NATIONAL ADVISORY COMMITTEE FOR AERONAUTICS

TECHNICAL NOTE 3628

AN ANALYSIS OF ESTIMATED AND

EXPERIMENTAL TRANSONIC DOWNWASH CHARACTERISTICS AS

AFFECTED BY PLAN FORM AND THICKNESS FOR WING AND

WING-FUSELAGE CONFIGURATIONS

By Joseph Weil, George S. Campbell,
and Margaret S. Diederich

Langley Aeronautical Laboratory
Langley Field, Va.

NACA

Washington
April 1956

.A

NATIONAL ADVISORY COMMITTEE FOR AERONAUTICS

TECHNICAL NOTE 3628

AN ANALYSIS OF ESTIMATED AND

EXPERIMENTAL TRANSONIC DOWNWASH CHARACTERISTICS AS

AFFECTED BY PLAN FORM AND THICKNESS FOR WING AND

WING-FUSELAGE CONFIGURATIONS[1]

By Joseph Weil, George S. Campbell,
and Margaret S. Diederich

SUMMARY

As part of a transonic research program the sensitivity of downwash at the tail plane to fairly systematic changes in wing plan form and thickness has been evaluated over a Mach number range of approximately 0.6 to 1.1, utilizing the transonic-bump technique. This paper presents a summary of information obtained from 11 transonic-bump investigations of wing and wing-fuselage configurations and compares the experimental results with theoretical estimations made for subsonic and supersonic Mach numbers.

Of the many variables investigated, the most powerful single factor influencing the character of downwash variation with Mach number appears to be wing thickness ratio. If the wing thickness is such that erratic lift variations are present at transonic speeds, similar effects on downwash can be expected. Available methods for estimating the downwash slope $\partial\epsilon/\partial C_L$ at high subsonic speeds or low supersonic speeds are probably sufficiently accurate for preliminary design purposes when applied at low lift coefficients, particularly for wings of small thickness ratio. With increases in sweep angle or aspect ratio, and decreases in taper ratio, the nonlinear downwash characteristics occurred at lower lift coefficients and were more severe; whereas changes in thickness ratio had little effect. The onset of nonlinear downwash characteristics was delayed to considerably higher lift coefficients and the severity of the nonlinearities was reduced considerably as the speed was increased from subsonic to low supersonic.

---

[1]Supersedes recently declassified NACA Research Memorandum L52I22 by Joseph Weil, George S. Campbell, and Margaret S. Diederich, 1952.

INTRODUCTION

Until recently, little information of a systematic nature has been available relative to the effects of wing geometry on downwash characteristics at transonic speeds. As part of a transonic research program, however, the effects of changes in wing plan form and thickness were investigated through a Mach number range of approximately 0.6 to 1.1 by utilizing the transonic-bump method. The results of 11 such studies are published in references 1 to 11.

The purpose of the present paper is to present a summary of the information gleaned from the various transonic-bump investigations of wing and wing-fuselage configurations at two representative tail heights and to compare these results with theoretical estimations made in the subsonic and supersonic Mach number range. At subsonic speeds, classical horseshoe-vortex methods were used to calculate theoretical downwash values. At supersonic Mach numbers, a recently developed line-vortex method (ref. 12) has been employed for similar downwash calculations. The theoretical results so obtained have been extended beyond the extremes of the experimental Mach number range so that downwash estimates are made available for this systematic series of wings at Mach numbers up to $\sqrt{2}$.

SYMBOLS AND ABBREVIATIONS

ϵ downwash angle, deg

ϵ' floating angle of free floating tails (corresponds to ϵ in refs. 1 to 11), deg

$\Delta\epsilon'$ increment in floating angle from zero lift, deg

α angle of attack, deg

C_L lift coefficient, $\dfrac{\text{Lift}}{qS}$

q dynamic pressure, lb/sq ft

S wing area, sq ft

M Mach number

b wing span, ft

b_t tail span, ft

x   distance between quarter chord of wing mean aerodynamic chord and tail mean aerodynamic chord, wing semispans

y   spanwise distance from plane of symmetry, wing semispans

z   tail height with respect to wing-chord plane, wing semispans

l distance from tail pivot axis to tail lifting line; lifting line and quarter-chord line assumed coincident at subsonic speeds

$\Lambda_{c/4}$ sweep of wing quarter-chord line, deg

A   aspect ratio

λ taper ratio

t   maximum streamwise-section wing thickness, ft

$\dfrac{c_l c}{C_L c_{av}}$ span load coefficient

c_l section-lift coefficient

c   local chord

c_{av} average wing chord, S/b

$\bar{c}$ mean aerodynamic chord, $\dfrac{2}{S}\displaystyle\int_0^{b/2} c^2 dy$

Subscripts:

t   tail

av   average

e   effective

EXPERIMENTAL METHODS

Scope of Test Data

Downwash characteristics are presented in references 1 to 11 for the wing and wing-fuselage configurations shown on table I. It is evident that the configurations investigated were sufficiently systematic to afford limited studies of the effects of sweepback, aspect ratio, taper ratio, and airfoil thickness. Data were obtained for five tail heights corresponding to a tail-height range of about ±40 percent semispan relative to the wing-chord plane extended. For reasons dictated by the test setup, the distance between the model pivot and location of the floating tails was maintained constant; therefore, inasmuch as wing area also remained constant, the ratio of tail length to wing semispan was a function of the aspect ratio. (See table I.) An angle-of-attack range of from about $-2°$ to $10°$ was covered over a Mach number range of about 0.6 to 1.1.

Because of the large bulk of downwash information obtained in the experimental investigations reported in references 1 to 11, a complete analysis at all tail heights was deemed impractical. The analysis included in the present paper, therefore, has been limited to tail heights on the chord plane extended and 30 percent of the wing semispan above the chord plane extended.

Test Technique

The experimental investigations were conducted in the Langley high-speed 7- by 10-foot tunnel by utilizing an adaptation of the NACA wing-flow technique for obtaining transonic speeds. The method used involves mounting a semispan model in the high-velocity flow field generated over the curved surface of a bump located on the tunnel floor. A more complete description of the transonic-bump test technique is presented in reference 13.

Effective downwash angles were determined by measuring the floating angles of a number of sweptback free-floating tails (wing 4 plan form of table I) located behind the various models. Typical test setups are shown in figure 1. Data were obtained for the five tail locations shown in two series of runs. (See fig. 1(a).) It was found from a preliminary investigation that the 2 inch tail spacing obtained in this manner enabled design information to be acquired with negligible interference between floating tails at transonic speeds. For studies of the downwash characteristics of the wing-fuselage configurations the centrally located tail was replaced by a geometrically similar tail mounted on the fuselage; therefore, a 0.4 inch more outboard spanwise region was

surveyed by the tail. (See fig. 1(b).) Further details of the test technique may be found in references 1 to 11.

No quantitative information is available as to the effect on wing-span-load distribution of factors that stem directly from the bump technique such as flow curvature, Mach number gradients, and low test Reynolds number (generally of the order of 6×10^5 to 8×10^5). As later concluded from the theoretical analysis, effects on span loading exert a much greater influence on downwash for tail locations on the chord plane extended than for considerably higher tail positions.

It should be pointed out that the tail floating angles obtained were a measure of the angle of zero pitching moment about the swept-tail pivot axis rather than the angle of zero lift (true effective downwash angle). The discrepancy between downwash and floating angles, however, caused by the presence of spanwise and chordwise downwash gradients was estimated to be generally less than 10 percent of the downwash angle for tails located on the chord plane extended and essentially zero for the high tail position analyzed.

THEORETICAL METHODS

Subsonic Method

Subsonic values of point downwash were calculated by summing the downwash contributions of 21 horseshoe vortices located along the wing quarter-chord line and having strengths determined by the theoretical span-load distribution. The analytical expression for the downwash induced by a single horseshoe vortex is given on page 197 of Glauert's text (ref. 14). Numerical values for the downwash in the $z = 0$ plane of a rectangular vortex were obtained from the tables of reference 15; similar values were calculated for the $z = 0.3$ plane. Since the time of these calculations, downwash in the field of a single horseshoe vortex has been presented for several tail heights in reference 16.

Two methods were used to calculate the wing-span-load distributions which determined the strength of the individual vortices. The most readily available wing loadings are those obtained from Weissinger's method and are given in the charts of reference 17. However, comparisons of Weissinger's 7-point solutions with lifting-surface theory and with experiment (refs. 18 and 19) indicate unsatisfactory prediction of loading shape for wings having a combination of moderately high sweep and aspect ratio. Somewhat more reliable loading shapes may be calculated as in reference 18 without undue labor. Wing loadings obtained from references 17 and 18 and the downwash from such loadings are compared in the present paper.

Results of calculations for several of the plan forms considered
in this paper indicated that Mach number variations in the subsonic
range had a negligible effect on the shapes of the span-loading curves.
It therefore was considered justifiable to account for Mach number effects
on $\partial\epsilon/\partial C_L$ by using the incompressible span loadings in conjunction with

an increase in tail length by the ratio $\dfrac{1}{\sqrt{1 - M^2}}$. Such a procedure

results from application of the three-dimensional Prandtl-Glauert trans-
formation. (See ref. 20.)

Supersonic Method

The theoretical supersonic downwash in this paper was calculated
using equations (41) and (46) of reference 12 for the downwash in the
field of swept and unswept supersonic line vortices. Calculations made
for representative plan forms and tail locations indicated that a con-
siderable saving in labor could be effected by replacement of the integral
terms in these equations with equivalent finite summations. At the same
time, accuracy was not perceptibly impaired when the span loading was
broken up into 20 steps across the span. Hence, the theoretical super-
sonic downwash presented in this paper was calculated by using such a
finite summation. The sweep and chordwise location of the line vortex
was chosen to approximate those of the curved line of local centers of
pressure.

The supersonic loadings presented in this paper and used in the
downwash calculations are subject to the usual limitations of small
perturbation theory. In the case of wings having supersonic leading
and trailing edges, the span loading was calculated by evaluating the
potential at the trailing edge, the expression for velocity potential
being given in reference 21. Design charts are now available in refer-
ence 22 for the span loading of such wings. Cohen's method (refs. 23
to 25) was used to calculate the loading of wings having subsonic edges.
For the intermediate case of subsonic leading edge and supersonic
trailing edge, the expressions of reference 26 for local pressure were
integrated analytically to provide spanwise loading.

Application

The theoretical downwash presented is directly applicable to iso-
lated wing configurations. The effects of wing-body interference have
not been considered. The principal effect of this interference on wing
span loading probably is experienced inboard near the juncture and, as
will be shown later, is apt to produce the largest effect on the down-
wash characteristics of tails located on the wake center line.

For most of the calculations the vortex sheet was assumed to be flat with displacement and rolling-up of the trailing vortex neglected. This assumption is believed justified in the low-lift range, particularly in view of the fact that the configurations studied were close-coupled and generally of moderate aspect ratio.

As will be shown later, in certain instances it was found desirable to estimate the downwash on the assumption that the entire semispan trailing vorticity could be concentrated in a single trailing vortex. For the low-lift range in which the estimations were applied, vortex displacement was neglected. The method used for these estimations may be found in reference 27.

As mentioned in a previous section, the experimental measurements did not represent true effective downwash angles, but rather a measure of the angle of zero pitching moment of the floating tail about its pivot axis. In order to compare theory with experiment it therefore was necessary to compute the tail floating angles for the swept tail used (wing 4 plan form). This computation was made by use of the following downwash-weighting relationship

$$\frac{\partial \epsilon'}{\partial C_L} = \frac{1}{l_{av}} \int_0^1 \epsilon C_{L_l} \left(\frac{c_l c}{C_L c_{av}}\right) d\left(\frac{y}{b_t/2}\right) \tag{1}$$

where $\dfrac{c_l c}{C_L c_{av}}$ for the assumed $45°$ swept tail can be found in figures 4 and 13.

The theoretical point downwash has been used not only to obtain the floating angles for correlation with experiment but also to obtain the theoretical effects of wing geometry on the downwash characteristics through a Mach number range considerably beyond the experimental range. For the latter computations a measure of the angle of zero lift of the floating tail (effective downwash) was computed by the following relation

$$\left(\frac{\partial \epsilon}{\partial C_L}\right)_e = \int_0^1 \frac{\partial \epsilon}{\partial C_L}\left(\frac{c_l c}{C_L c_{av}}\right) d\left(\frac{y}{b_t/2}\right) \tag{2}$$

PRESENTATION OF RESULTS

A summary of figures presenting the results of the subject investigation is as follows:

ANALYSIS AND DISCUSSION

Theoretical Downwash

Subsonic.- The comparison of the span-load distributions obtained
from the charts of reference 17 and the methods of reference 18 is fairly

good except for the wings of the highest sweep angles and aspect ratios (wings 5 and 7). (See figs. 5 and 7.) Decreasing wing taper ratio, sweep angle, or aspect ratio is shown to produce a more favorable comparison between the two methods. It is interesting to note that, whereas differences in span-load gradient attributable to the method of calculation represent sizeable differences in estimated downwash angle per unit lift for tails located on the wing-chord plane extended, very little sensitivity to the exact shape of the span-loading curve is indicated when the tail surface is located 30 percent of the wing semispan above the chord plane extended.

In view of the fact that the methods of reference 17 are apt to produce somewhat erroneous results for certain of the wings considered, all subsonic downwash estimations presented and discussed in the remainder of this paper utilize span loadings calculated by the methods of reference 18. The values of lift-curve slope and the lateral center of pressure for the incompressible finite-step loadings are presented in table II.

An inspection of figures 2 to 10 indicates in many instances a rather large spanwise gradient of $\partial\epsilon/\partial C_L$ with a minimum value occurring at the plane of symmetry. For the higher tail position investigated ($z = 0.3$), the gradients in $\partial\epsilon/\partial C_L$ are generally negligible.

Increasing the tail length to infinity generally reduced the downwash angles by about 10 to 15 percent. This magnitude also represents the maximum first-order effects of compressibility on the subsonic downwash angles, since the downwash angles in compressible flow can be obtained by calculating the incompressible downwash with the tail length increased by $\dfrac{1}{\sqrt{1 - M^2}}$.

Supersonic.- The span-load distributions for the series of wings investigated showed appreciable effects of Mach number at supersonic speeds, which is in marked contrast to the negligible changes in wing loading found at subsonic speeds. (See figs. 11 to 19.) As may be seen from the span-loading shapes or from the values of lateral center of pressure, increasing Mach number at supersonic speeds shifted the center of load progressively outboard in all instances with the exception of the delta wing (fig. 18) for which no change in loading shape is indicated.

Spanwise downwash gradients in the chord plane extended were generally much greater at supersonic speeds than at subsonic speeds. Inasmuch as relatively small differences are shown between the downwash characteristics for finite and infinite tail lengths, it is evident that the large spanwise gradients are primarily attributable to the shape of the load-grading curve rather than caused by fundamental differences in the

nature of the subsonic and supersonic calculations. Raising the tail
0.3 semispan above the chord plane greatly reduced the spanwise downwash
gradients and generally reduced the effect of Mach number on $\partial\epsilon/\partial C_L$.

Variations with Mach number.- The theoretical point values of $\partial\epsilon/\partial C_L$
presented in figures 2 to 19 were weighted by use of equation (2) to
obtain estimated $\left(\partial\epsilon/C_L\right)_e$ variations with Mach number for the nine plan

forms investigated and for the tail configurations shown in table I. The
variation of $\left(\partial\epsilon/\partial\alpha\right)_e$ with Mach number was calculated by a similar
weighting process. Estimations are presented for tail heights of 0
and 0.3 semispan above the wing-chord plane extended at finite and infi-
nite tail lengths. (See figs. 20 to 31.) Although it is realized that
the "Trefftz plane" results are physically inaccurate because of wake-
distortion effects, the infinite-tail-length estimations were included
because they give at least a fair evaluation of the differences between
rather short coupled configurations and those having large tail lengths.
An arbitrary dashed-line fairing has been used in the Mach number range
from M = 0.8 to 1.1 to connect the subsonic and supersonic values of
$\left(\partial\epsilon/C_L\right)_e$ and $\left(\partial\epsilon/\partial\alpha\right)_e$.

An inspection of the various curves (figs. 20 to 31) shows several
interesting differences between the subsonic and supersonic downwash
characteristics. The downwash slopes are a maximum in the chord plane
extended at subsonic speeds but this is not always true at supersonic

speeds. Increase in tail length reduced $\left(\partial\epsilon/\partial C_L\right)_e$ and $\left(\partial\epsilon/\partial\alpha\right)_e$ at
subsonic speeds but the reverse condition was generally indicated at
supersonic speeds.

From the data it would appear that the smallest change in downwash
parameter $\left(\partial\epsilon/\partial C_L\right)_e$ with Mach number at low C_L might be expected for
a high tail at relatively large tail length. In the sweep series, Mach
number effects were smallest for the $60°$ configuration (fig. 21). At
all speeds the wings having lowest aspect ratio and taper ratio had the
largest computed downwash slopes.

Experimental Downwash

Effect of sweep angle.- The basic data of figures 32 to 42 have
been used to determine the variation of $\partial\epsilon'/\partial C_L$ with Mach number in the
low-lift range. For the wing-alone condition, the unswept wing gener-
ally produced the highest value of $\partial\epsilon'/\partial C_L$ and also demonstrated the
most erratic changes in $\partial\epsilon'/\partial C_L$ above M = 0.85. (See fig. 43.) It
should be pointed out that the unswept-wing data (ref. 1) showed similar

irregularities in the lateral center of pressure. This result indicates
that sizeable changes occur in the span load distribution of the unswept
wing at transonic speeds which are directly reflected in $\partial\epsilon'/\partial C_L$. The
sweptback wings showed rather small variations of $\partial\epsilon'/\partial C_L$ with M par-
ticularly at $z = 0.3$.

The addition of the fuselage had the largest effect on the wings of
greatest sweep. For the tail located on the chord plane extended, it
should be remembered that the increases in $\partial\epsilon'/\partial C_L$ shown for the $45°$ and
$60°$ wings are at least partially caused by the more outboard spanwise
location of the floating tail in conjunction with large spanwise down-
wash gradients indicated by theory. (See fig. 43.)

Comparisons of the experimental and estimated floating-angle param-
eter $\partial\epsilon'/\partial C_L$ for the sweep series as a function of Mach number are
shown in figures 44 to 47. A smooth arbitrary fairing was used in the
Mach number range between lift-force break and the lowest point for
which supersonic estimations were made. In contradiction with what
might be anticipated, the floating angles for the wing-fuselage configu-
rations agree better with estimations for the low tail position at sub-
sonic speeds than do the corresponding wing-alone configurations. For
$z = 0$ the estimated floating-angle slope is generally considerably
higher than the experimental results. (See figs. 44 and 45.) The over-
all agreement between experimental and estimated results is seen to be
considerably better for $z = 0.3$ (figs. 46 and 47), however, perhaps
because $\partial\epsilon'/\partial C_L$ is more dependent upon the total lift at the higher
tail position and less influenced by small deviations in the span
loading. (See figs. 44 and 46.)

The variations of floating-angle increments with lift coefficient
are presented in figures 48 to 51 for Mach numbers of 0.8 and 1.1. Only
limited conclusions regarding the downwash characteristics at higher lift
coefficients can be drawn from these data because of the restricted angle
range obtained in the original investigations. It is apparent, however,
that the extent of the linear range of $\Delta\epsilon'$ against C_L decreases with
increasing wing sweep. The lift coefficient at which the lateral center
of pressure departs from linearity (refs. 1 to 11) has been indicated
in the figures by a small vertical tick. It is evident that the onset
of nonlinearity in variation of $\Delta\epsilon'$ with C_L is directly related to
the lift coefficient at which changes in span loading are known to occur.
For the swept wings, the center of pressure moves inboard at the higher
lift coefficients and a corresponding increase in $\partial\epsilon'/\partial C_L$ is indicated;
for the unswept wing the reverse is true. At $M = 1.1$, changes in span
loading are delayed to a higher lift coefficient than at $M = 0.8$ and
this effect is reflected in the extension of linear ϵ'.

In view of the preceding discussion, it is apparent that correlation between experimental and predicted results can be defined by the slopes shown in figures 44 to 47 up to the lift coefficients indicated by the ticks in figures 48 to 51.

Effect of aspect ratio.- The effects of aspect ratio on $\partial\epsilon'/\partial C_L$ are presented in figures 52 to 60. Increasing wing aspect ratio almost always reduced the floating-angle slope and produced a somewhat smaller variation of $\partial\epsilon'/\partial C_L$ with Mach number. A sizeable but rather inconsistent fuselage effect is also shown. (See figs. 52, 55, and 58.)

The most significant effect of aspect ratio on the floating-angle characteristics at the higher lift coefficients is indicated for the 45° swept plan form which shows a large increase in $\partial\epsilon'/\partial C_L$ above $C_L \approx 0.4$ for the wing of aspect ratio 6 at subsonic speeds. Although the limited lift range precludes a definite conclusion, it is apparent that the linearity of the curve of $\Delta\epsilon'$ against C_L is maintained to a somewhat higher C_L for the wing with an aspect ratio of 4. The foregoing trends, which may be affected by the low scale of the test, are directly traceable to earlier occurrence of flow changes on the higher-aspect-ratio wing and were reflected by movements of the spanwise center of pressure. (See vertical ticks, fig. 56.)

In general, the effects of aspect ratio as determined experimentally were either always less than or approximately equal to the estimated increments. The largest discrepancies between the estimated and experimental results were evident for the wing with an aspect ratio of 2 and $\Lambda_{c/4} = 60^\circ$ (fig. 58). For this wing the chord-plane-extended slopes were much smaller than those estimated by assuming no distortion of the vortex sheet. This latter effect becomes more critical as the aspect ratio is reduced and may be responsible in part for the very poor agreement.

Effects of taper ratio.- For the two wings having approximately 35° sweep the effects of changing wing taper ratio were considerably less than estimated for $z = 0$ at subsonic speeds. At low supersonic speeds, however, the agreement between experiment and estimation was quite good. (See fig. 61.) Mach number effects were not materially greater for wings of either taper ratio.

For the triangular wing, changes in wing span loading, as indicated by the vertical ticks on figure 62, occurred at considerably lower lift coefficients than for the wing of $\lambda = 0.6$ and this effect was generally reflected in the earlier occurrence of unstable trends in the higher lift downwash characteristics. The addition of the fuselage to the triangular wing produced more unstable downwash characteristics in the higher lift range throughout the speed range.

Decreasing the taper ratio from 0.6 to 0.3 on the 45° swept plan form delayed and reduced the pronounced decrease in $\partial\epsilon'/\partial C_L$ for the wing fuselage condition ($z = 0$) at transonic speeds. (See fig. 64.) The agreement between experiment and estimations is seen to be rather poor for the low-tail position. For the tail in the raised position, the experimental results indicate a rather ragged variation with M, but the absolute values agree fairly well with estimations. The data are insufficient to explain the cause of the sharp hump in the variation of $\partial\epsilon'/\partial C_L$ between $M = 1.05$ and 1.1 for $\lambda = 0.3$, $z = 0.30$.

Effects of wing thickness.- The effects of reducing the thickness of the unswept wing from 6 to 4 percent and of the 45° swept wing of aspect ratio 6 from 9 to 6 percent are presented in figures 67 to 70. It is evident that, for both plan forms, reducing the wing thickness produced better agreement between the estimated and experimental results at transonic speeds.

The largest effects of thickness were present for the swept wing where, for the 9-percent-thick configuration, loss in tip loading in the low-lift range near $M = 1.0$ (ref. 8) caused a large increase in $\partial\epsilon'/\partial C_L$. For general application, a rough idea of the combination of thickness ratio, aspect ratio, and sweep for which erratic downwash variations might be expected in the low-lift range at transonic speeds can be obtained from references 28 and 29. The increase in $\partial\epsilon'/\partial C_L$ for the swept wing in the higher lift range at subsonic speeds was little affected by thickness changes.

Summary of correlation between experimental and estimated results.- The values of $\partial\epsilon/\partial C_L$ at $M = 0.8$ estimated by the assumption of a flat vortex sheet were almost always considerably higher than values obtained from the experimental wing-alone data. (See fig. 71.) Surprisingly enough, the addition of the fuselage actually resulted in somewhat better correlation. In the higher tail location considerably better agreement was obtained with most points falling within the lines indicating ±20 percent departure from the line of perfect agreement. With the possible exception of wing 9, it might be expected that the assumption of a flat vortex sheet should be valid at low C_L. Nevertheless, inasmuch as the correlation for the chord plane extended results was considered rather poor, it was decided to calculate the downwash on the improbable assumption that the trailing vorticity was completely rolled up into two discrete vortices. The correlation obtained by use of this method is shown by the flagged symbols of figure 71. It is seen that the agreement using a single horseshoe vortex is much improved for the low tail position. The correlation for $z = 0.30$ is essentially the same for either method and is considered acceptable for preliminary design estimates.

A correlation between experimental $\partial\epsilon'/\partial C_L$ at $M = 1.1$ and values calculated on the basis of line-vortex theory (assuming a flat sheet) is presented in figure 72. As was shown in the subsonic correlation, the degree to which $\partial\epsilon'/\partial C_L$ can be predicted is considerably better for $z = 0.30$ than for tails located on the wake center line. The presence of the fuselage did not materially affect the correlation. As previously pointed out, increasing the thickness ratio from 6 percent (wing 7) to 9 percent (wing 8) results in large span load changes which produce a detrimental effect on the correlation.

The replacement of the wing by a single horseshoe vortex, which was shown to work so well at $M = 0.8$ was also tried at $M = 1.1$. The general correlation at $M = 1.1$, however, was materially worse when the rolled-up vortex assumption was used, and it is not suggested that this approach be used in most instances even for preliminary estimates. It might be added, however, that the experimental data for wing 9 ($A = 2$, $\Lambda_{c/4} = 60°$), which were in very poor agreement with the linear theory result at $z = 0$, were brought into almost perfect agreement with the value estimated on the assumption of a rolled-up vortex; this result indicates that the assumption of a rolled-up vortex might still offer the best approach at low supersonic speeds for wings of very low aspect ratio.

CONCLUDING REMARKS

A study of the effects of plan form and thickness on the estimated and experimentally determined transonic downwash characteristics of various wing and wing fuselage configurations indicated a number of points of special interest which are summarized in the following paragraphs.

The thin wings investigated in the present paper generally showed rather smooth transonic downwash characteristics with no important consistent effects of sweep angle, aspect ratio, taper ratio, or tail height on the variation of the rate of change of downwash slope $\partial\epsilon/\partial C_L$ with Mach number in the low lift range. Although data pertaining to thickness effects were meager, indications were that the use of wings having thickness large enough to produce erratic variations of lift slope at transonic speeds very likely will produce similar erratic variations on downwash characteristics. The addition of the fuselage to the isolated wing affected the absolute magnitude of downwash slope more than it affected the variation of the downwash slope with Mach number.

At subsonic speeds, a somewhat better correlation between estimated and experimental downwash slope $\partial\epsilon/\partial C_L$ was obtained for tails located on the chord plane extended by the physically improbable assumption of a

completely rolled-up vortex sheet instead of a flat vortex sheet. For a tail position considerably above the wake center line, assumption of either a flat or rolled-up vortex sheet gave an acceptable correlation with experiment. At low supersonic speeds use of line-vortex theory with a flat vortex sheet produced results that were in fair agreement with experiment.

Any conclusions drawn concerning the downwash characteristics at higher lift coefficients are somewhat restricted because of the limited angle-of-attack range of most of the test data. It was found, however, that the lateral center-of-pressure data obtained in the investigations of the various wings could be used to determine the lift coefficient at which nonlinearities in downwash might be expected at all Mach numbers. Increase in sweep angle and aspect ratio and decrease in taper ratio produced earlier and more pronounced increases in downwash slope at higher lift coefficients, whereas thickness change had little effect. The onset of nonlinear downwash characteristics was delayed to considerably higher lift coefficients and the severity of the nonlinearities reduced considerably as the speed was increased from subsonic to low supersonic.

Langley Aeronautical Laboratory,
    National Advisory Committee for Aeronautics,
        Langley Field, Va., September 19, 1952.

REFERENCES

1. Goodson, Kenneth W., and Morrison, William D., Jr.: Aerodynamic Characteristics of a Wing With Unswept Quarter-Chord Line, Aspect Ratio 4, Taper Ratio 0.6, and NACA 65A006 Airfoil Section. Transonic-Bump Method. NACA RM L9H22, 1949.

2. Myers, Boyd C., II, and Wiggins, James W.: Aerodynamic Characteristics of a Wing With Unswept Quarter-Chord Line, Aspect Ratio 4, Taper Ratio 0.6, and NACA 65A004 Airfoil Section. Transonic-Bump Method. NACA RM L50C16, 1950.

3. Sleeman, William C., Jr., and Becht, Robert E.: Aerodynamic Characteristics of a Wing With Quarter-Chord Line Swept Back 35°, Aspect Ratio 4, Taper Ratio 0.6, and NACA 65A006 Airfoil Section. Transonic-Bump Method. NACA RM L9B25, 1949.

4. Weil, Joseph, and Goodson, Kenneth W.: Aerodynamic Characteristics of a Wing With Quarter-Chord Line Swept Back 45°, Aspect Ratio 4, Taper Ratio 0.6, and NACA 65A006 Airfoil Section. Transonic-Bump Method. NACA RM L9A21, 1949.

5. King, Thomas J., Jr., and Myers, Boyd C., II: Aerodynamic Characteristics of a Wing With Quarter-Chord Line Swept Back 60°, Aspect Ratio 4, Taper Ratio 0.6, and NACA 65A006 Airfoil Section. Transonic-Bump Method. NACA RM L9G27, 1949.

6. Sleeman, William C., Jr., and Morrison, William D., Jr.: Aerodynamic Characteristics of a Wing With Quarter-Chord Line Swept Back 35°, Aspect Ratio 6, Taper Ratio 0.6, and NACA 65A006 Airfoil Section. Transonic-Bump Method. NACA RM L9K10a, 1949.

7. Goodson, Kenneth W., and Few, Albert G., Jr.: Aerodynamic Characteristics of a Wing With Quarter-Chord Line Swept Back 45°, Aspect Ratio 6, Taper Ratio 0.6, and NACA 65A006 Airfoil Section. Transonic-Bump Method. NACA RM L9I08, 1949.

8. Spreemann, Kenneth P., Morrison, William D., Jr., and Pasteur, Thomas B., Jr.: Aerodynamic Characteristics of a Wing With Quarter-Chord Line Swept Back 45°, Aspect Ratio 6, Taper Ratio 0.6, and NACA 65A009 Airfoil Section. Transonic-Bump Method. NACA RM L50B03a, 1950.

9. Myers, Boyd C., II, and King, Thomas J., Jr.: Aerodynamic Characteristics of a Wing With Quarter-Chord Line Swept Back 60°, Aspect Ratio 2, Taper Ratio 0.6, and NACA 65A006 Airfoil Section. Transonic-Bump Method. NACA RM L50A12, 1950.

10. Sleeman, William C., Jr., and Becht, Robert E.: Aerodynamic Charac-
    teristics of a Delta Wing With Leading Edge Swept Back 45°, Aspect
    Ratio 4, and NACA 65A006 Airfoil Section. Transonic-Bump Method.
    NACA RM L9G22a, 1949.

11. Myers, Boyd C., II, and King, Thomas J., Jr.: Aerodynamic Charac-
    teristics of a Wing With Quarter-Chord Line Swept Back 45°, Aspect
    Ratio 4, Taper Ratio 0.3, and NACA 65A006 Airfoil Section.
    Transonic-Bump Method. NACA RM L9E25, 1949.

12. Mirels, Harold, and Haefeli, Rudolph C.: Line-Vortex Theory for
    Calculation of Supersonic Downwash. NACA Rep. 983, 1950.

13. Schneiter, Leslie E., and Ziff, Howard L.: Preliminary Investiga-
    tion of Spoiler Lateral Control on a 42° Sweptback Wing at Tran-
    sonic Speeds. NACA RM L7F19, 1947.

14. Glauert, H.: The Elements of Aerofoil and Airscrew Theory. Second
    ed., Cambridge Univ. Press, 1947. (Reprinted 1948.)

15. Staff of Mathematics Division, N.P.L.: Tables of Complete Downwash
    Due to a Rectangular Vortex. R. & M. No. 2461, British A.R.C.,
    July 21, 1947.

16. Diederich, Franklin W.: Charts and Tables for Use in Calculations
    of Downwash of Wings of Arbitrary Plan Form. NACA TN 2353, 1951.

17. DeYoung, John, and Harper, Charles W.: Theoretical Symmetric Span
    Loading at Subsonic Speeds for Wings Having Arbitrary Plan Form.
    NACA Rep. 921, 1948.

18. Campbell, George S.: A Finite-Step Method for the Calculation of
    Span Loadings of Unusual Plan Forms. NACA RM L50L13, 1951.

19. Schneider, William C.: A Comparison of the Spanwise Loading Calcu-
    lated by Various Methods With Experimental Loadings Obtained
    on a 45° Sweptback Wing of Aspect Ratio 8.02 at a Reynolds Number
    of 4.0×10^6. NACA Rep. 1208, 1954. (Supersedes NACA RM L51G30.)

20. Nielsen, Jack N., and Sweberg, Harold H.: Note on Compressibility
    Effects on Downwash at the Tail at Subcritical Speeds. NACA WR L-19,
    1945. (Formerly NACA CB L5C09.)

21. Harmon, Sidney M., and Jeffreys, Isabella: Theoretical Lift and
    Damping in Roll of Thin Wings With Arbitrary Sweep and Taper at
    Supersonic Speeds. Supersonic Leading and Trailing Edges. NACA
    TN 2114, 1950.

22. Martin, John C., and Jeffreys, Isabella: Span Load Distributions
    Resulting From Angle of Attack, Rolling, and Pitching for Tapered
    Sweptback Wings With Streamwise Tips — Supersonic Leading and
    Trailing Edges. NACA TN 2643, 1952.

23. Cohen, Doris: The Theoretical Lift of Flat Swept-Back Wings at
    Supersonic Speeds. NACA TN 1555, 1948.

24. Cohen, Doris: Theoretical Loading at Supersonic Speeds of Flat
    Swept-Back Wings With Interacting Trailing and Leading Edges.
    NACA TN 1991, 1949.

25. Cohen, Doris: Formulas and Charts for the Supersonic Lift and Drag
    of Flat Swept-Back Wings With Interacting Leading and Trailing
    Edges. NACA TN 2093, 1950.

26. Malvestuto, Frank S., Jr., Margolis, Kenneth, and Ribner, Herbert S.:
    Theoretical Lift and Damping in Roll at Supersonic Speeds of Thin
    Sweptback Tapered Wings With Streamwise Tips, Subsonic Leading Edges,
    and Supersonic Trailing Edges. NACA Rep. 970, 1950. (Supersedes
    NACA TN 1860.)

27. Spreiter, John R., and Sacks, Alvin H.: The Rolling Up of the
    Trailing Vortex Sheet and Its Effect on the Downwash Behind Wings.
    Jour. Aero. Sci., vol. 18, no. 1, Jan. 1951, pp. 21-32, 72.

28. Polhamus, Edward C.: Summary of Results Obtained by Transonic-Bump
    Method on Effects of Plan Form and Thickness on Lift and Drag
    Characteristics of Wings at Transonic Speeds. NACA TN 3469, 1955.
    (Supersedes NACA RM L51H30.)

29. Nelson, Warren H., and McDevitt, John B.: The Transonic Character-
    istics of 22 Rectangular, Symmetrical Wing Models of Varying Aspect
    Ratio and Thickness. NACA TN 3501, 1955. (Supersedes NACA
    RM A51A12.)

Table I

Model Geometry
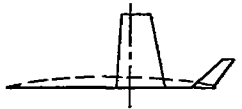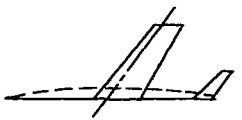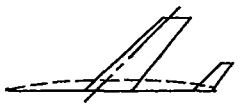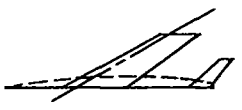
Wing No. and Ref.		$\Lambda \frac{c}{4}$ (deg)	A	λ	NACA Section	x	$\dfrac{b_f}{b}$
1		0	4	.6	65A006	1.2	.38
2					65A004		
3		35	4	.6	65A006	1.2	.38
4		45	4	.6	65A006	1.2	.38
5		60	4	.6	65A006	1.2	.38
6		35	6	.6	65A006	1.0	.31
7		45	6	.6	65A006	1.0	.31
8					65A009		
9		60	2	.6	65A006	1.7	.53
10		36.9	4	0	65A006	1.2	.38
11		45	4	.3	65A006	1.2	.38

TABLE II

SUMMARY OF THEORETICAL LIFT-CURVE SLOPES

AND LATERAL CENTERS OF PRESSURE[1]

M \ Wing	Lift-curve slope, per degree					Lateral center of pressure, percent semispan				
	0	1.1	1.2	1.3	$\sqrt{2}$	0	1.1	1.2	1.3	$\sqrt{2}$
1,2	0.0658	0.1149	0.0901	0.0747	0.0636	43.6	40.4	41.2	41.8	42.8
4	0.0556	0.0756	0.0751	0.0734	0.0683	46.0	46.4	48.6	49.7	50.0
5	0.0429	0.0505	0.0505	0.0507	0.0506	47.1	47.9	48.4	49.0	49.5
6	0.0681	0.1097	0.1013	0.0893	0.0765	46.1	48.8	50.1	50.4	50.0
7,8	0.0608	0.0834	0.0845	0.0853	0.0803	46.7	48.3	49.7	51.5	51.8
9	0.0361	0.0427	0.0421	0.0418	0.0417	45.7	43.6	45.2	46.2	47.0
10	0.0588	0.0991	0.0859	0.0773	0.0698	40.4	42.4	42.4	42.4	42.4
11	0.0572	0.0825	0.0793	0.0738	0.0686	44.5	46.5	47.6	47.8	48.1

M \ Wing	0	1.13	1.25	$\sqrt{2}$	0	1.13	1.25	$\sqrt{2}$
3	0.0606	0.0930	0.0819	0.0683	45.3	47.2	48.0	48.7

[1]Values shown for zero Mach number calculated by method of reference 18.
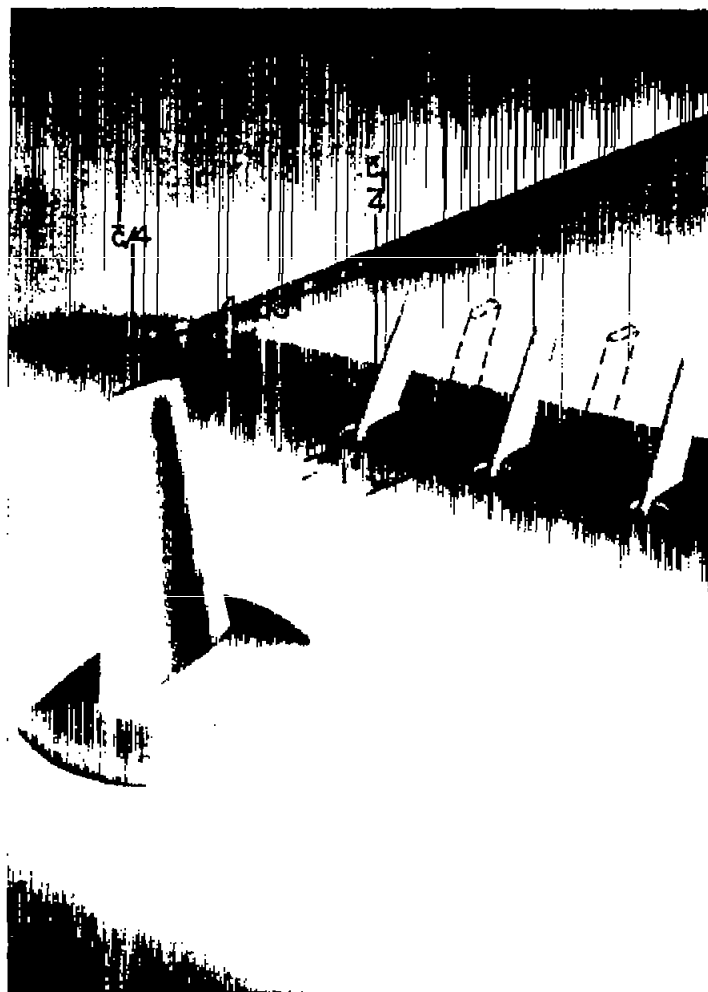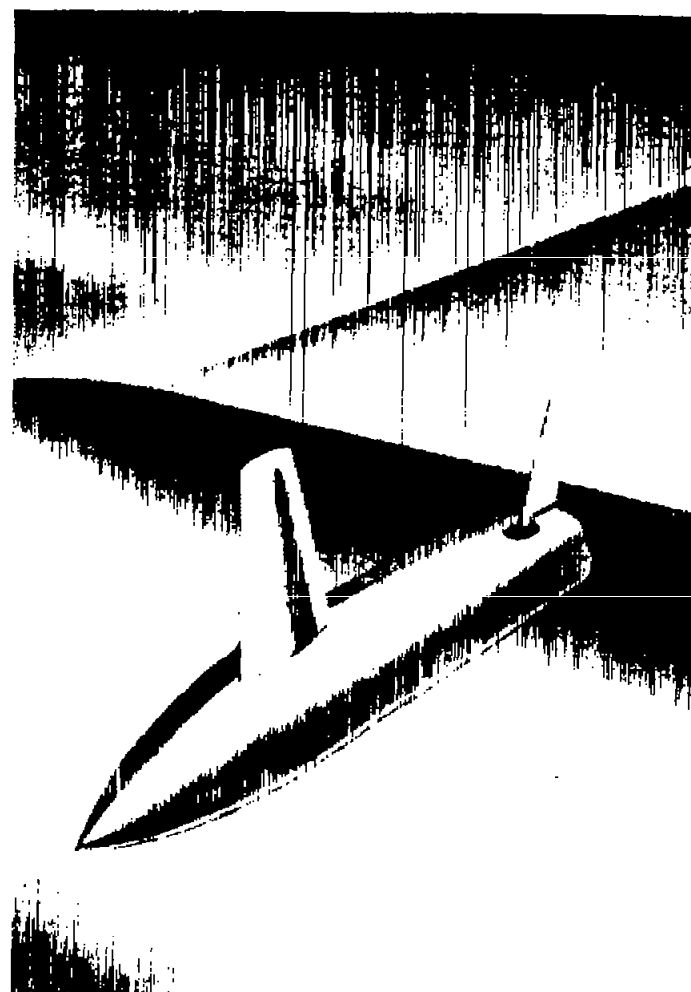
(a) Wing alone.　　　　(b) Wing fuselage.

L-76117

Figure 1.- Pictorial representation showing test setup on transonic bump.
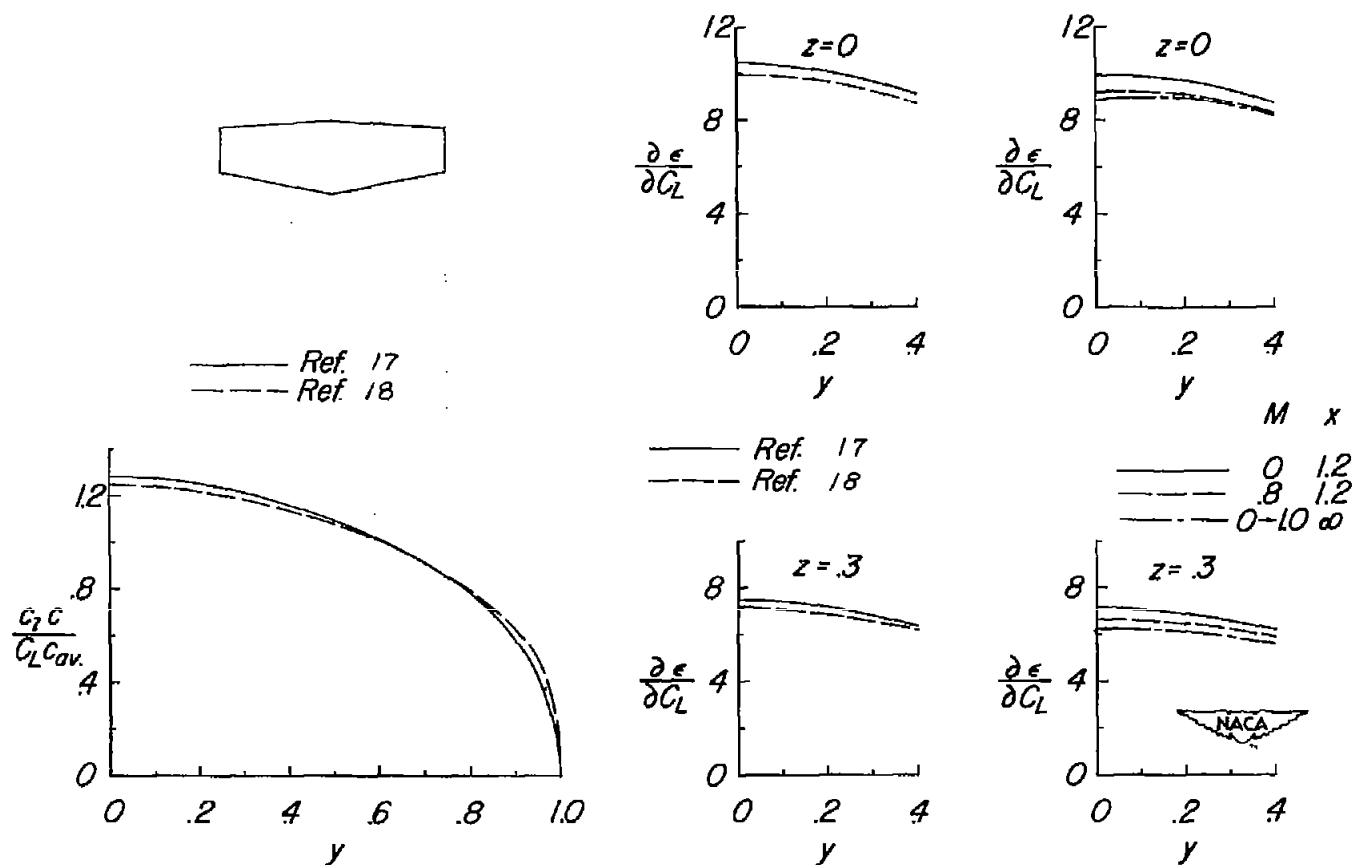
(a) Comparison of span load distribution computed by two different methods.

(b) Effect of span load distribution on the spanwise variation of downwash parameter $\partial\epsilon/\partial C_L$. $x = 1.2$.

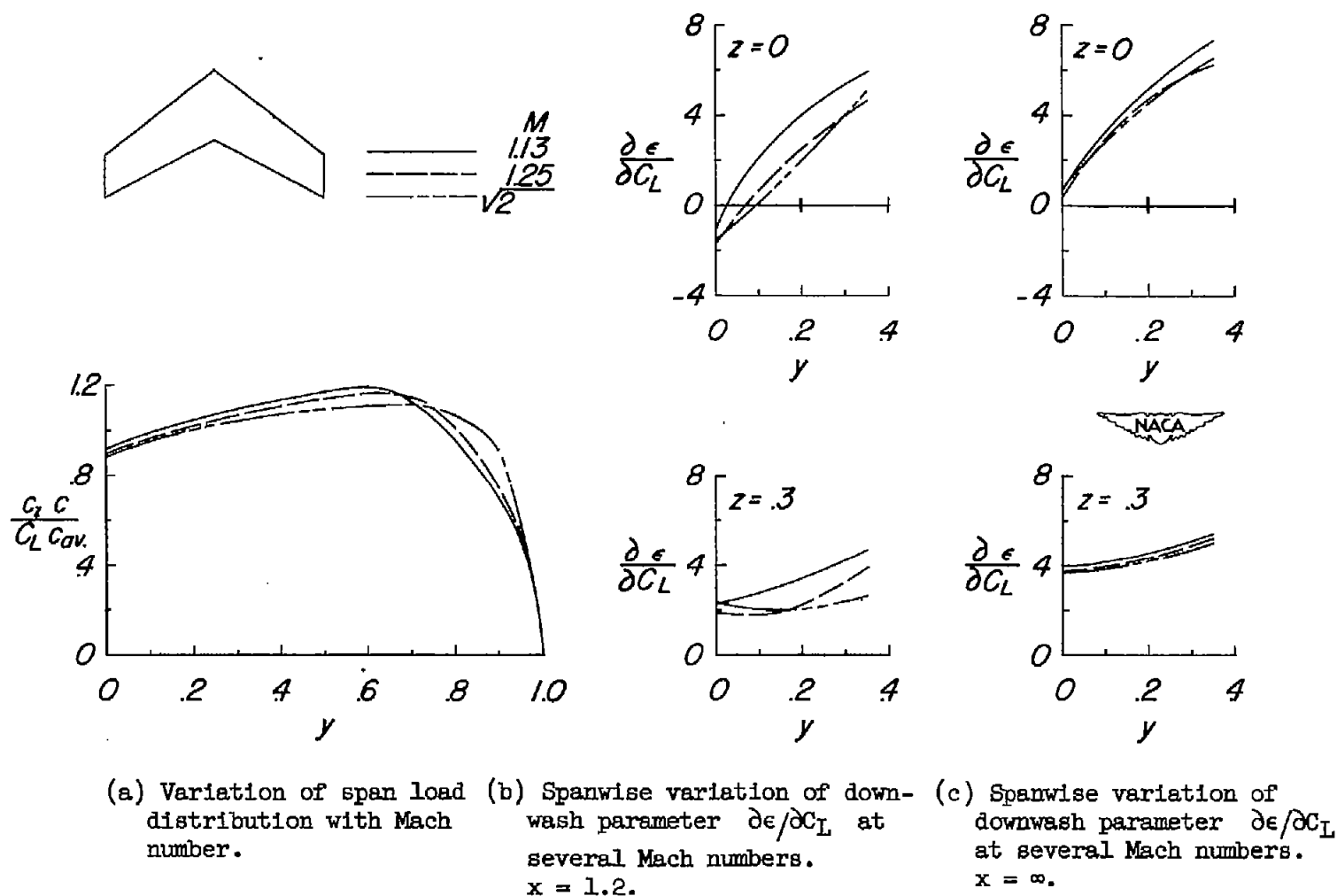(c) Effect of tail length and Mach number on spanwise variation of downwash parameter $\partial\epsilon/\partial C_L$.

Figure 2.- Theoretical span load distribution and spanwise downwash characteristics at subsonic speeds. Wings 1 and 2; $\Lambda_{c/4} = 0^O$; $A = 4$; $\lambda = 0.6$.
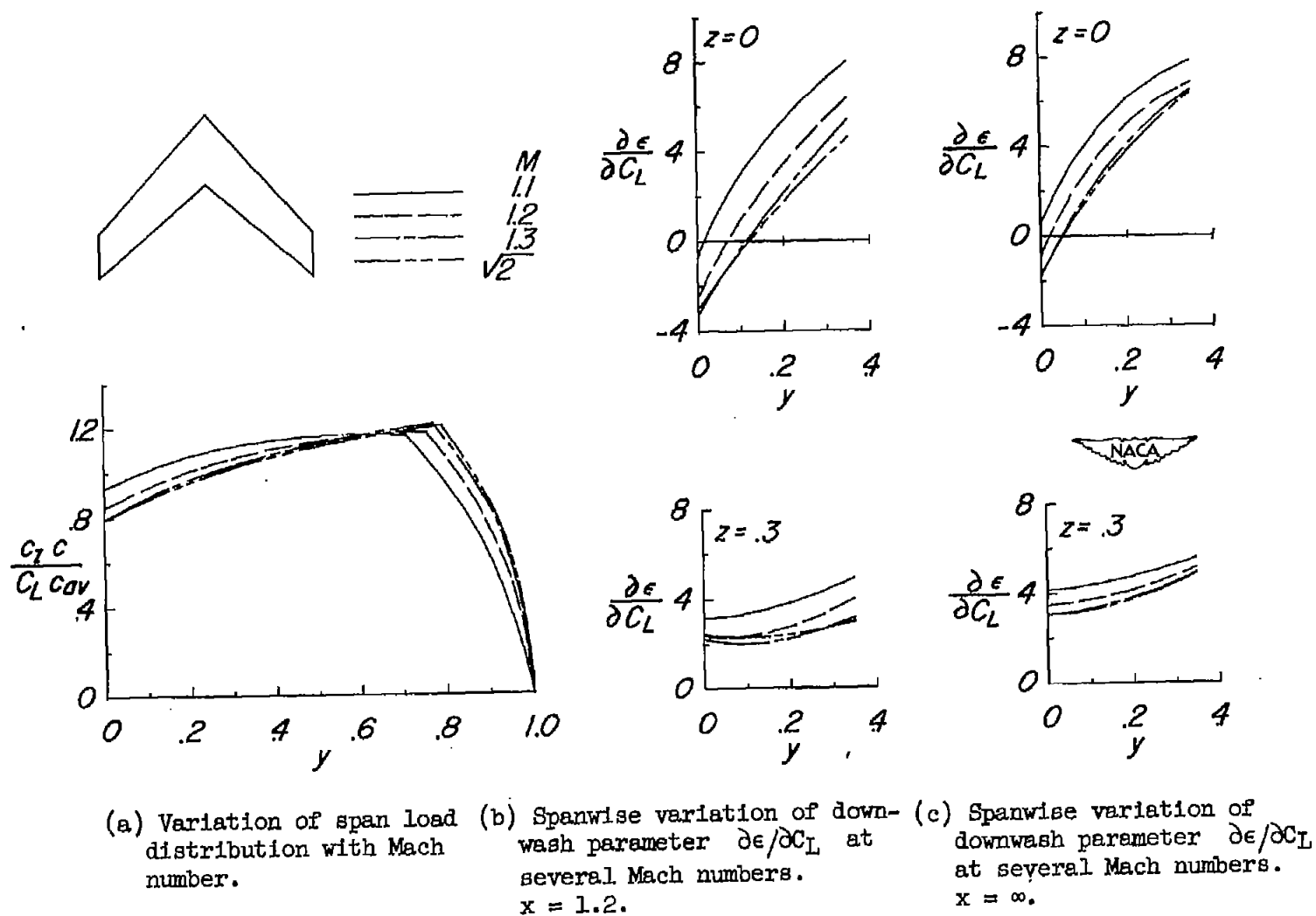
(a) Comparison of span load distribution computed by two different methods.

(b) Effect of span load distribution on the spanwise variation of downwash parameter $\partial\epsilon/\partial C_L$. $x = 1.2$.

(c) Effect of tail length and Mach number on spanwise variation of downwash parameter $\partial\epsilon/\partial C_L$.
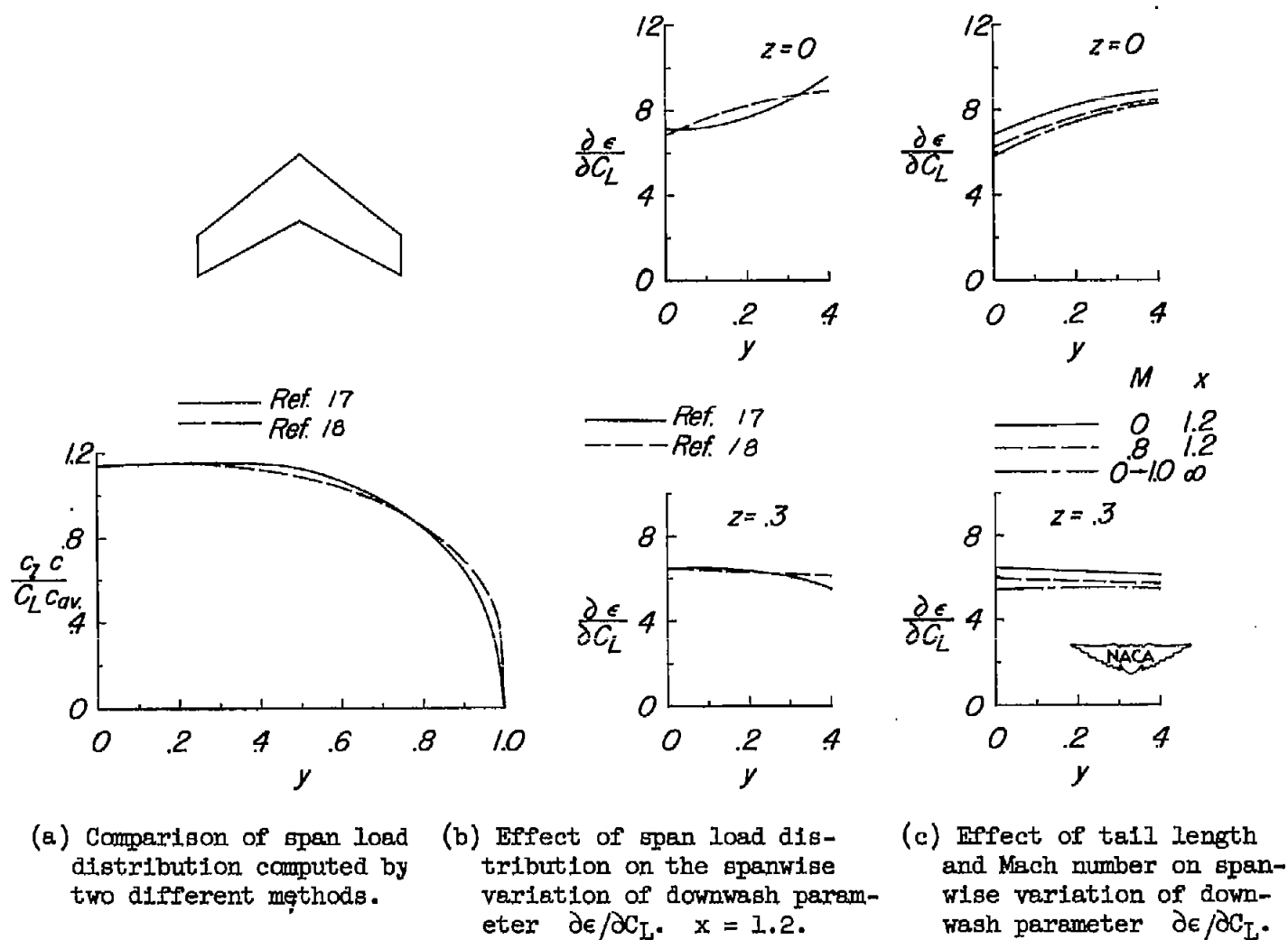
Figure 3.- Theoretical span load distribution and spanwise downwash characteristics at subsonic speeds. Wing 3; $\Lambda_{c/4} = 35°$; $A = 4$; $\lambda = 0.6$.
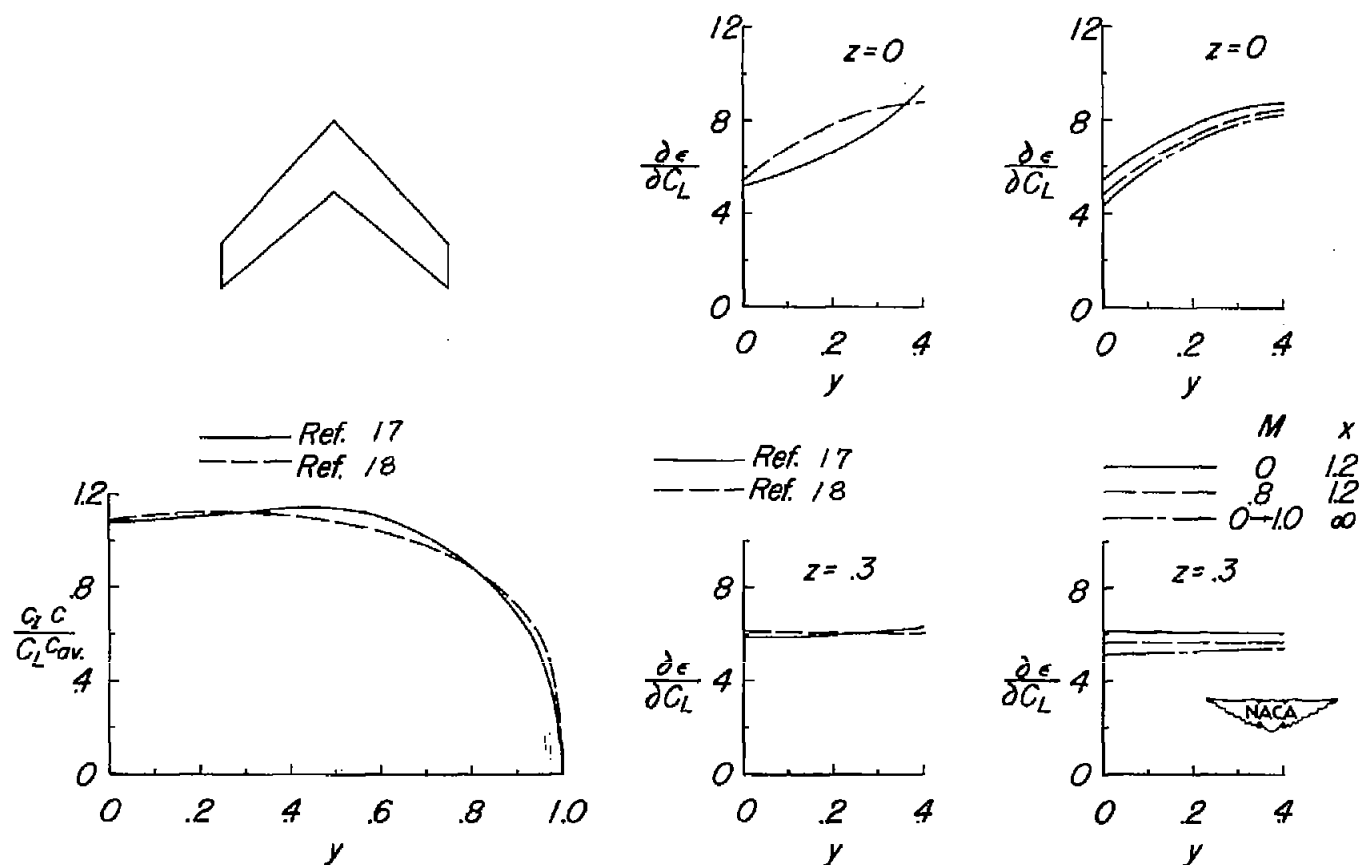
(a) Comparison of span load distribution computed by two different methods.

(b) Effect of span load distribution on the spanwise variation of downwash parameter $\partial\epsilon/\partial C_L$. $x = 1.2$.

(c) Effect of tail length and Mach number on spanwise variation of downwash parameter $\partial\epsilon/\partial C_L$.

Figure 4.- Theoretical span load distribution and spanwise downwash characteristics at subsonic speeds. Wing 4; $\Lambda_{c/4} = 45°$; $A = 4$; $\lambda = 0.6$.
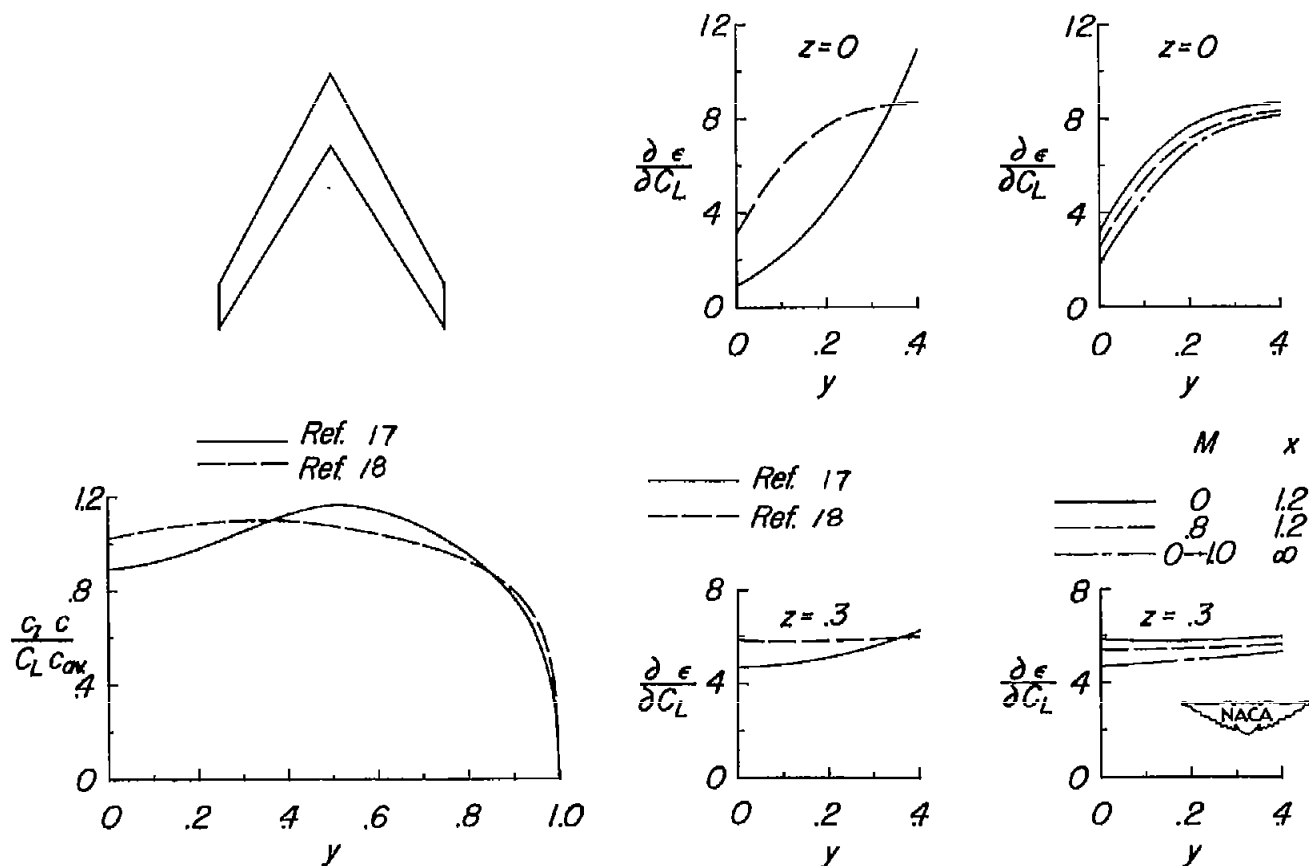
(a) Comparison of span load distribution computed by two different methods.

(b) Effect of span load distribution on the spanwise variation of downwash parameter $\partial\epsilon/\partial C_L$. x = 1.2.

(c) Effect of tail length and Mach number on spanwise variation of downwash parameter $\partial\epsilon/\partial C_L$.

Figure 5.- Theoretical span load distribution and spanwise downwash characteristics at subsonic speeds. Wing 5; $\Lambda_{c/4}$ = 60°; A = 4; λ = 0.6.

(a) Comparison of span load distribution computed by two different methods.

(b) Effect of span load distribution on the spanwise variation of downwash parameter $\partial\epsilon/\partial C_L$. $x = 1.2$.

(c) Effect of tail length and Mach number on spanwise variation of downwash parameter $\partial\epsilon/\partial C_L$.
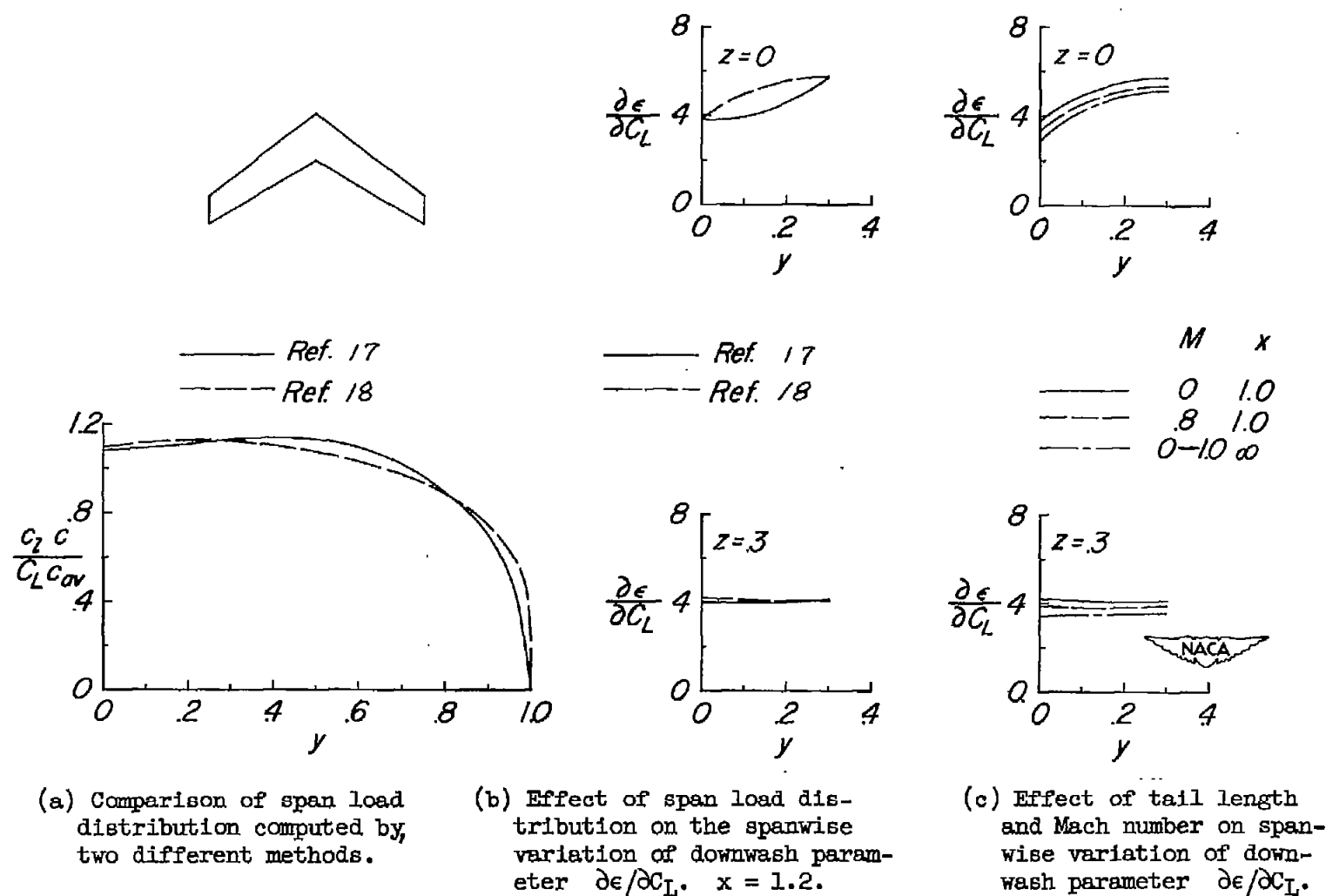
Figure 6.- Theoretical span load distribution and spanwise downwash characteristics at subsonic speeds. Wing 6; $\Lambda_{c/4} = 35°$; $A = 6$; $\lambda = 0.6$.

──────── Ref. 17
── ── ── Ref. 18

──────── Ref. 17
── ── ── Ref. 18

	M	x
────────	0	1.0
── ── ──	.8	1.0
──── ────	0→1.0	∞

(a) Comparison of span load distribution computed by two different methods.

(b) Effect of span load distribution on the spanwise variation of downwash parameter $\partial\epsilon/\partial C_L$. x = 1.2.

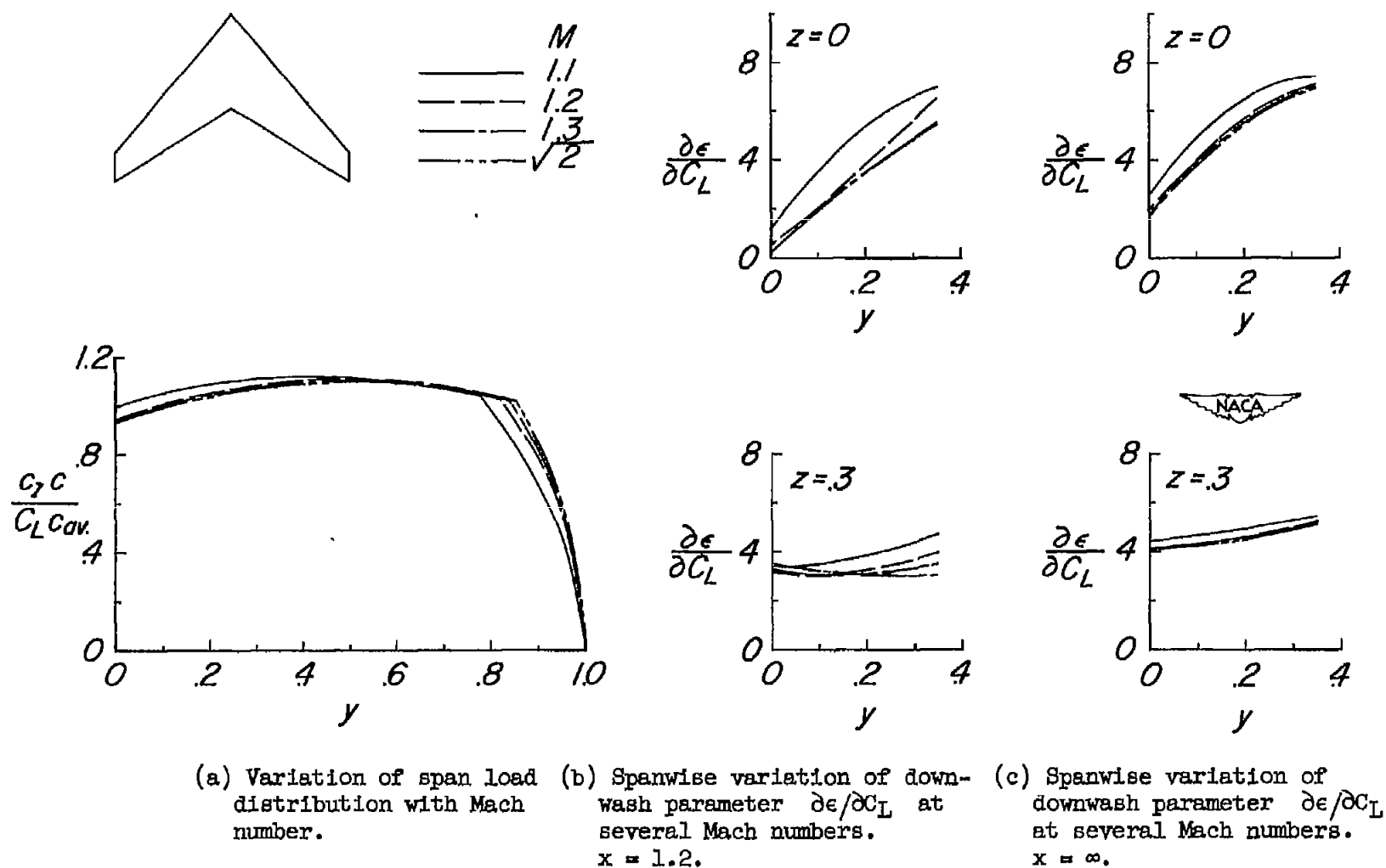(c) Effect of tail length and Mach number on spanwise variation of downwash parameter $\partial\epsilon/\partial C_L$.
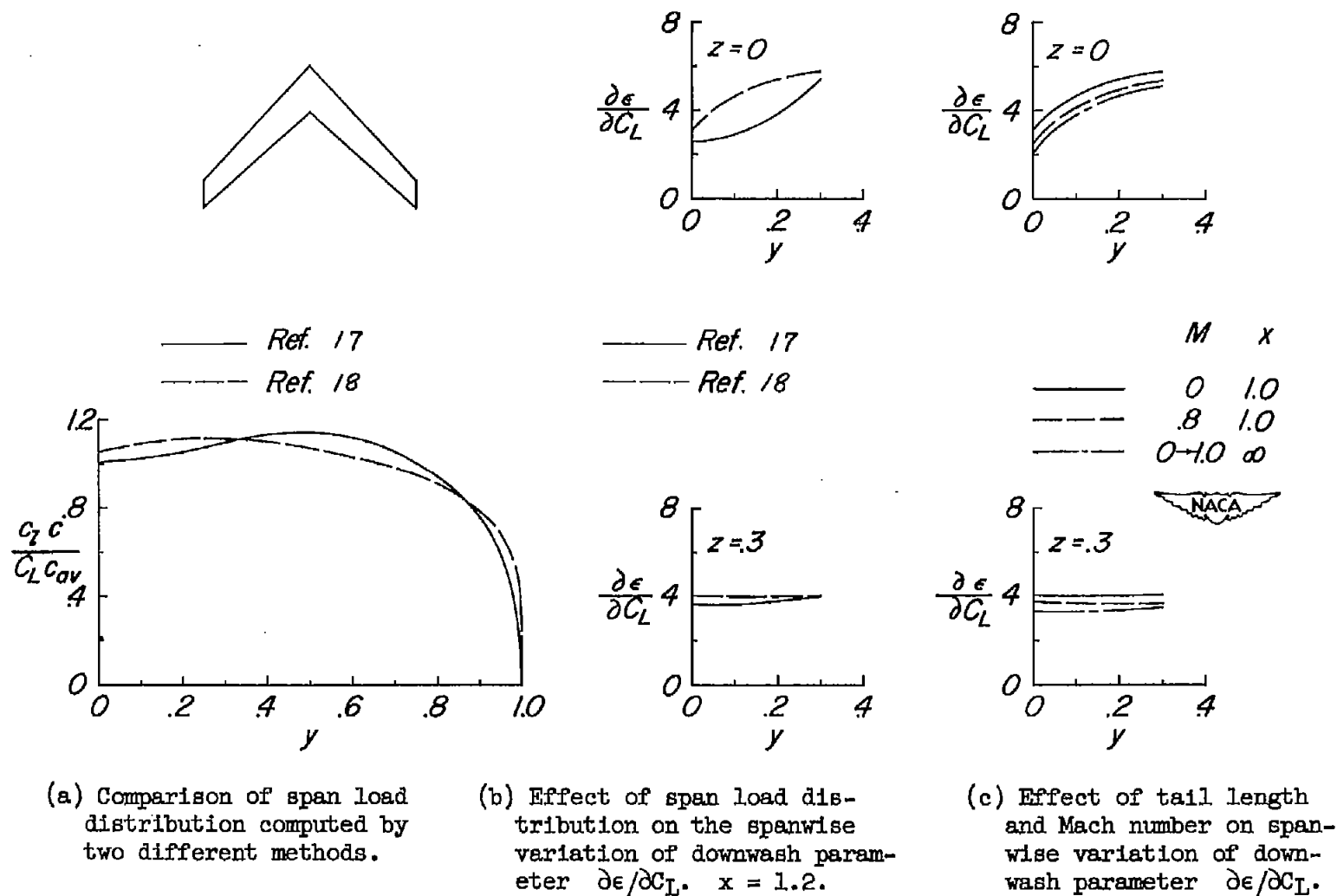
Figure 7.- Theoretical span load distribution and spanwise downwash characteristics at subsonic speeds. Wings 7 and 8; $\Lambda_{c/4} = 45°$; A = 6; $\lambda = 0.6$.
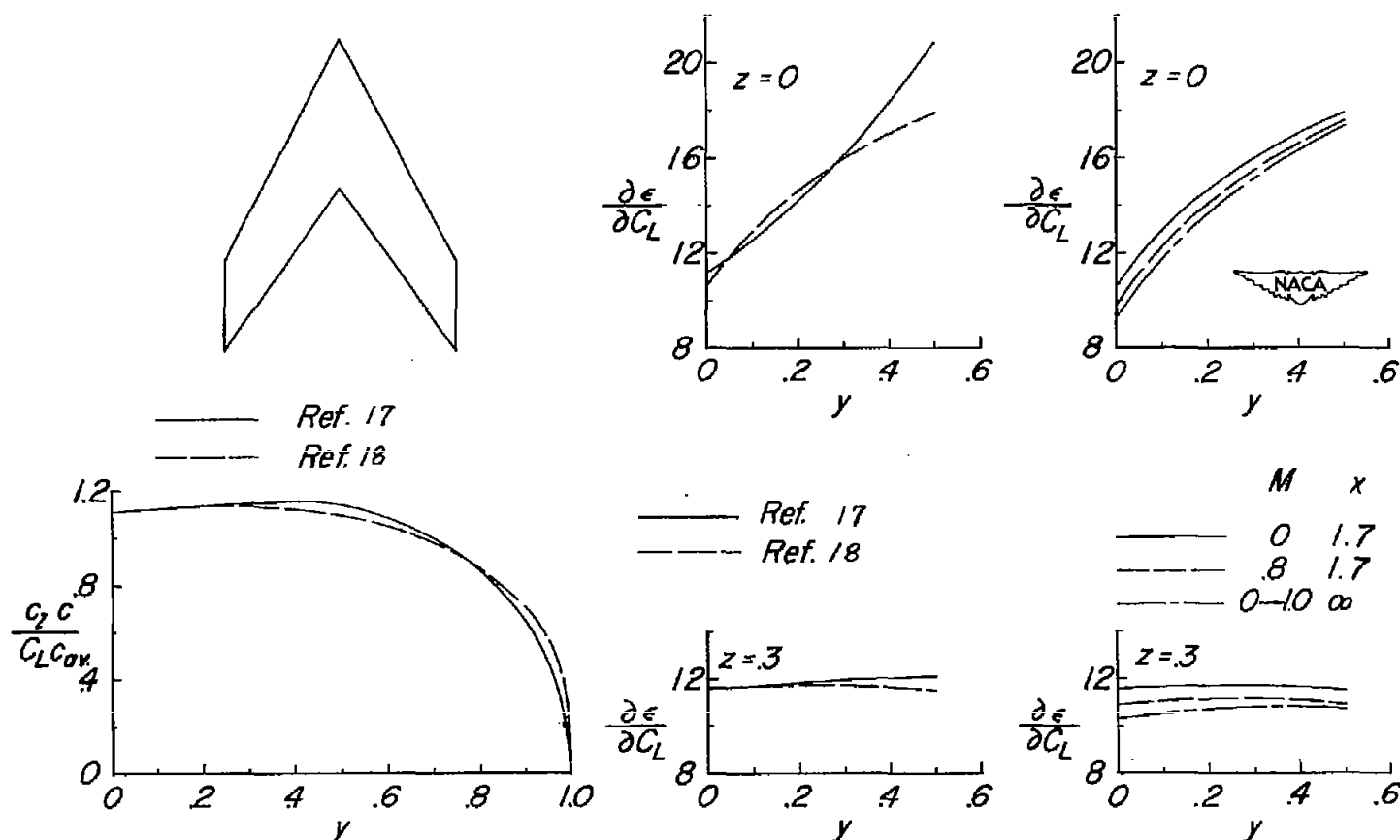
(a) Comparison of span load distribution computed by two different methods.

(b) Effect of span load distribution on the spanwise variation of downwash parameter $\partial\epsilon/\partial C_L$. $x = 1.2$.

(c) Effect of tail length and Mach number on spanwise variation of downwash parameter $\partial\epsilon/\partial C_L$.

Figure 8.- Theoretical span load distribution and spanwise downwash characteristics at subsonic speeds. Wing 9; $\Lambda_{c/4} = 60°$; $A = 2$; $\lambda = 0.6$.

(a) Comparison of span load distribution computed by two different methods.

(b) Effect of span load distribution on the spanwise variation of downwash parameter $\partial\epsilon/\partial C_L$. x = 1.2.

(c) Effect of tail length and Mach number on spanwise variation of downwash parameter $\partial\epsilon/\partial C_L$.
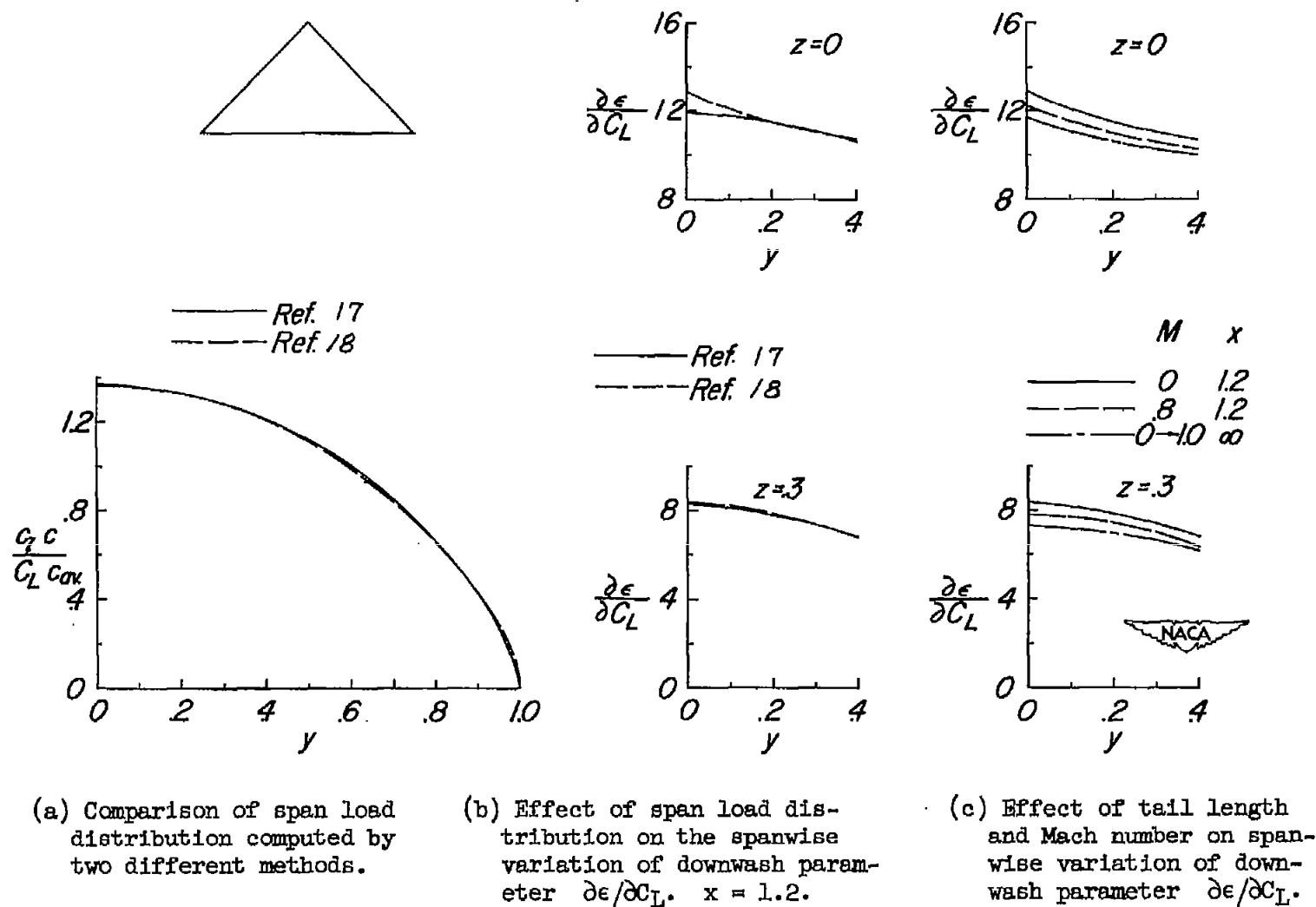
Figure 9.- Theoretical span load distribution and spanwise downwash characteristics at subsonic speeds. Wing 10; $\Lambda_{c/4}$ = 36.9°; A = 4; λ = 0.
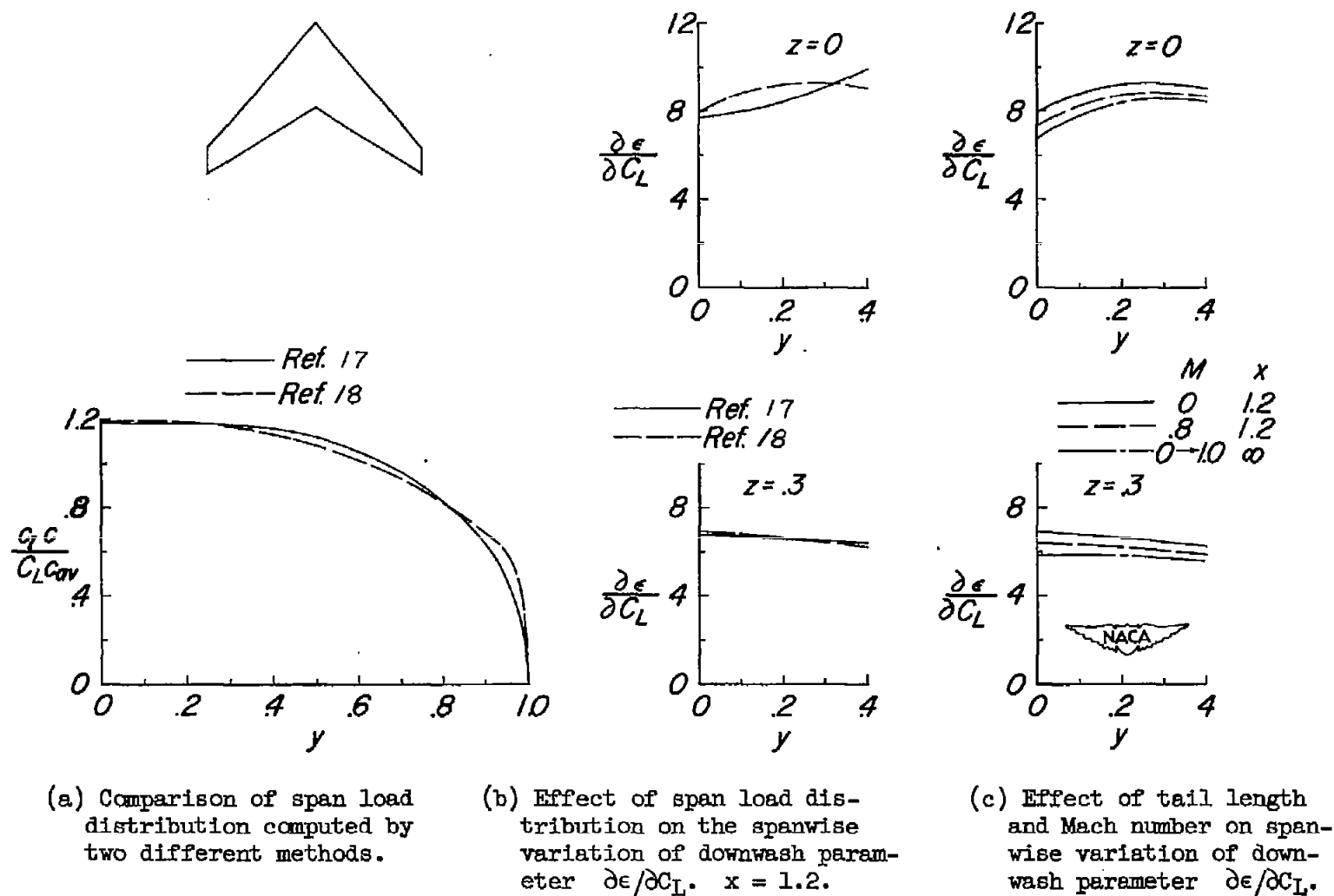
(a) Comparison of span load distribution computed by two different methods.

(b) Effect of span load distribution on the spanwise variation of downwash parameter $\partial\epsilon/\partial C_L$. $x = 1.2$.

(c) Effect of tail length and Mach number on spanwise variation of downwash parameter $\partial\epsilon/\partial C_L$.

Figure 10.- Theoretical span load distribution and spanwise downwash characteristics at subsonic speeds.   Wing 11; $\Lambda_{c/4} = 45^{\circ}$; $A = 4$; $\lambda = 0.3$.

(a) Variation of span load distribution with Mach number.

(b) Spanwise variation of downwash parameter $\partial\epsilon/\partial C_L$ at several Mach numbers. $x = 1.2$.

(c) Spanwise variation of downwash parameter $\partial\epsilon/\partial C_L$ at several Mach numbers. $x = \infty$.
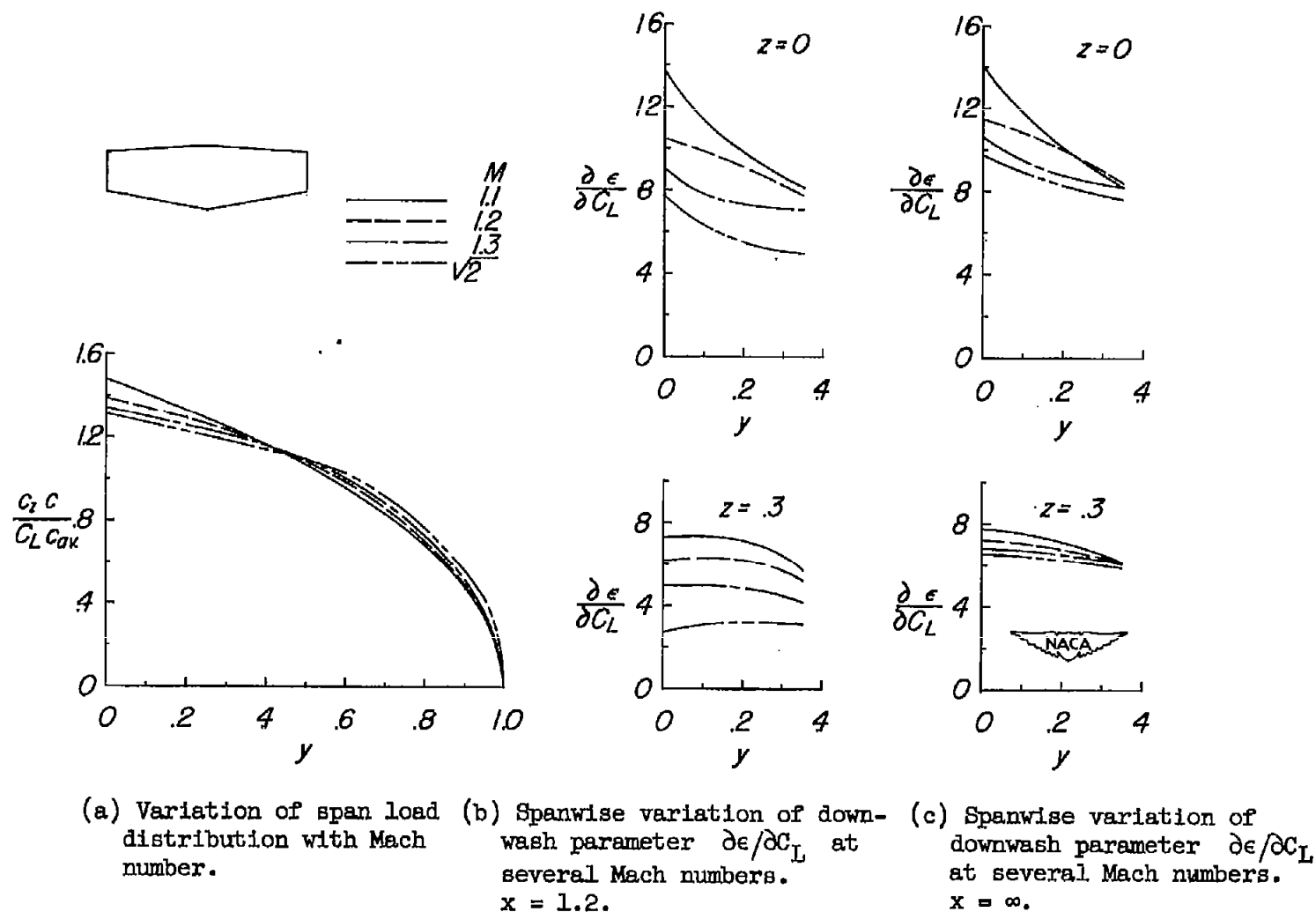
Figure 11.- Theoretical span load distribution and spanwise downwash characteristics at supersonic speeds. Wings 1 and 2; $\Lambda_{c/4} = 0°$; $A = 4$; $\lambda = 0.6$.

(a) Variation of span load distribution with Mach number.

(b) Spanwise variation of downwash parameter $\partial\epsilon/\partial C_L$ at several Mach numbers. $x = 1.2$.

(c) Spanwise variation of downwash parameter $\partial\epsilon/\partial C_L$ at several Mach numbers. $x = \infty$.

Figure 12.- Theoretical span load distribution and spanwise downwash characteristics at supersonic speeds. Wing 3; $\Lambda_{c/4} = 35°$; $A = 4$; $\lambda = 0.6$.

(a) Variation of span load distribution with Mach number.

(b) Spanwise variation of down-wash parameter $\partial\epsilon/\partial C_L$ at several Mach numbers. $x = 1.2$.

(c) Spanwise variation of downwash parameter $\partial\epsilon/\partial C_L$ at several Mach numbers. $x = \infty$.

Figure 13.— Theoretical span load distribution and spanwise downwash characteristics at supersonic speeds. Wing 4; $\Lambda_{c/4} = 45°$; $A = 4$; $\lambda = 0.6$.
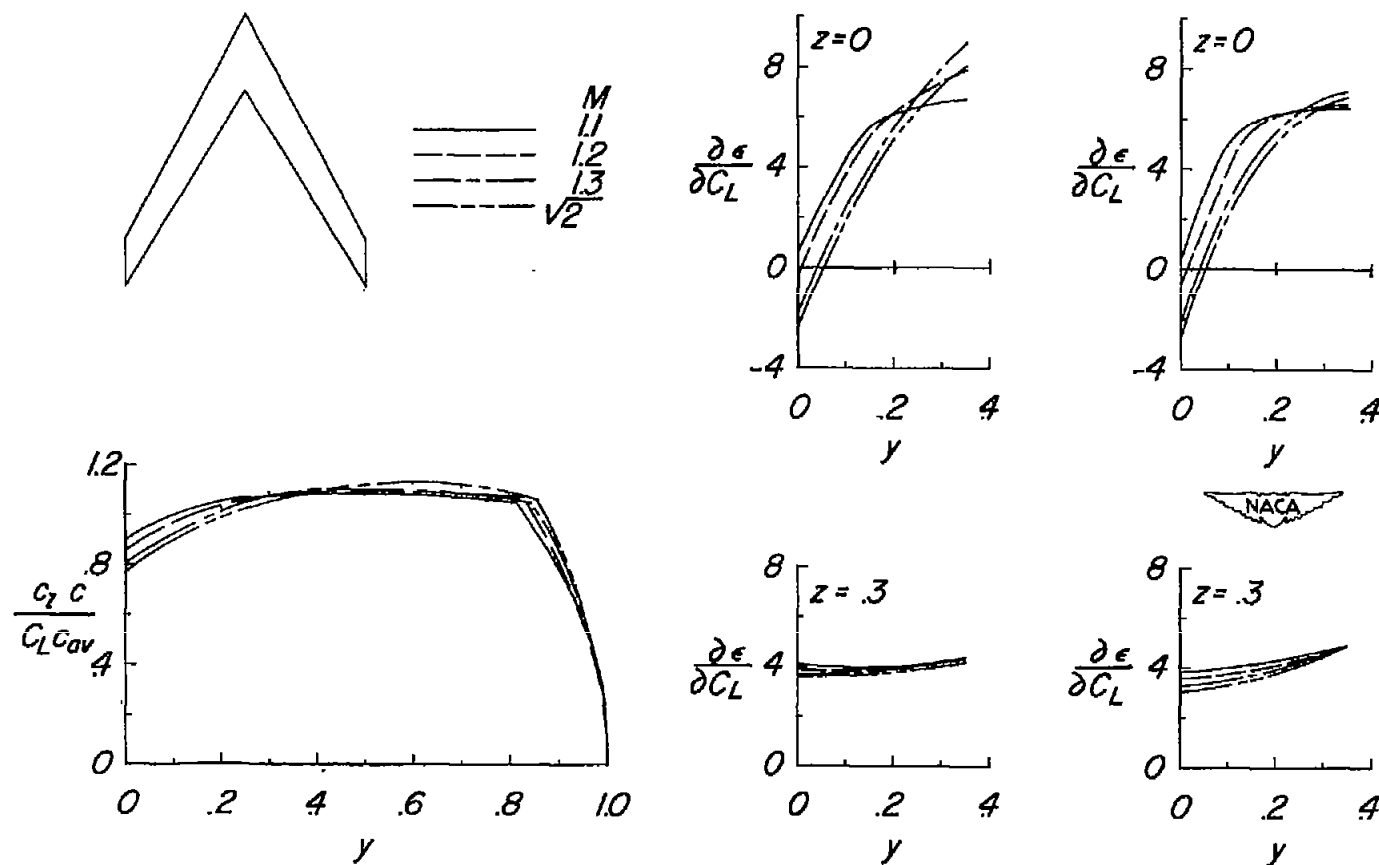
(a) Variation of span load distribution with Mach number.

(b) Spanwise variation of downwash parameter $\partial\epsilon/\partial C_L$ at several Mach numbers. $x = 1.2$.

(c) Spanwise variation of downwash parameter $\partial\epsilon/\partial C_L$ at several Mach numbers. $x = \infty$.

Figure 14.- Theoretical span load distribution and spanwise downwash characteristics at supersonic speeds. Wing 5; $\Lambda_{c/4} = 60°$; $A = 4$; $\lambda = 0.6$.

(a) Variation of span load distribution with Mach number.

(b) Spanwise variation of downwash parameter $\partial\epsilon/\partial C_L$ at several Mach numbers. $x = 1.2$.

(c) Spanwise variation of downwash parameter $\partial\epsilon/\partial C_L$ at several Mach numbers. $x = \infty$.
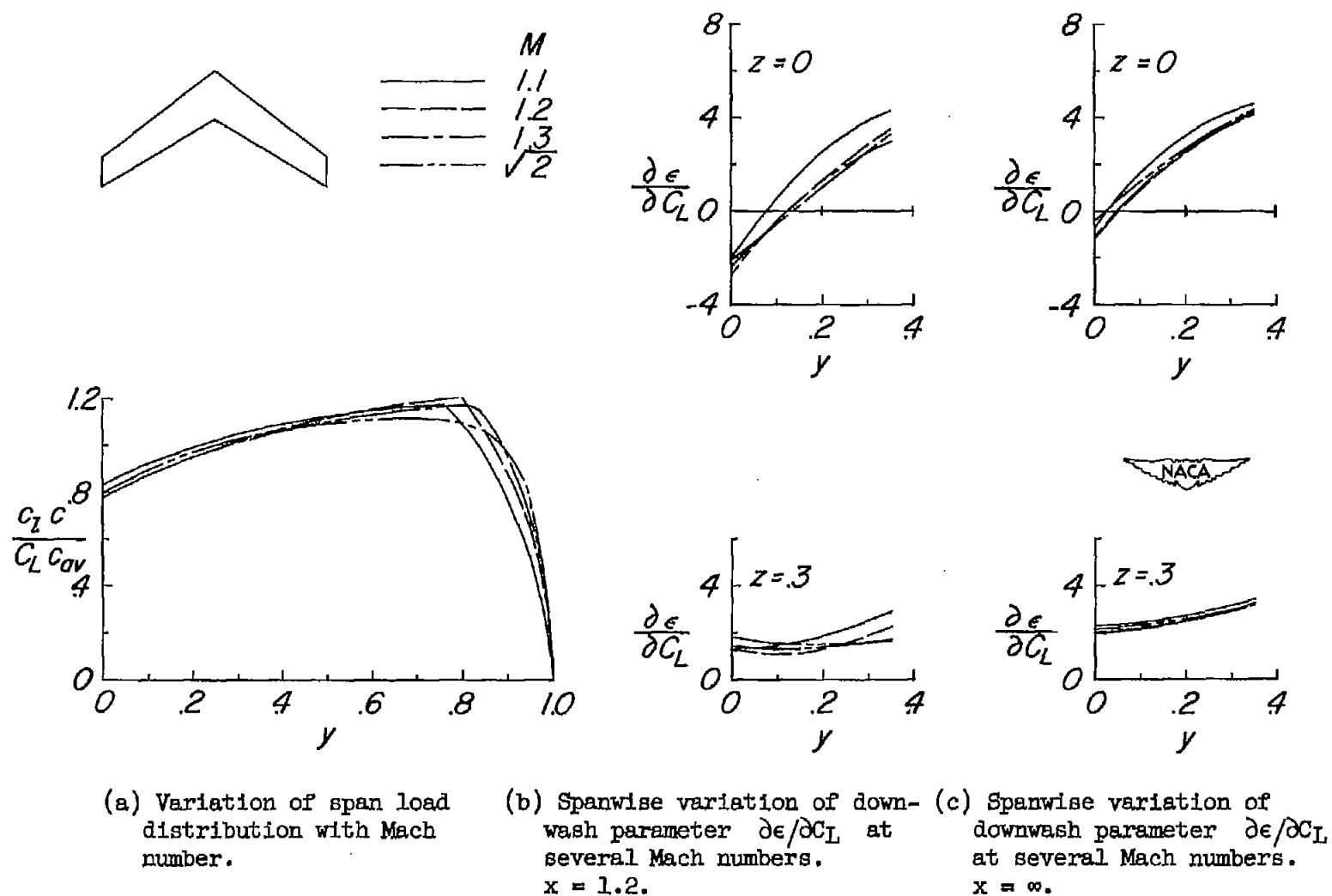
Figure 15.- Theoretical span load distribution and spanwise downwash characteristics at supersonic speeds. Wing 6; $\Lambda_{c/4} = 35°$; $A = 6$; $\lambda = 0.6$.

(a) Variation of span load distribution with Mach number.

(b) Spanwise variation of downwash parameter $\partial\epsilon/\partial C_L$ at several Mach numbers. $x = 1.2$.

(c) Spanwise variation of downwash parameter $\partial\epsilon/\partial C_L$ at several Mach numbers. $x = \infty$.
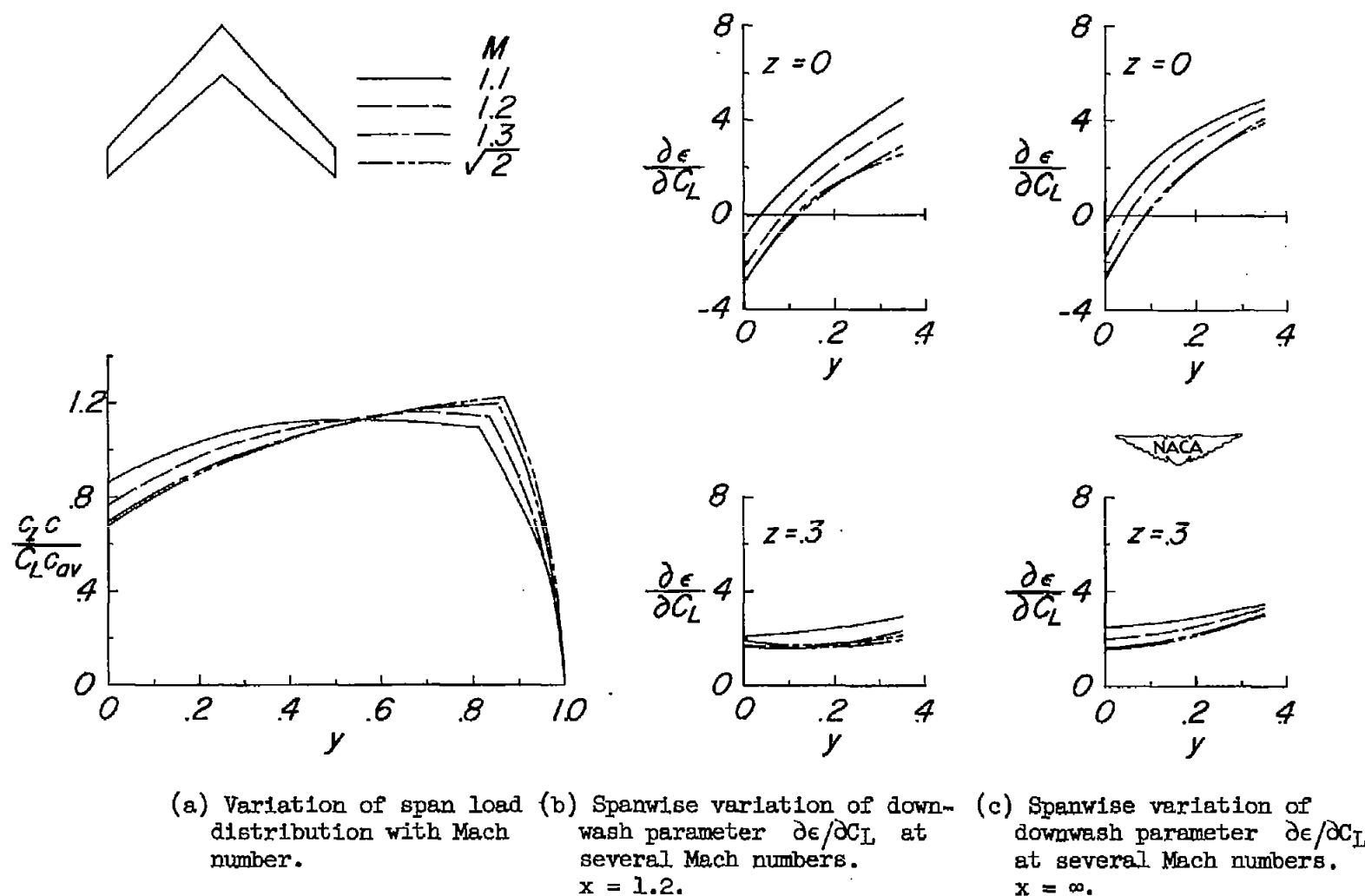
Figure 16.- Theoretical span load distribution and spanwise downwash characteristics at supersonic speeds. Wings 7 and 8; $\Lambda_{c/4} = 45°$; $A = 6$; $\lambda = 0.6$.
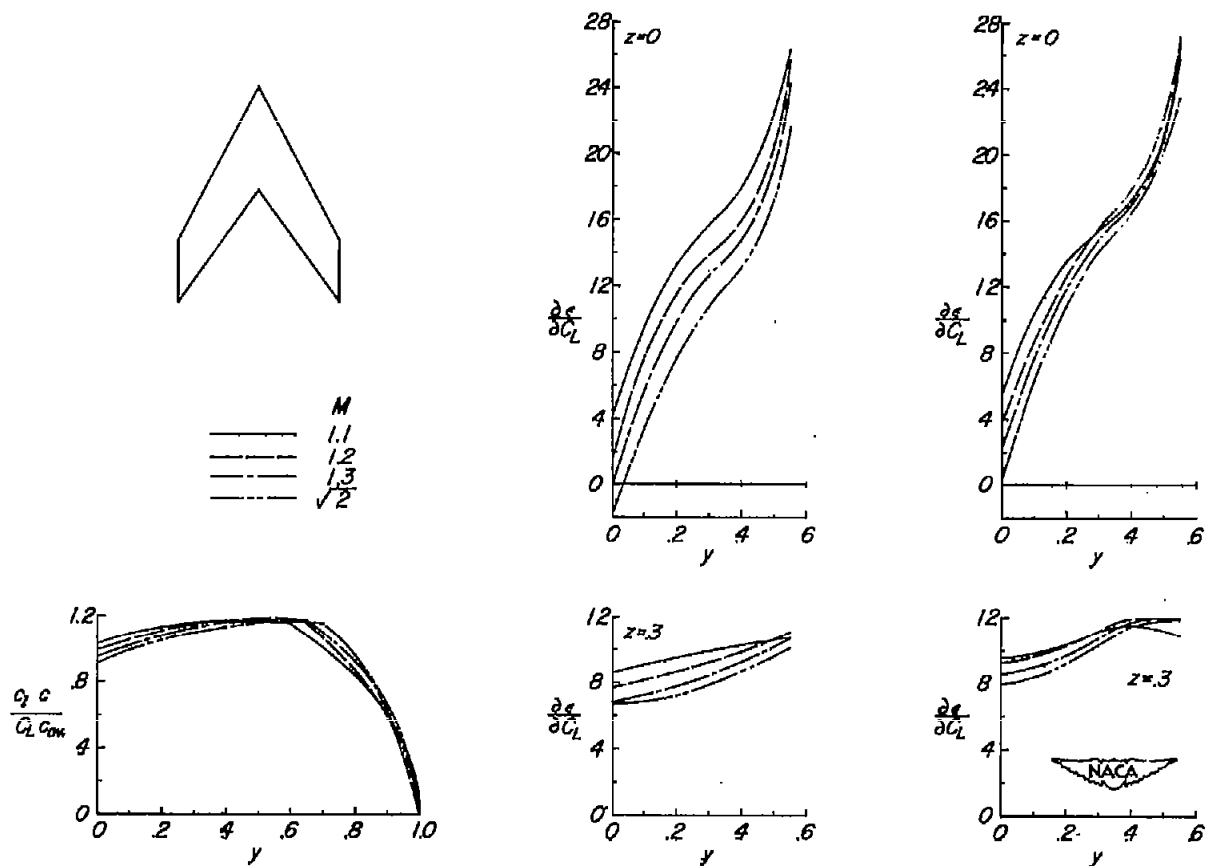
(a) Variation of span load distribution with Mach number.

(b) Spanwise variation of downwash parameter $\partial\epsilon/\partial C_L$ at several Mach numbers. $x = 1.2$.

(c) Spanwise variation of downwash parameter $\partial\epsilon/\partial C_L$ at several Mach numbers. $x = \infty$.

Figure 17.- Theoretical span load distribution and spanwise downwash characteristics at supersonic speeds. Wing 9; $\Lambda_{c/4} = 60°$; $A = 2$; $\lambda = 0.6$.
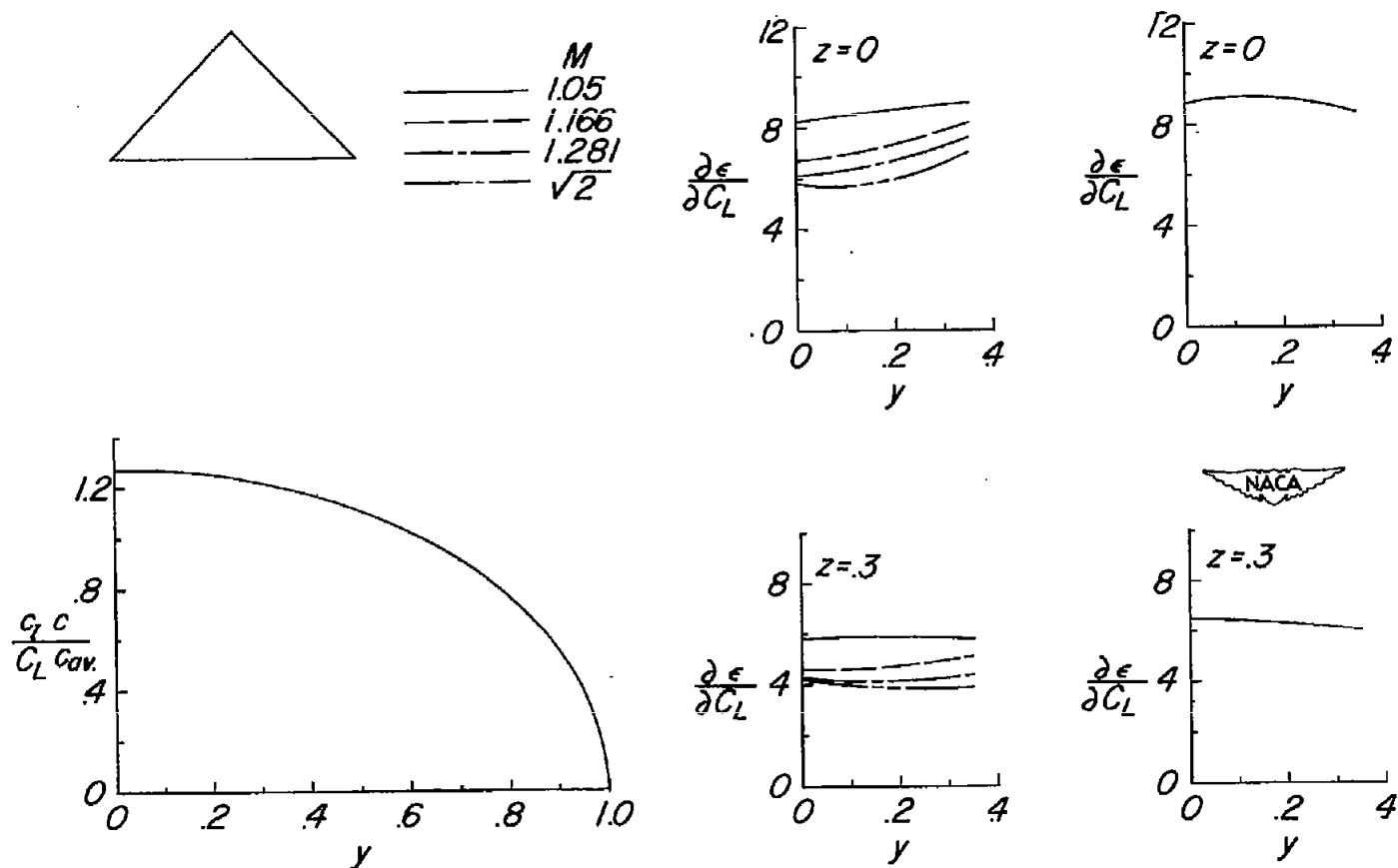
(a) Variation of span load distribution with Mach number.

(b) Spanwise variation of downwash parameter $\partial\epsilon/\partial C_L$ at several Mach numbers. $x = 1.2$.

(c) Spanwise variation of downwash parameter $\partial\epsilon/\partial C_L$ at several Mach numbers. $x = \infty$.

Figure 18.- Theoretical span load distribution and spanwise downwash characteristics at supersonic speeds. Wing 10; $\Lambda_{c/4} = 36.9^{\circ}$; $A = 4$; $\lambda = 0$.

(a) Variation of span load distribution with Mach number.

(b) Spanwise variation of downwash parameter $\partial\epsilon/\partial C_L$ at several Mach numbers. $x = 1.2$.

(c) Spanwise variation of downwash parameter $\partial\epsilon/\partial C_L$ at several Mach numbers. $x = \infty$.

Figure 19.- Theoretical span load distribution and spanwise downwash characteristics at supersonic speeds. Wing 11; $\Lambda_{c/4} = 45°$; $A = 4$; $\lambda = 0.3$.
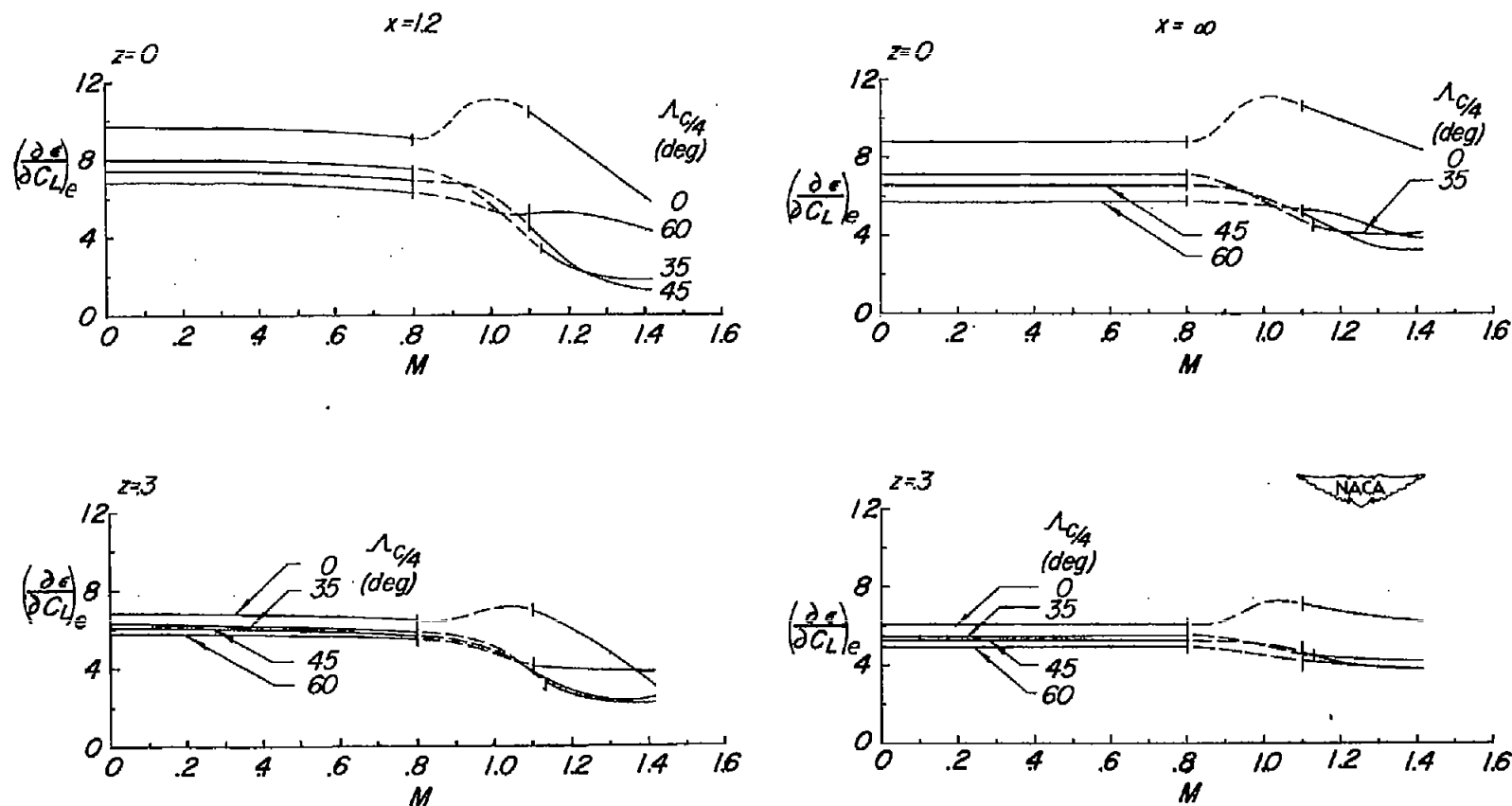
Figure 20.- Effect of sweep angle on variation of downwash parameter $\left(\partial\epsilon/\partial C_L\right)_e$ with Mach number. $A = 4$; $\lambda = 0.6$.
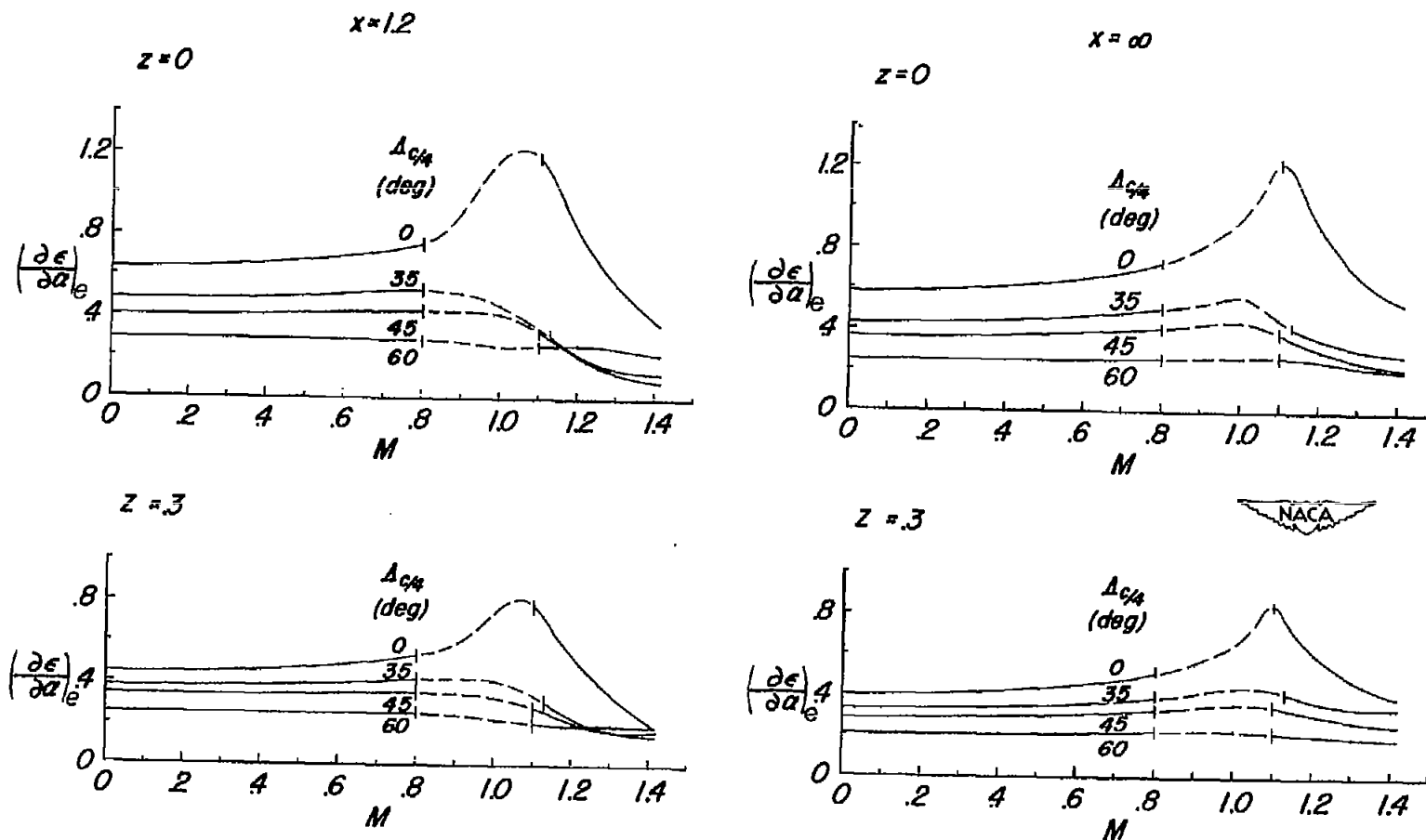
Figure 21.- Effect of sweep angle on variation of downwash parameter $(\partial\epsilon/\partial\alpha)_e$ with Mach number. $A = 4$; $\lambda = 0.6$.
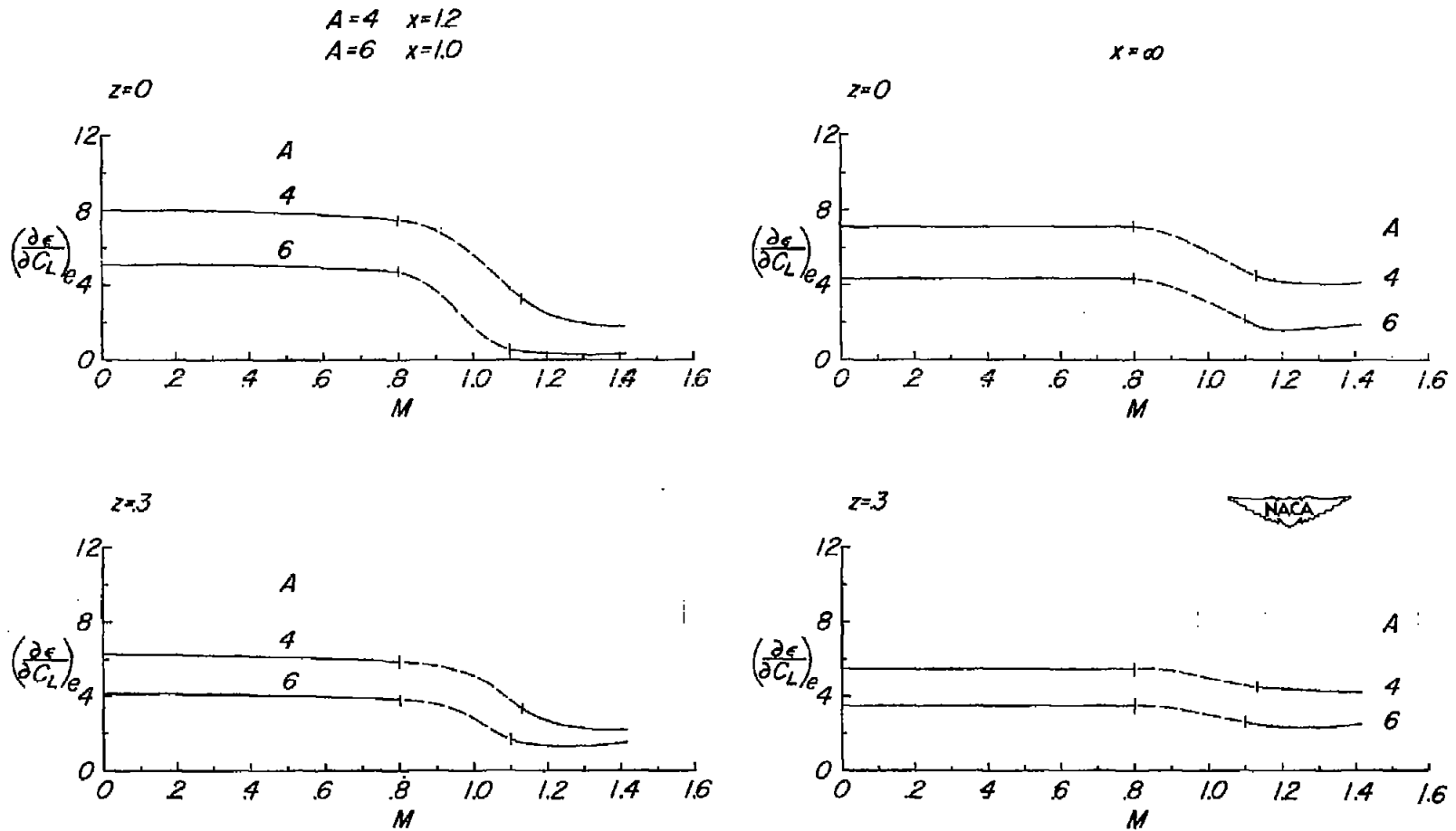
Figure 22.- Effect of aspect ratio on variation of downwash parameter $\left(\partial\epsilon/\partial C_L\right)_e$ with Mach number. $\Lambda_{c/4} = 35°$; $\lambda = 0.6$.
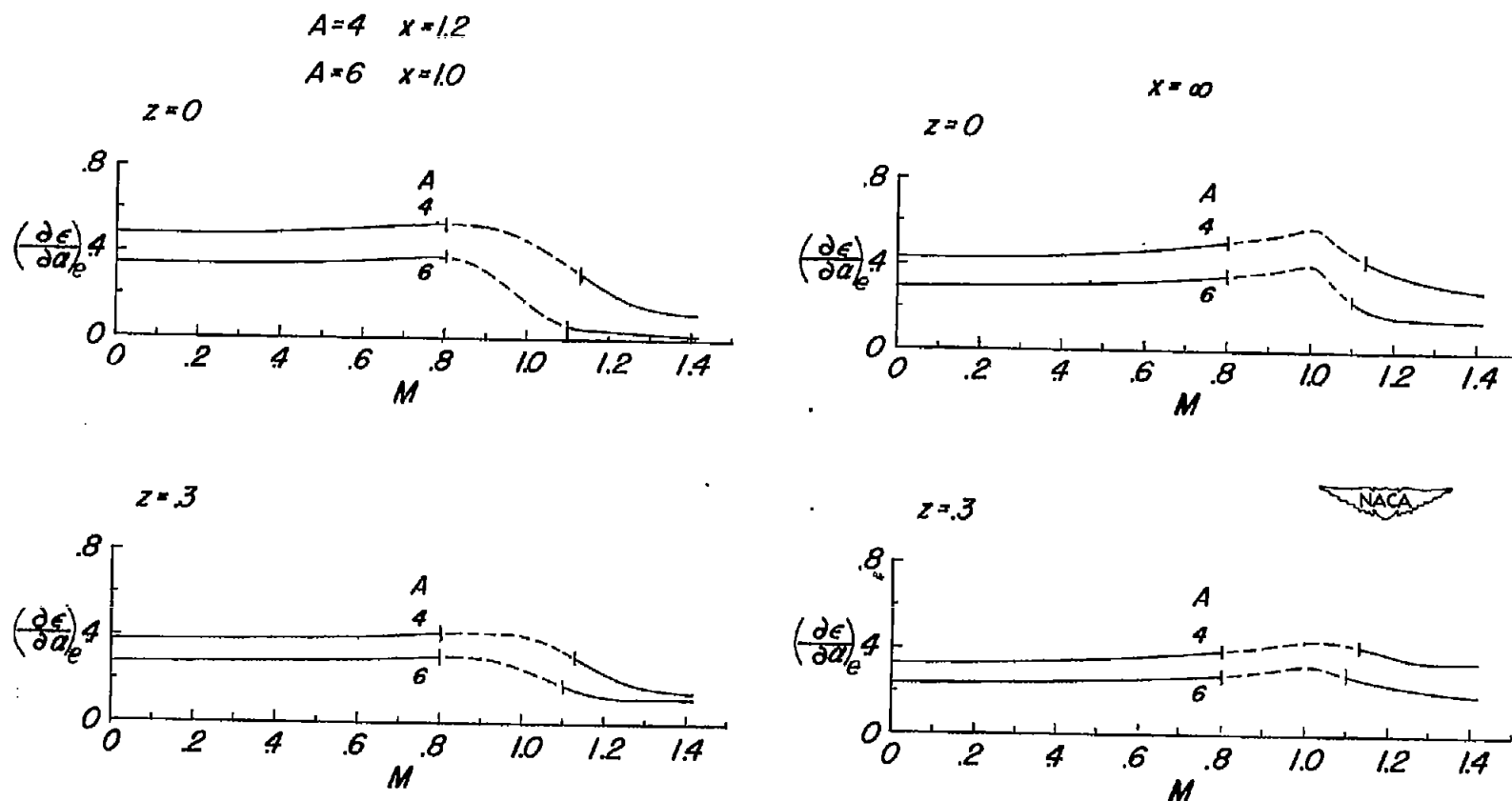
Figure 23.- Effect of aspect ratio on variation of downwash parameter $(\partial\epsilon/\partial\alpha)_e$ with Mach number. $\Lambda_{c/4} = 35°$; $\lambda = 0.6$.

$A=4 \quad \chi=1.2$
$A=6 \quad \chi=1.0$

$\chi = \infty$

$z=0$

$z=0$

$z=.3$

$z=.3$
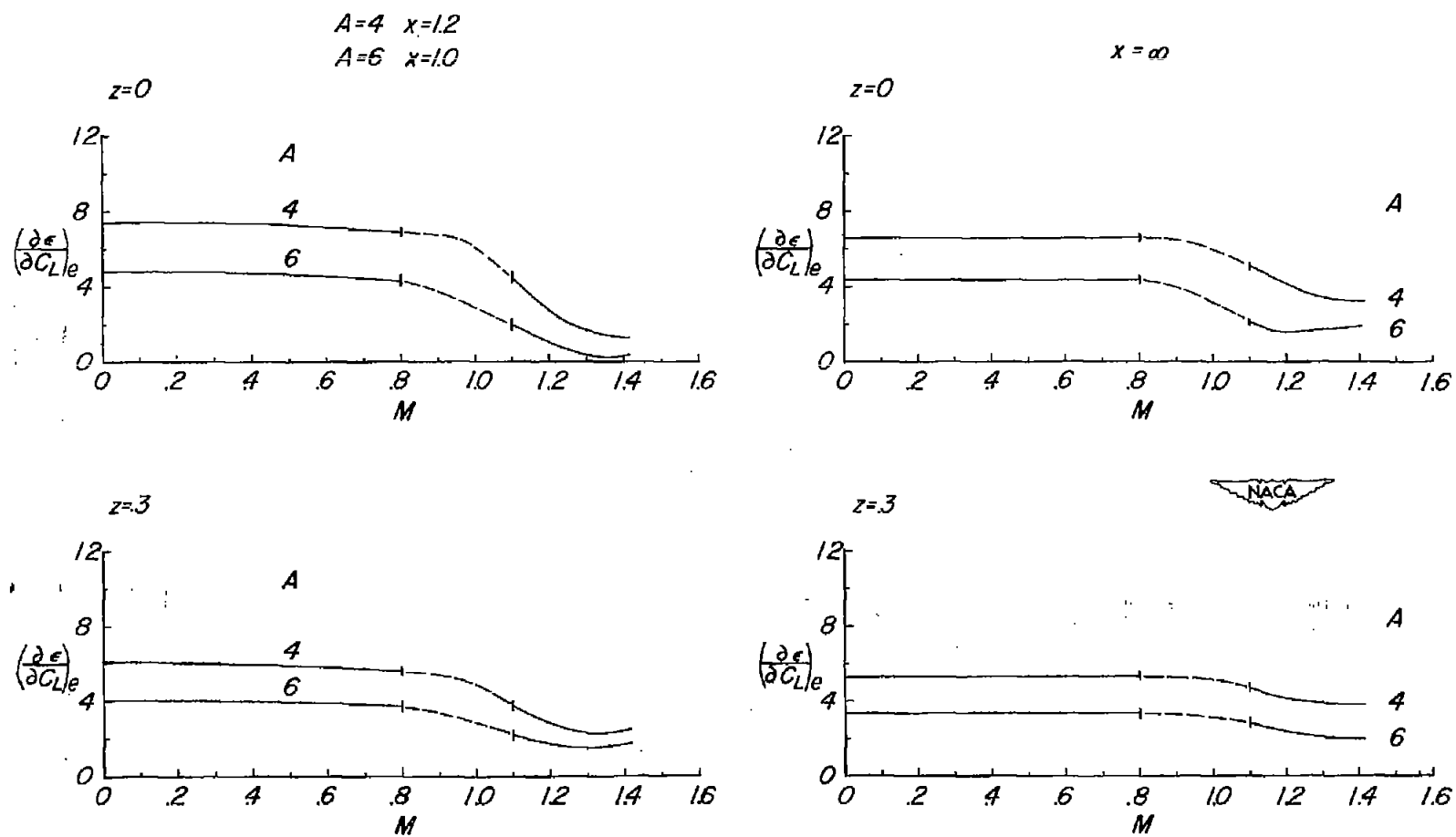
Figure 24.- Effect of aspect ratio on variation of downwash parameter $\left(\partial\epsilon/\partial C_L\right)_e$ with Mach number. $\Lambda_{c/4} = 45°$; $\lambda = 0.6$.
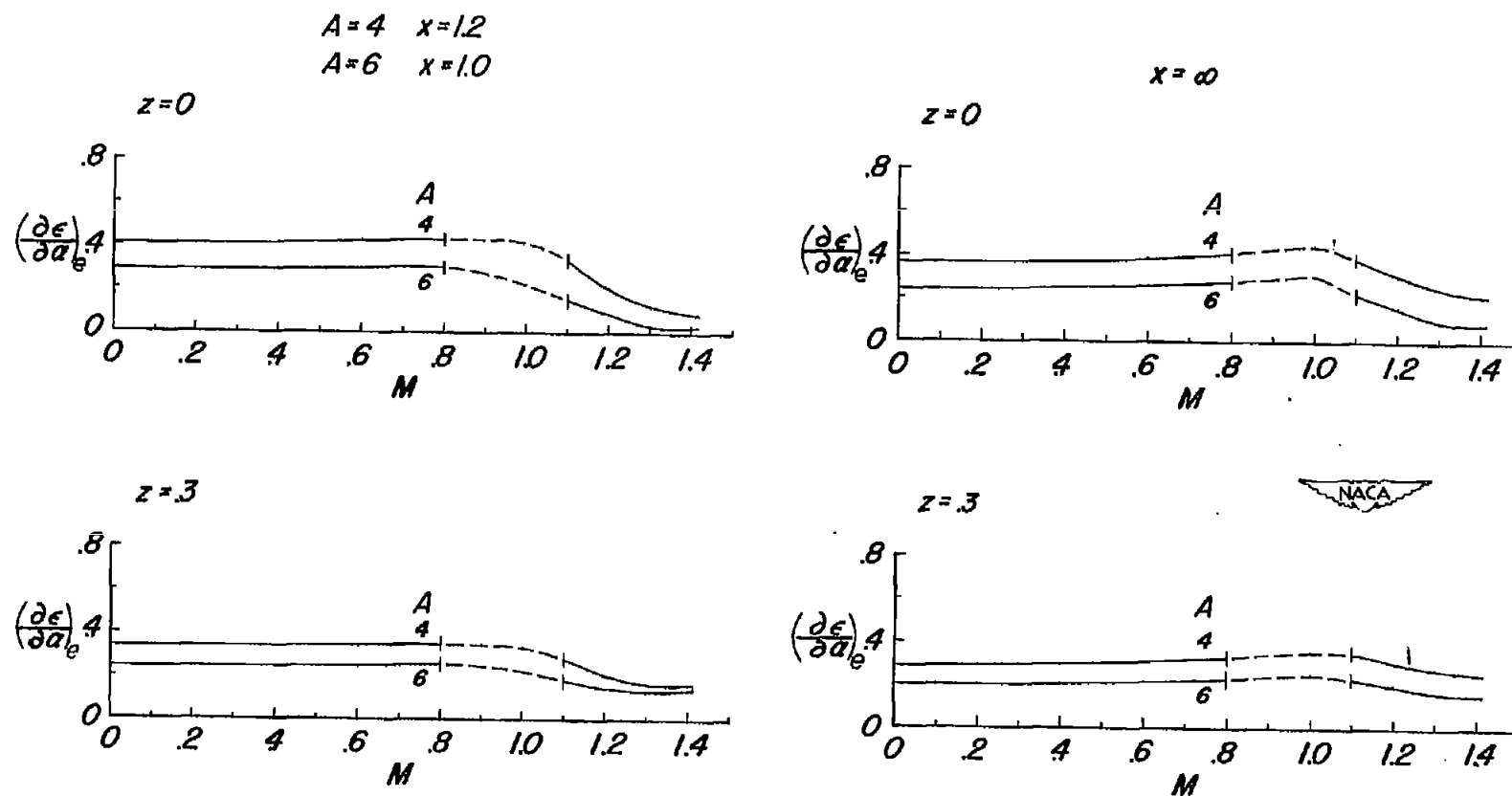
Figure 25.- Effect of aspect ratio on variation of downwash parameter $(\partial\epsilon/\partial\alpha)_e$ with Mach number. $\Lambda_{c/4} = 45°$; $\lambda = 0.6$.

A=2 x=1.7
A=4 x1.2

X = ∞

z=0

z=0

$$\left(\frac{\partial \epsilon}{\partial C_L}\right)_e$$

A

2

4

$$\left(\frac{\partial \epsilon}{\partial C_L}\right)_e$$

A

2

4

z=.3

z=.3

$$\left(\frac{\partial \epsilon}{\partial C_L}\right)_e$$

A

2

4

$$\left(\frac{\partial \epsilon}{\partial C_L}\right)_e$$

A

2

4
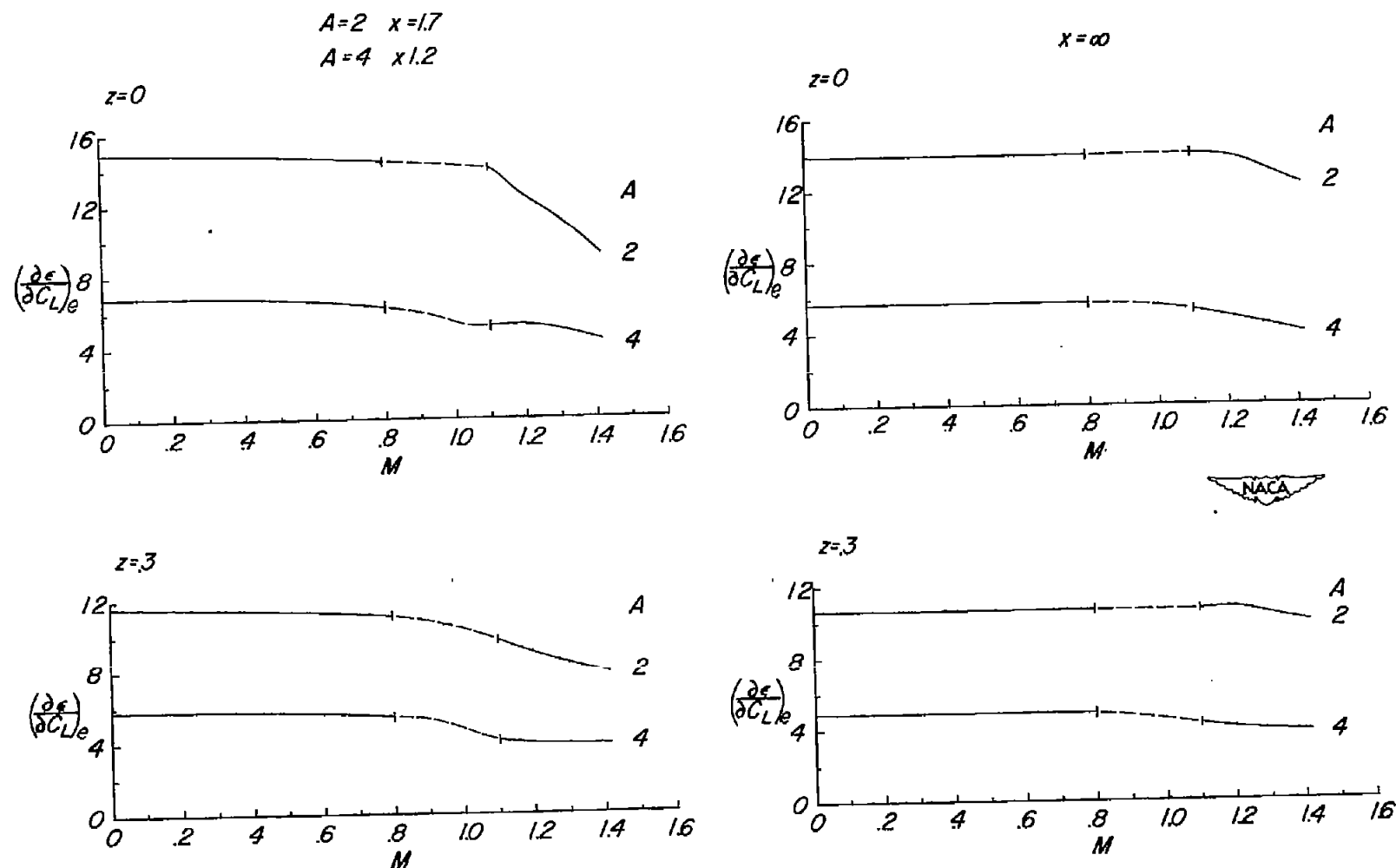
Figure 26.- Effect of aspect ratio on variation of downwash parameter $\left(\partial\epsilon/\partial C_L\right)_e$ with Mach number. $\Lambda_{c/4} = 60°$; $\lambda = 0.6$.
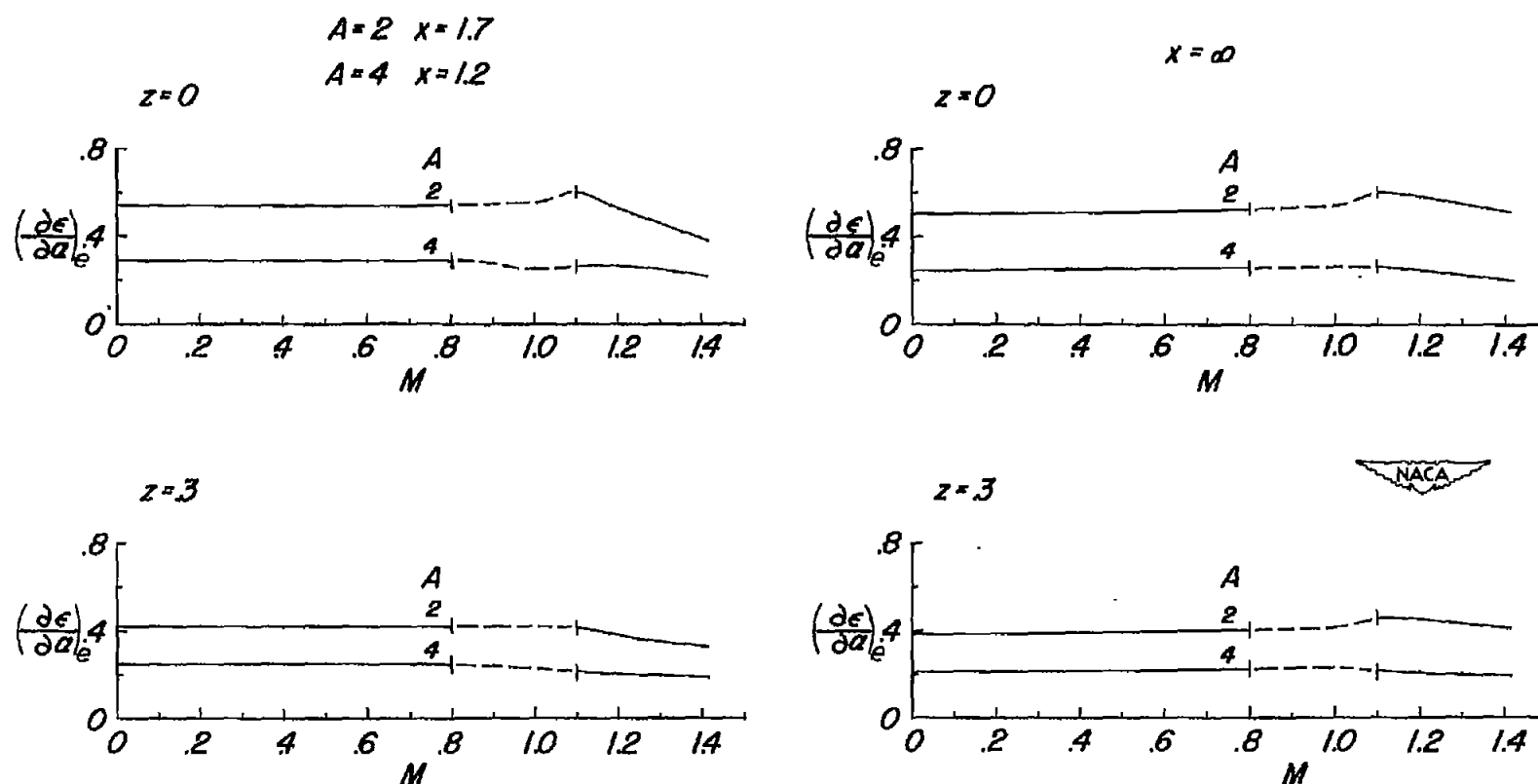
Figure 27.- Effect of aspect ratio on variation of downwash parameter $(\partial\epsilon/\partial\alpha)_e$ with Mach number. $\Lambda_{c/4} = 60^\circ$; $\lambda = 0.6$.
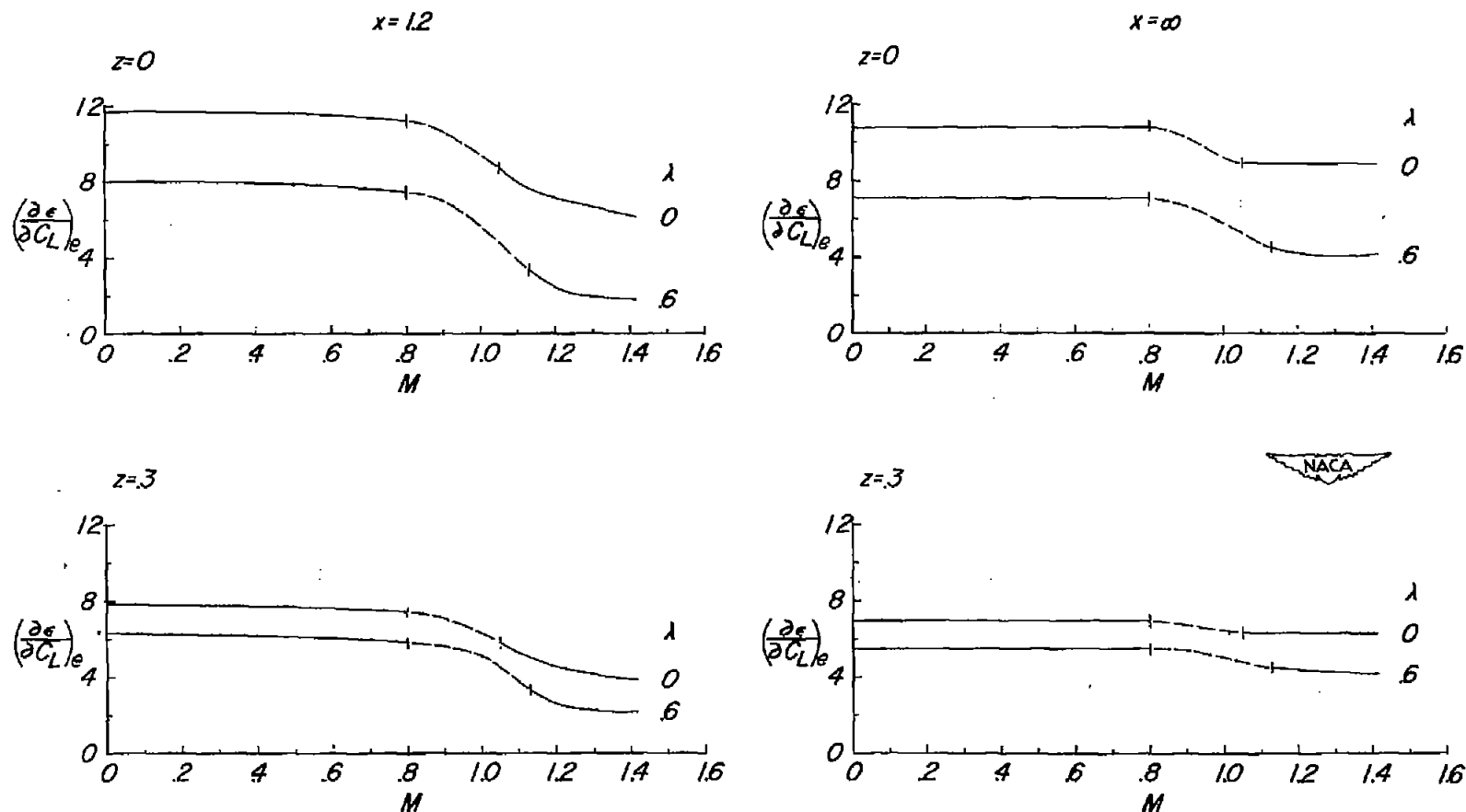
Figure 28.- Effect of taper ratio on variation of downwash parameter $\left(\partial \epsilon / \partial C_L\right)_e$ with Mach number. $\Lambda_{c/4} = 35^o$; $A = 4$.
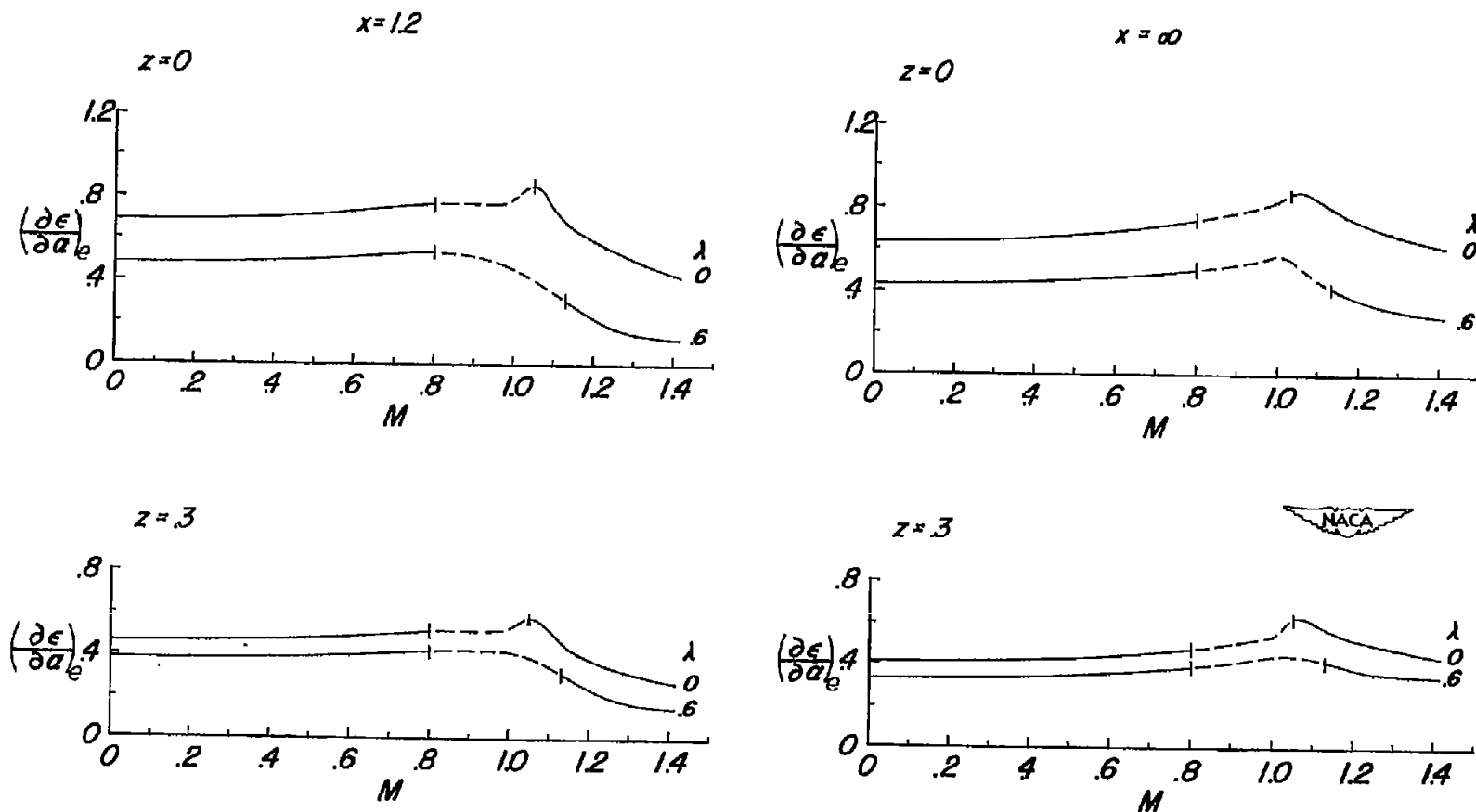
Figure 29.- Effect of taper ratio on variation of downwash parameter $(\partial\epsilon/\partial\alpha)_e$ with Mach number. $\Lambda_{c/4} = 35°$; A = 4.
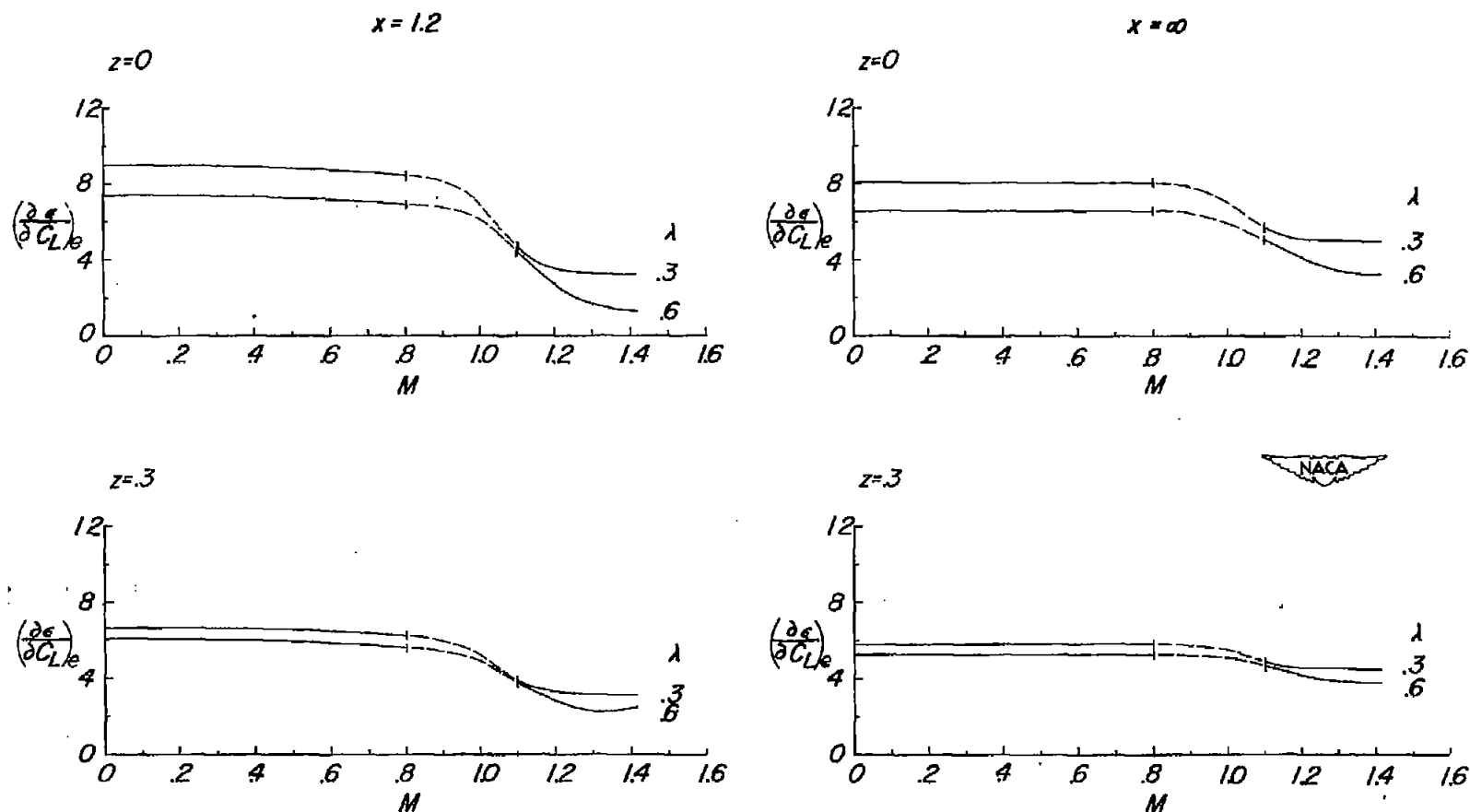
Figure 30.- Effect of taper ratio on variation of downwash parameter $\left(\partial\epsilon/\partial C_L\right)_e$ with Mach number. $\Lambda_{c/4} = 45°$; $A = 4$.
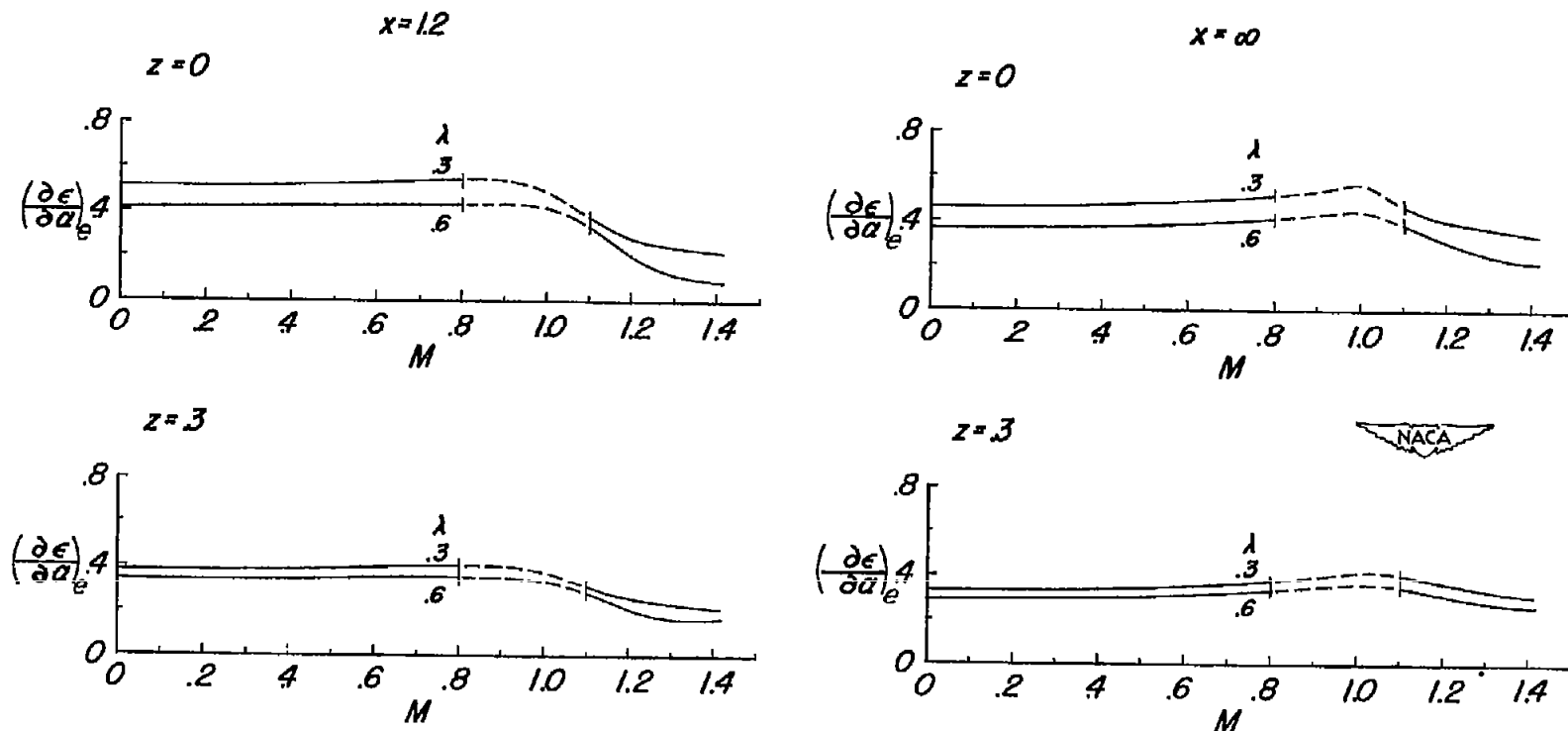
Figure 31.- Effect of taper ratio on variation of downwash parameter $(\partial\epsilon/\partial\alpha)_e$ with Mach number. $\Lambda_{c/4} = 45^\circ$; $A = 4$.

Wing alone
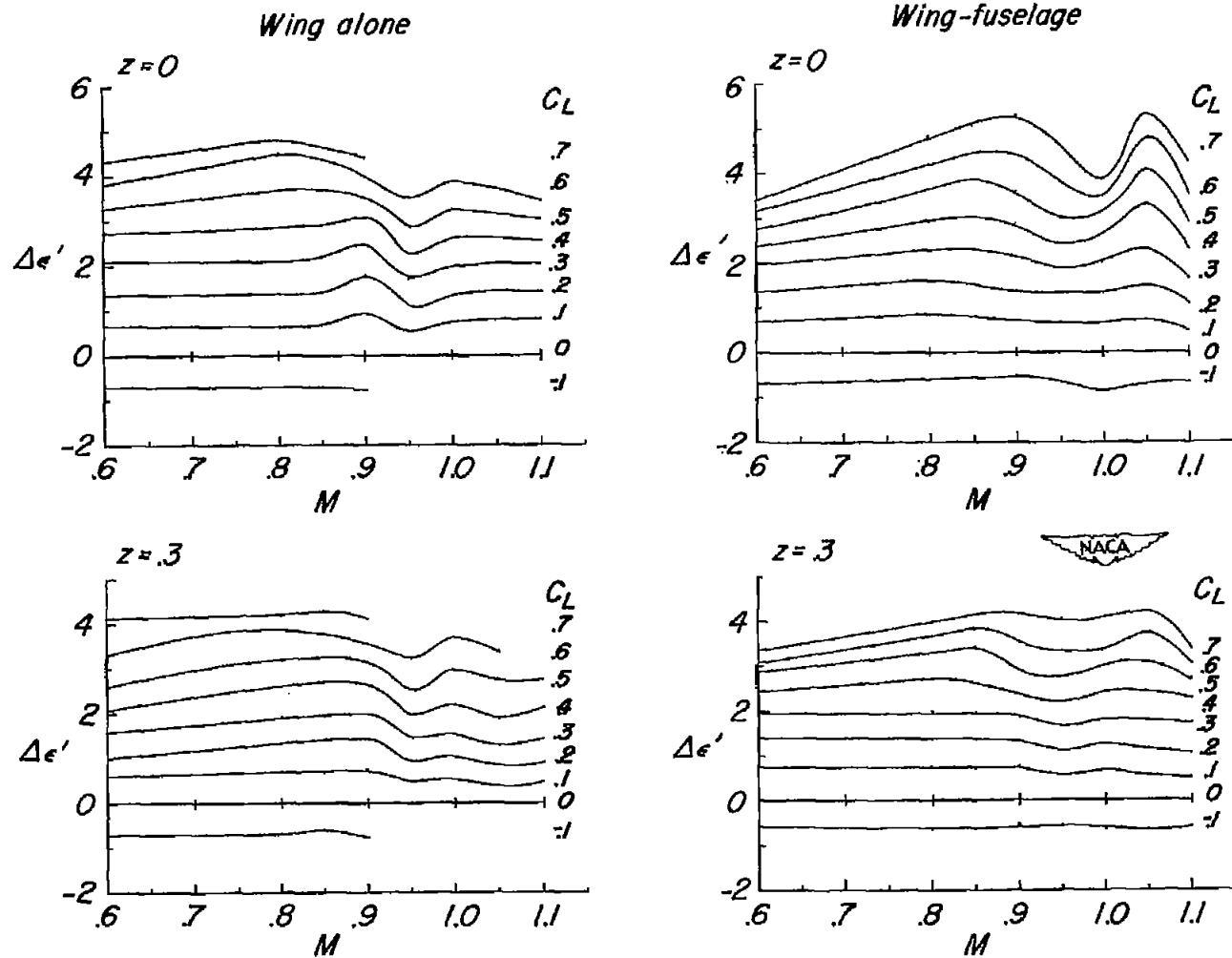
Wing-fuselage

Figure 32.- Variation of experimental floating angle with Mach number for wing-alone and wing-fuselage configurations at two tail heights. Wing 1; $\Lambda_{c/4} = 0°$; $A = 4$; $\lambda = 0.6$; $\frac{t}{c} = 0.06$.

Wing alone
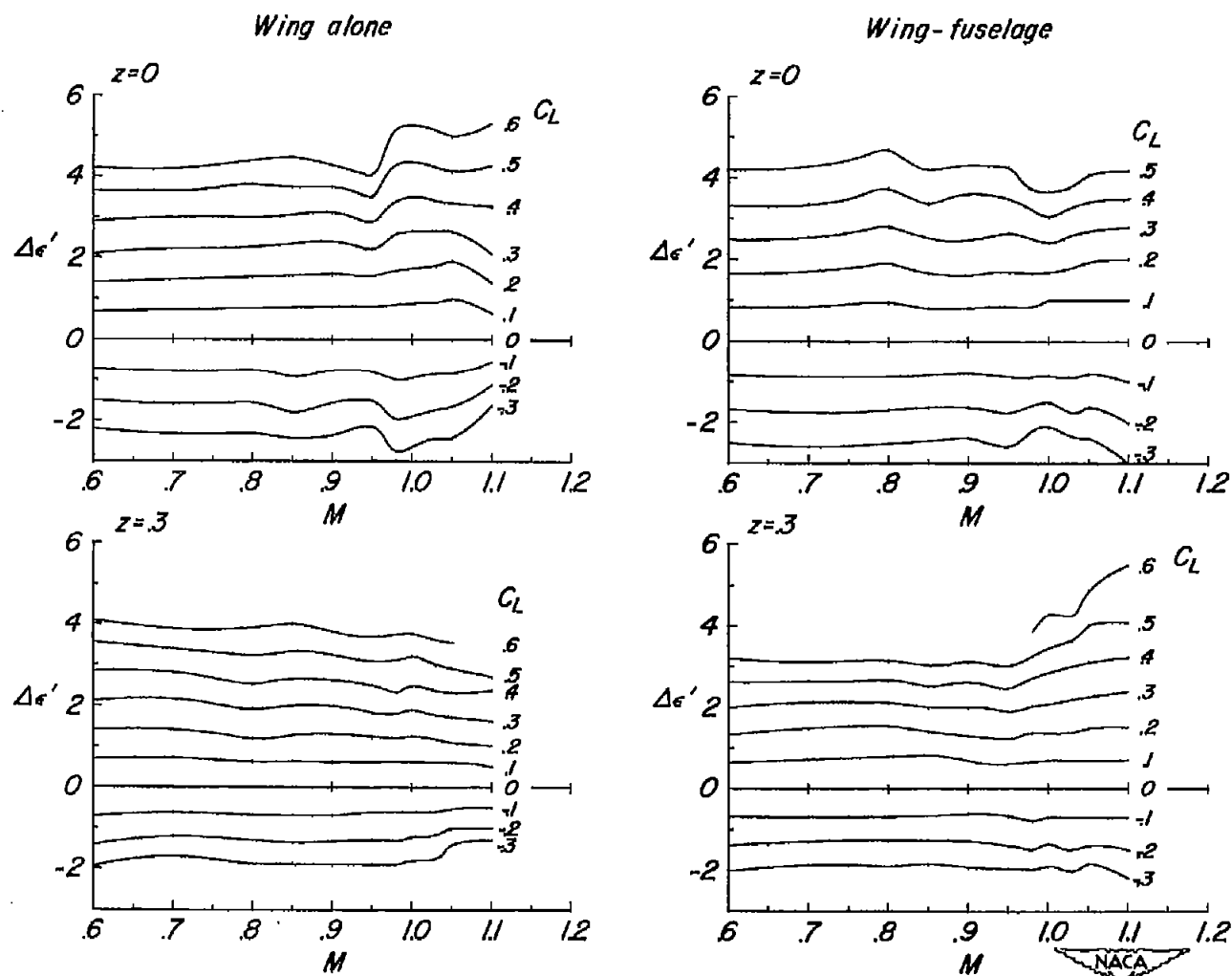
Wing-fuselage

Figure 33.- Variation of experimental floating angle with Mach number.
for wing-alone and wing-fuselage configurations at two tail heights.

Wing 2; $\Lambda_{c}/_{4} = 0^{\circ}$; $A = 4$; $\lambda = 0.6$; $\frac{t}{c} = 0.04$.

Wing alone
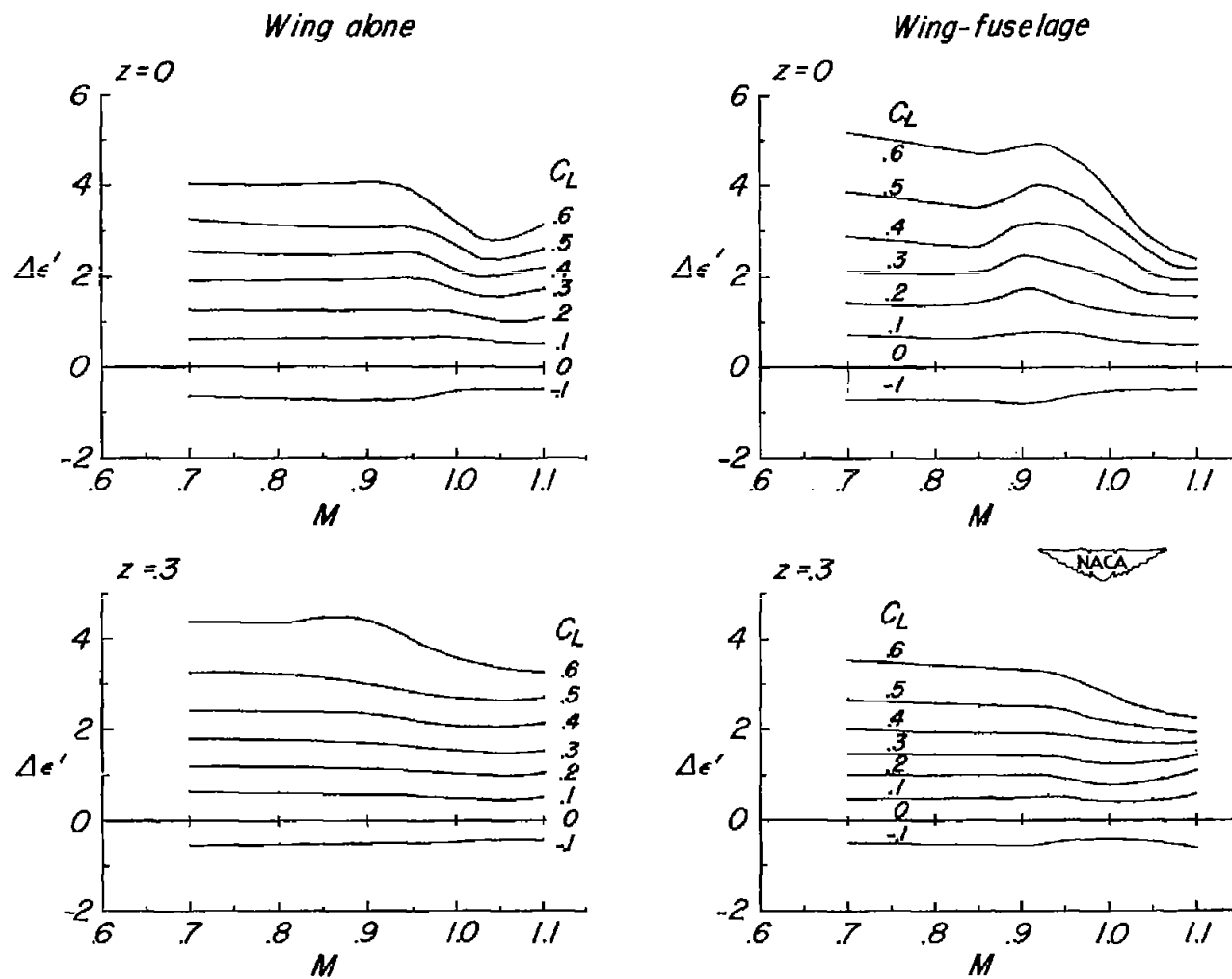
Wing-fuselage

Figure 34.- Variation of experimental floating angle with Mach number for wing-alone and wing-fuselage configurations at two tail heights.

Wing 3; $\Lambda_{c/4} = 35°$; $A = 4$; $\lambda = 0.6$; $\frac{t}{c} = 0.06$.

Wing alone
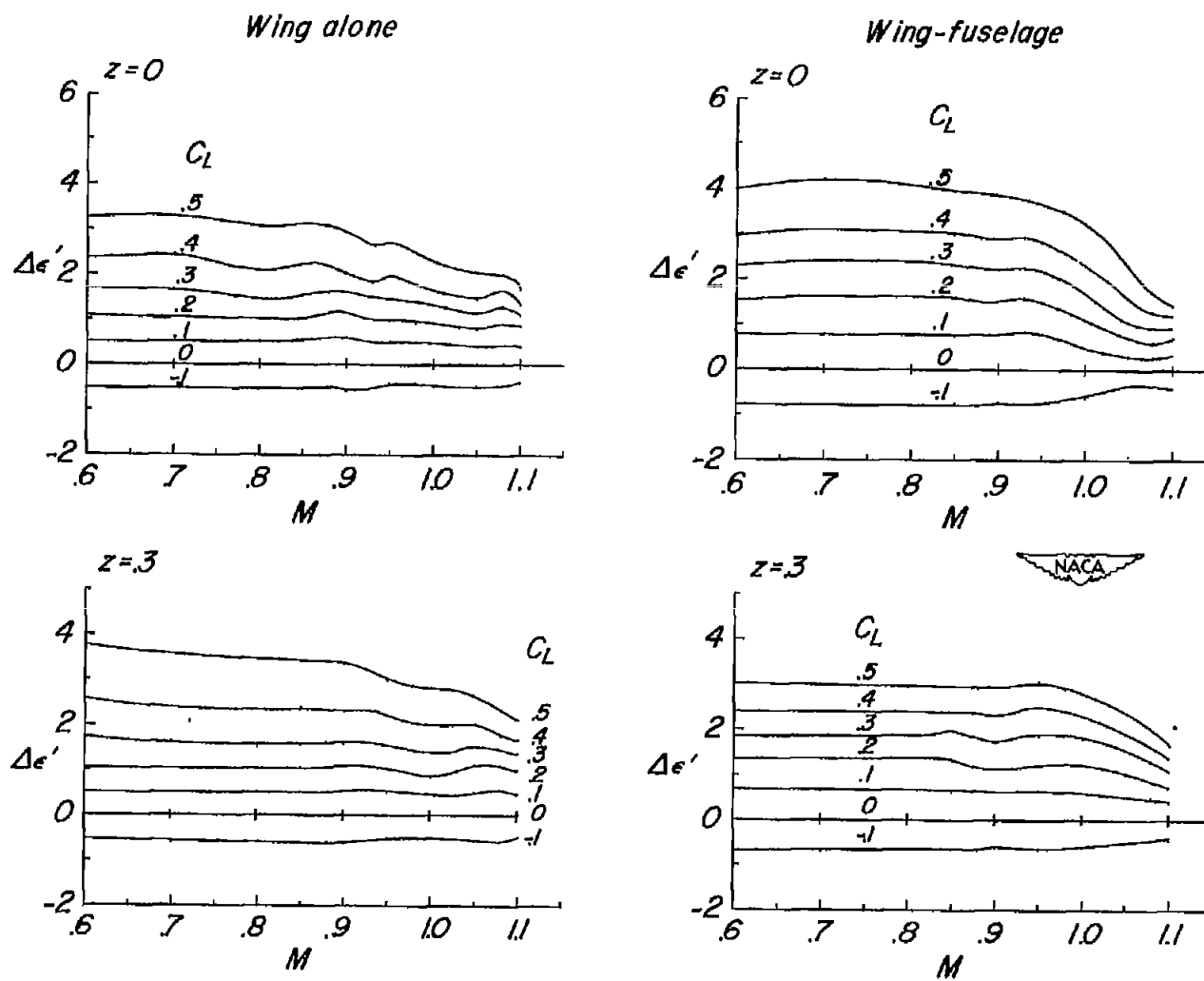
Wing-fuselage

Figure 35.- Variation of experimental floating angle with Mach number for wing-alone and wing-fuselage configurations at two tail heights.

Wing 4; $\Lambda_{c/4} = 45^\circ$; $A = 4$; $\lambda = 0.6$; $\frac{t}{c} = 0.06$.

Wing alone
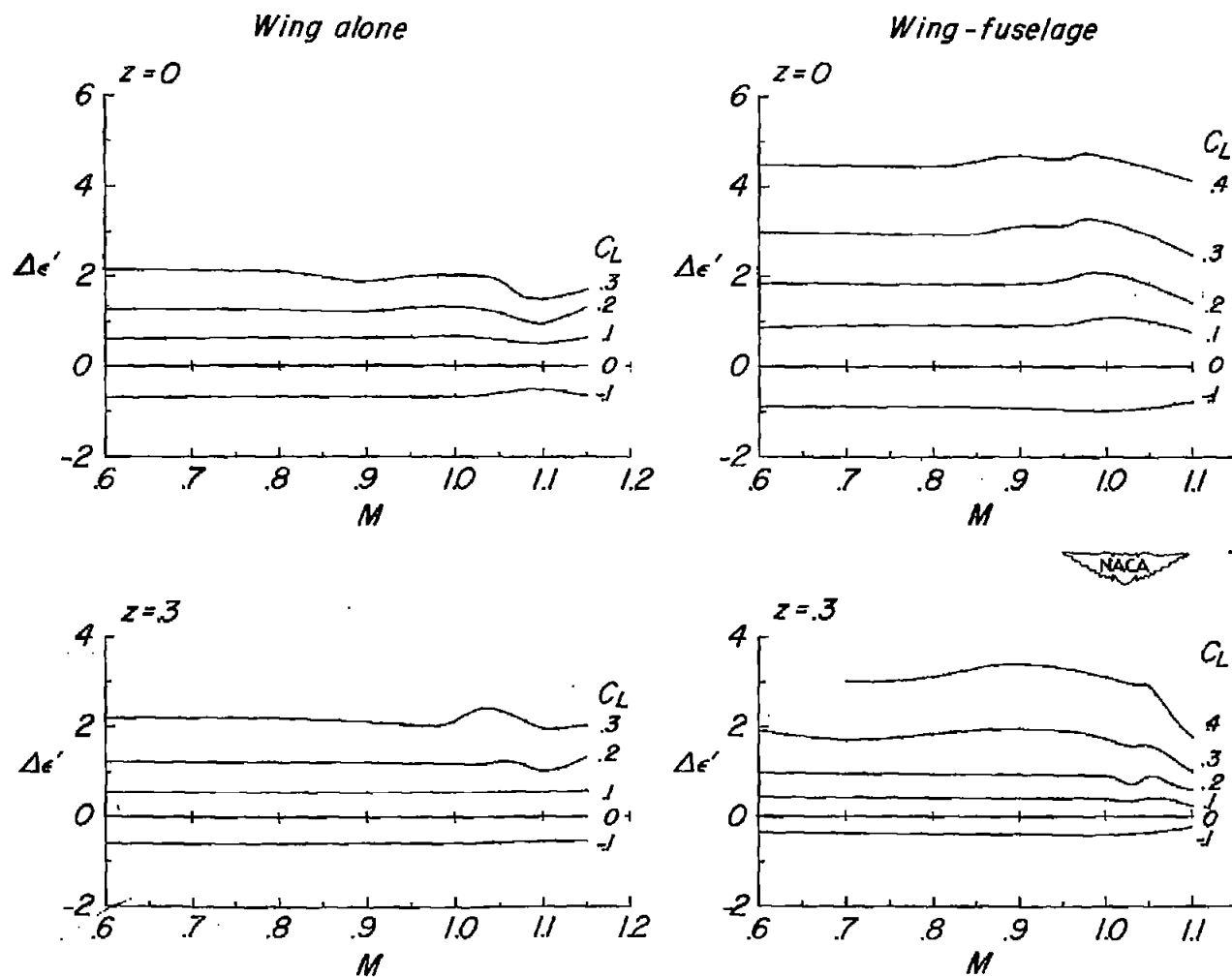
Wing-fuselage

Figure 36.- Variation of experimental floating angle with Mach number for wing-alone and wing-fuselage configurations at two tail heights. Wing 5; $\Lambda_{c/4} = 60°$; $A = 4$; $\lambda = 0.6$; $\frac{t}{c} = 0.06$.
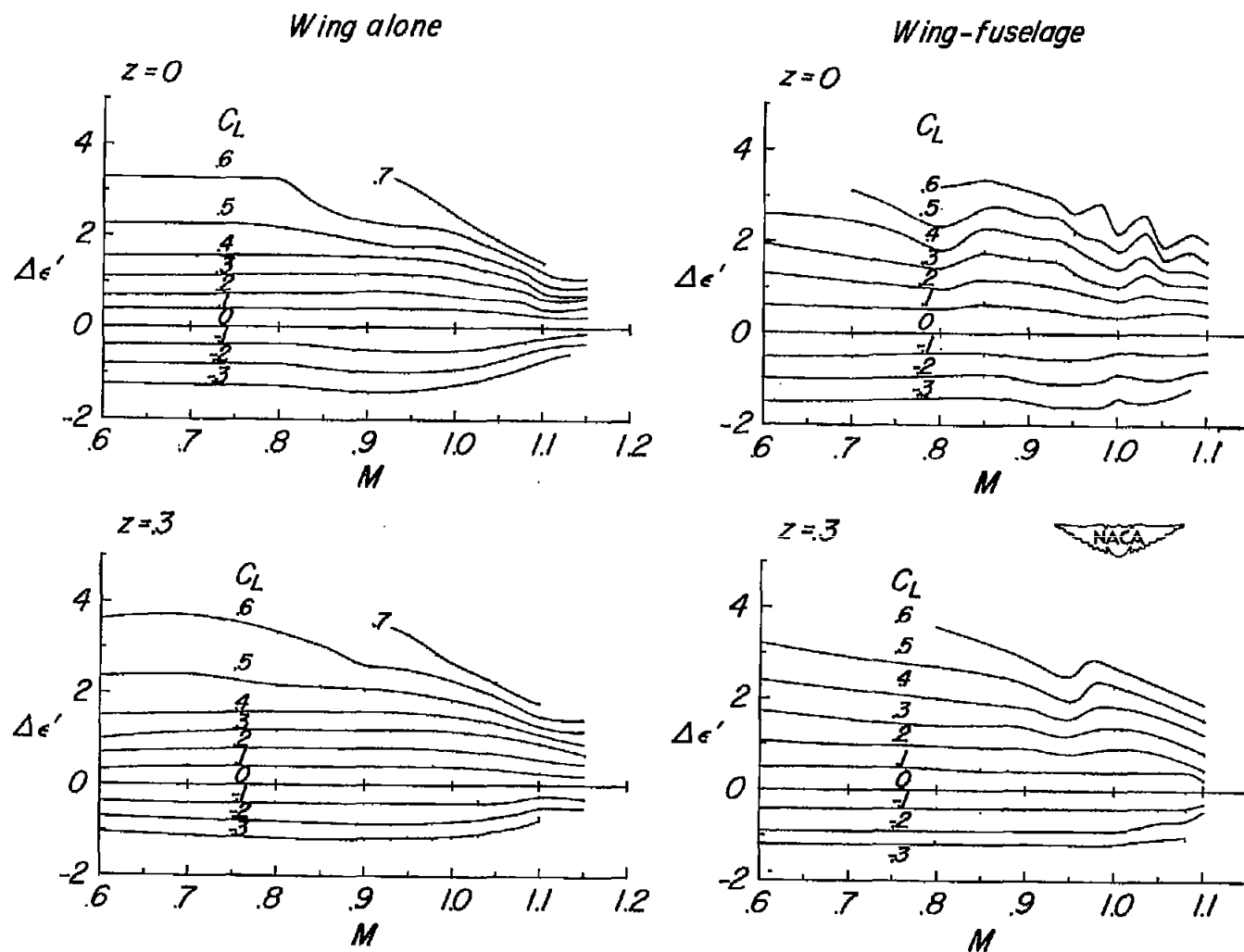
Figure 37.- Variation of experimental floating angle with Mach number for wing-alone and wing-fuselage configurations at two tail heights. Wing 6; $\Lambda_{c/4} = 35^\circ$; $A = 6$; $\lambda = 0.6$; $\frac{t}{c} = 0.06$.

Wing alone
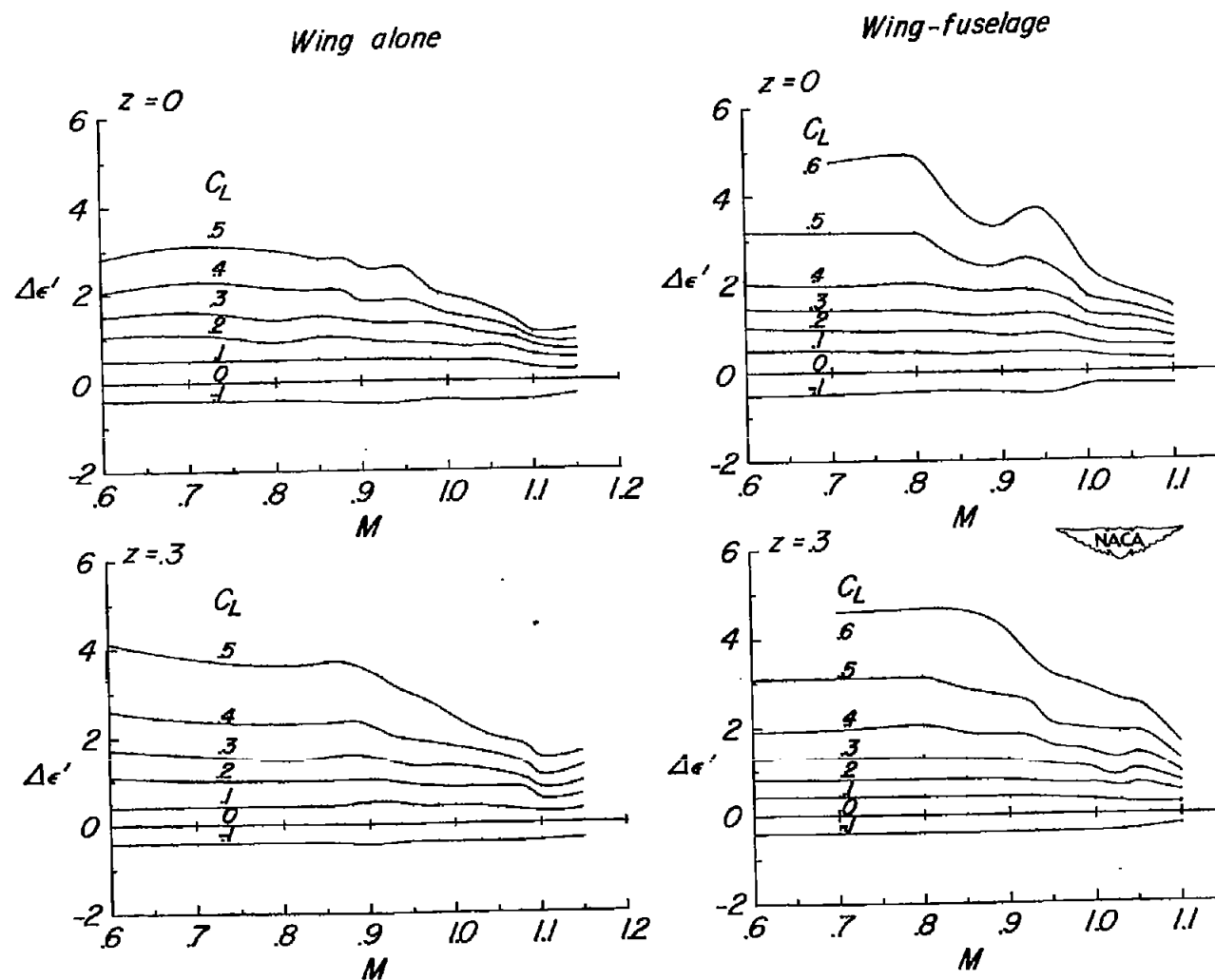
Wing-fuselage

Figure 38.- Variation of experimental floating angle with Mach number for wing-alone and wing-fuselage configurations at two tail heights.

Wing 7; $\Lambda_{c/4} = 45°$; A = 6; $\lambda = 0.6$; $\frac{t}{c} = 0.06$.
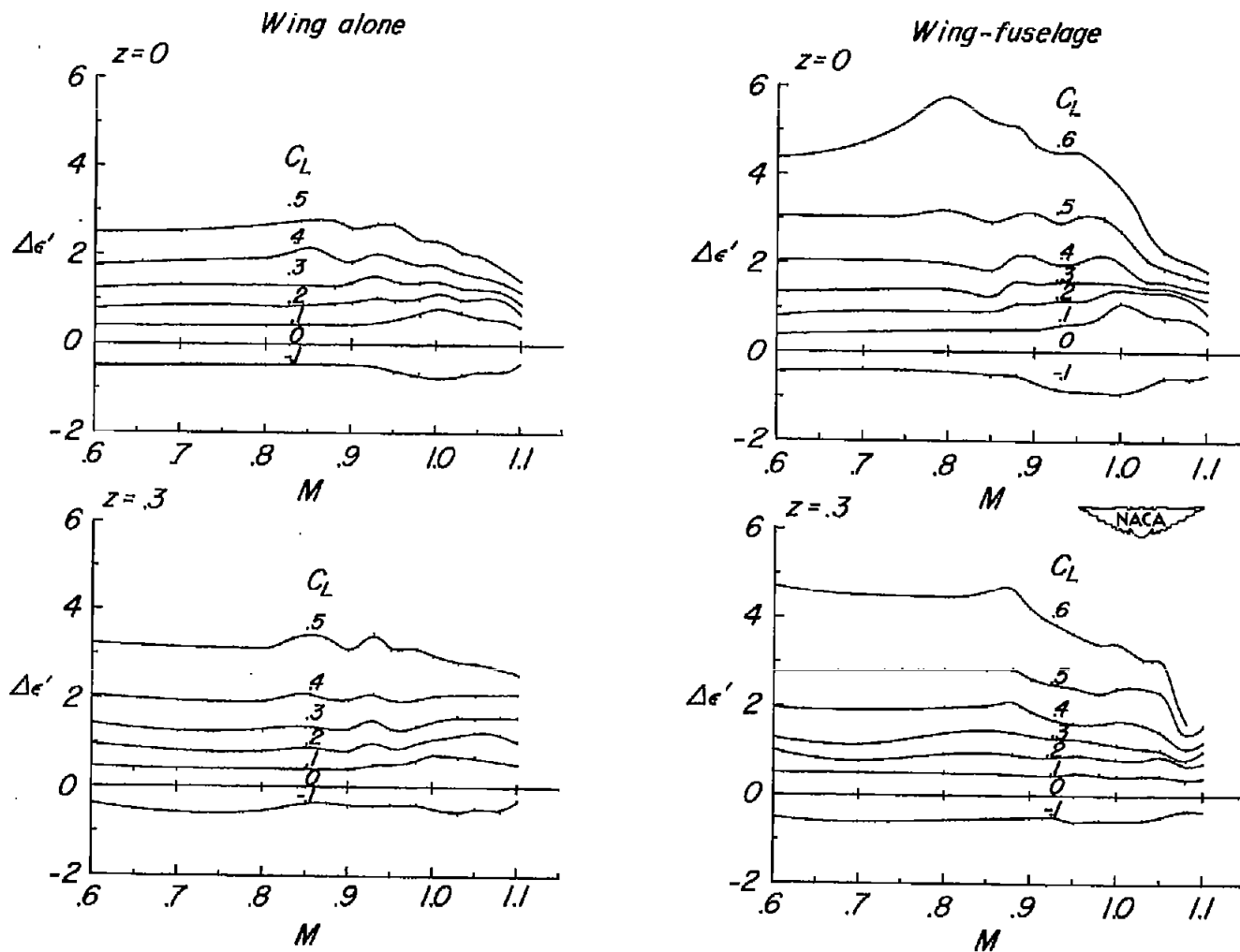
Figure 39.- Variation of experimental floating angle with Mach number for wing-alone and wing-fuselage configurations at two tail heights. Wing 8; $\Lambda_{c/4} = 45°$; $A = 6$; $\lambda = 0.6$; $\frac{t}{c} = 0.09$.
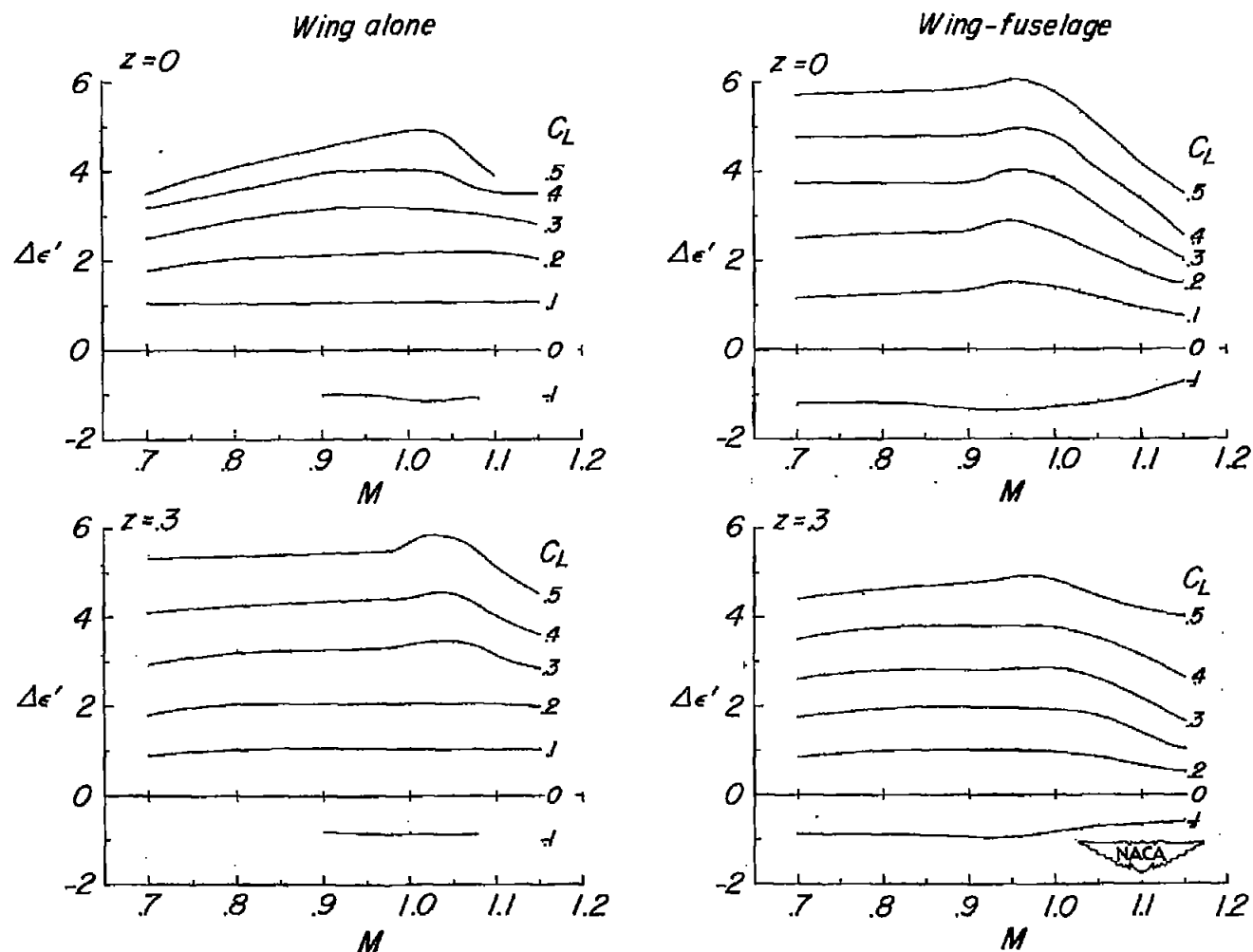
Figure 40.- Variation of experimental floating angle with Mach number
for wing-alone and wing-fuselage configurations at two tail heights.

Wing 9; $\Lambda_{c/4} = 60°$; $A = 2$; $\lambda = 0.6$; $\frac{t}{c} = 0.06$.

Wing alone
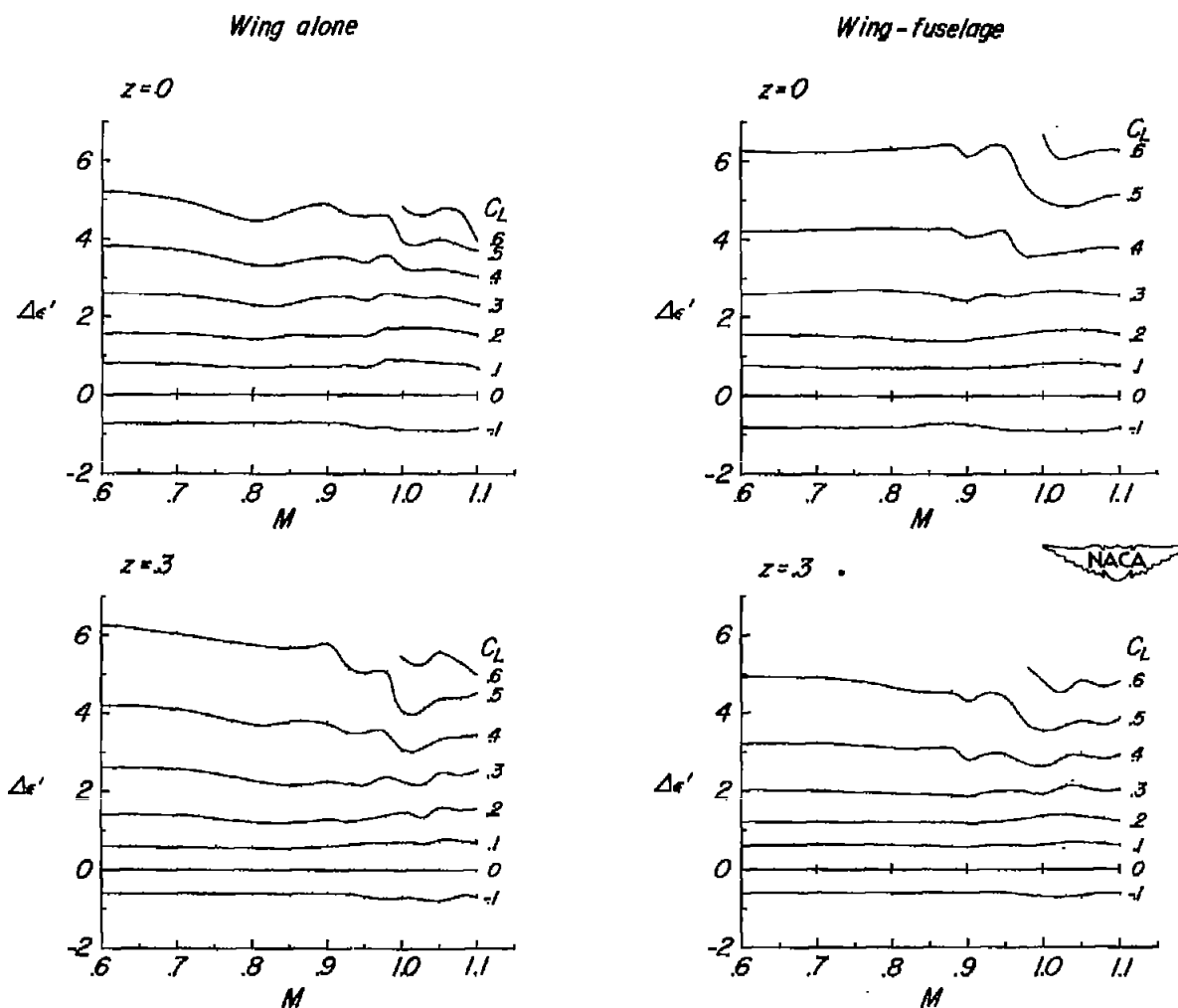
Wing - fuselage

Figure 41.- Variation of experimental floating angle with Mach number for wing-alone and wing-fuselage configurations at two tail heights.

Wing 10; $\Lambda_{c/4} = 36.9°$; $A = 4$; $\lambda = 0$; $\frac{t}{c} = 0.06$.
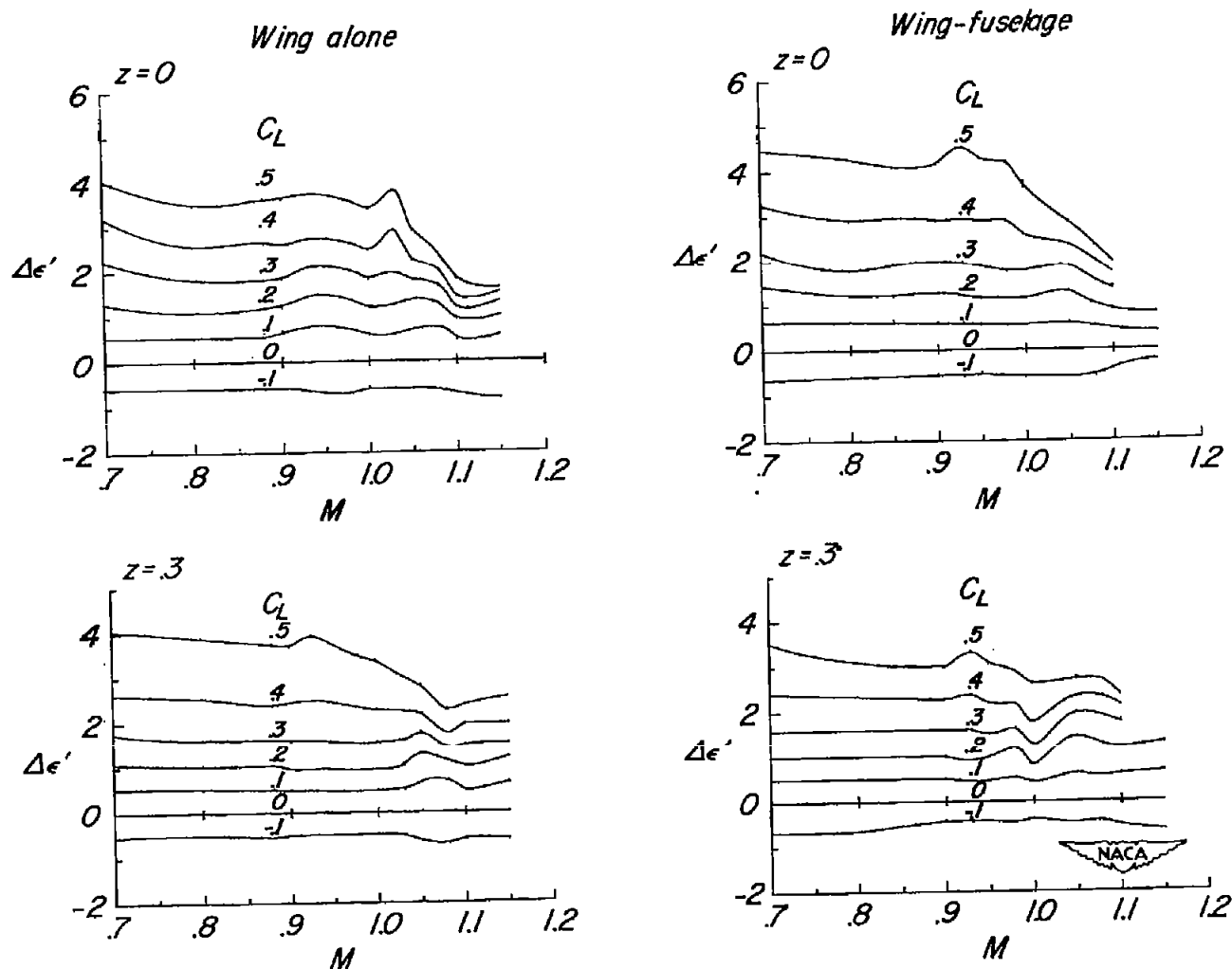
Figure 42.- Variation of experimental floating angle with Mach number for wing-alone and wing-fuselage configurations at two tail heights.

Wing 11; $\Lambda_{c/4} = 45°$; $A = 4$; $\lambda = 0.3$; $\frac{t}{c} = 0.06$.
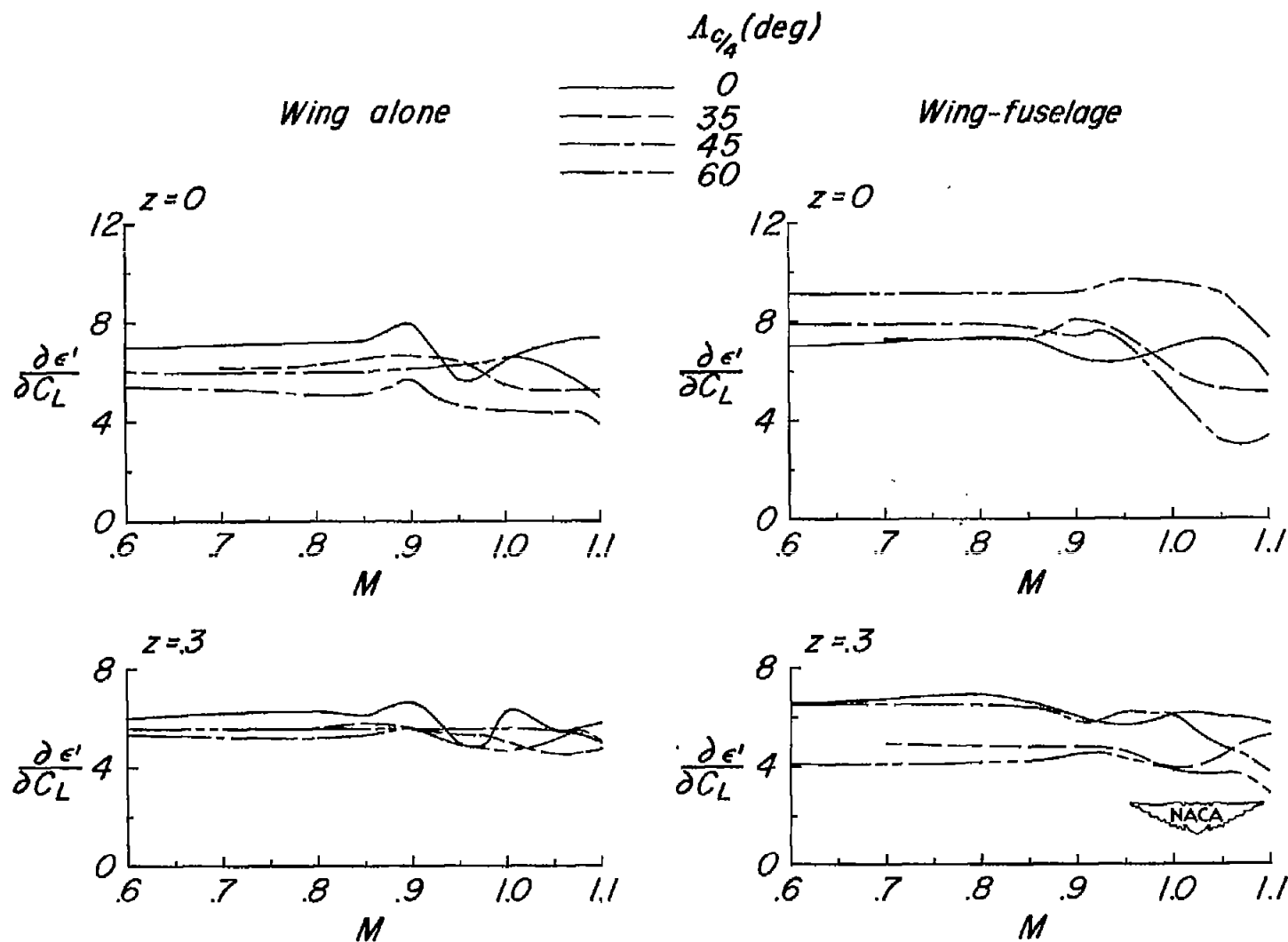
Figure 43.— Effect of sweep angle on the variation of experimental floating angle parameter $\partial\epsilon'/\partial C_L$ with Mach number. $A = 4$; $\lambda = 0.6$; $\frac{t}{c} = 0.06$.
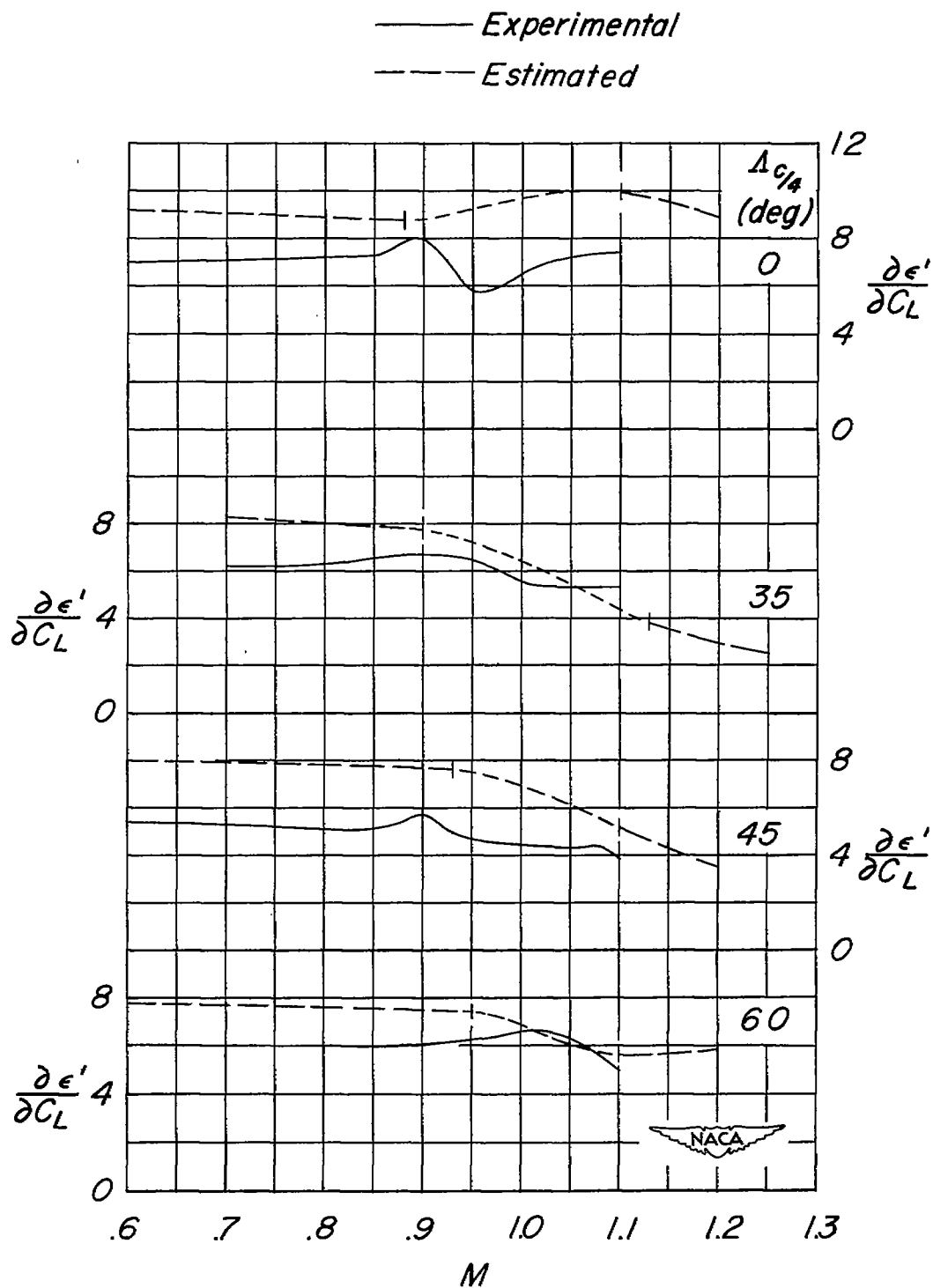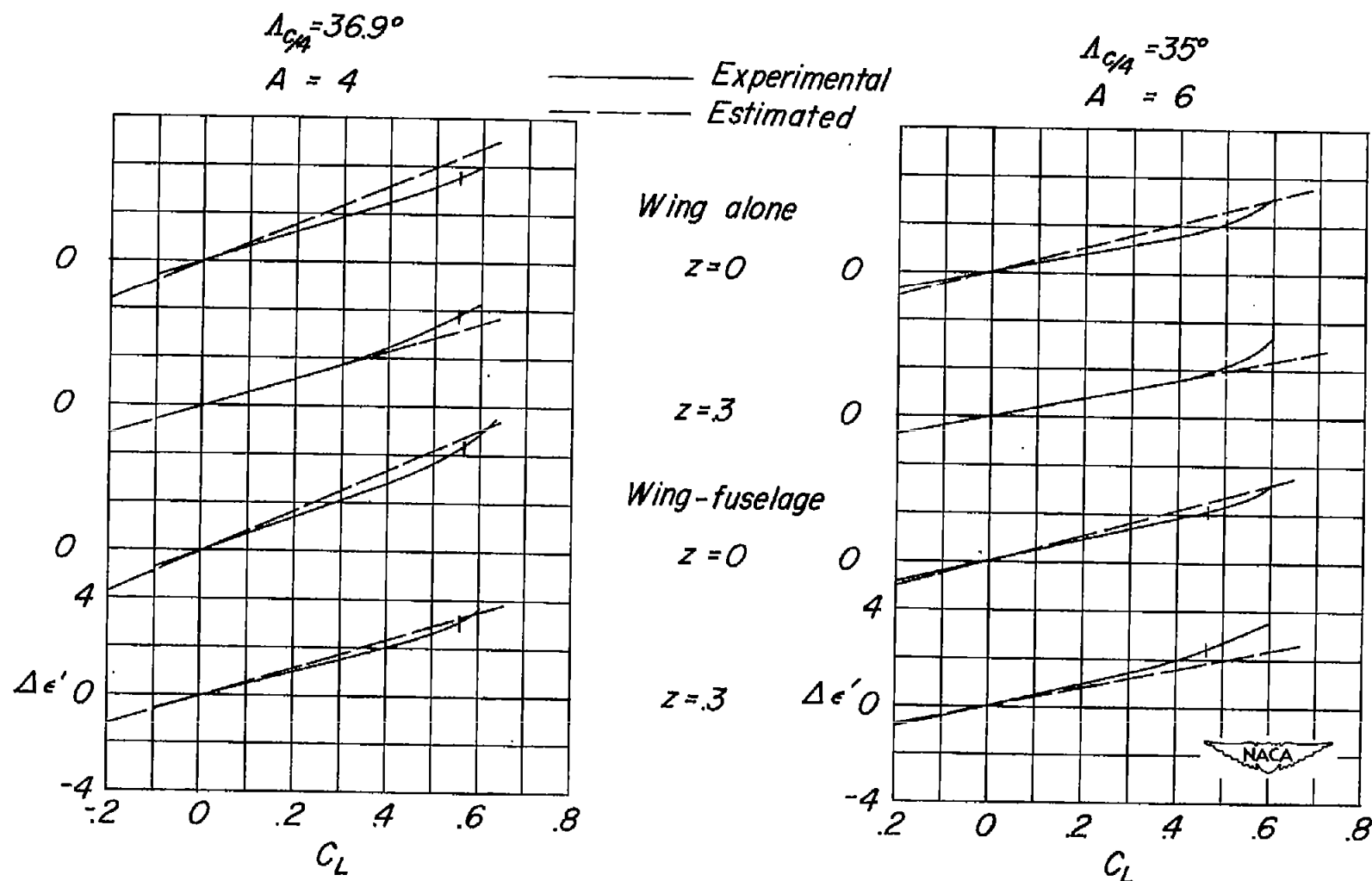
Figure 44.- Comparison of experimental and estimated variation of
floating-angle parameter $\partial \epsilon'/\partial C_L$ with Mach number for various
sweep angles. Wing alone; $z = 0$; $A = 4$; $\lambda = 0.6$; $\frac{t}{c} = 0.06$.
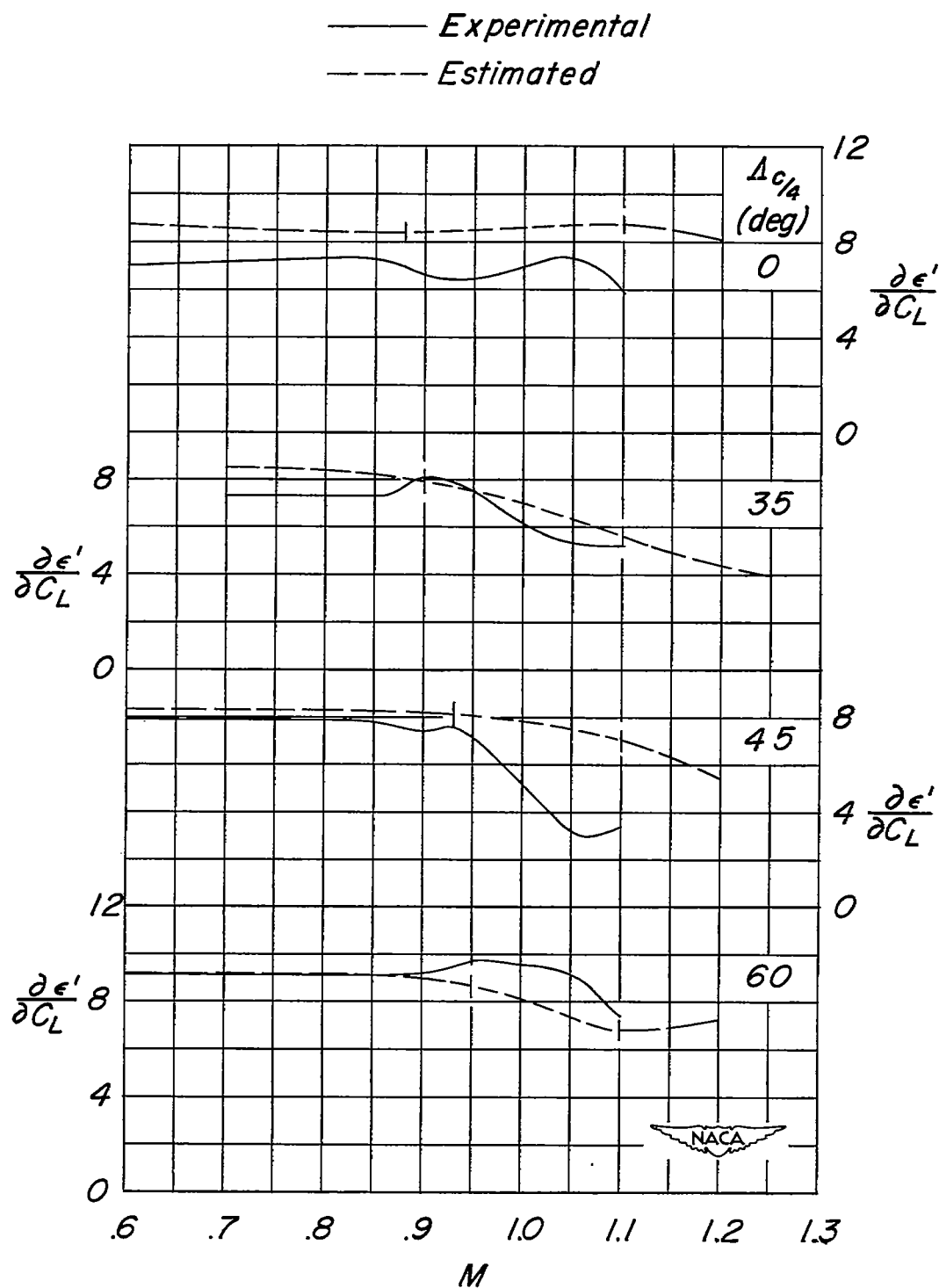
Figure 45.- Comparison of experimental and estimated variation of floating-angle parameter $\partial\epsilon'/\partial C_L$ with Mach number for various sweep angles. Wing and fuselage; $z = 0$; $A = 4$; $\lambda = 0.6$; $\frac{t}{c} = 0.06$.
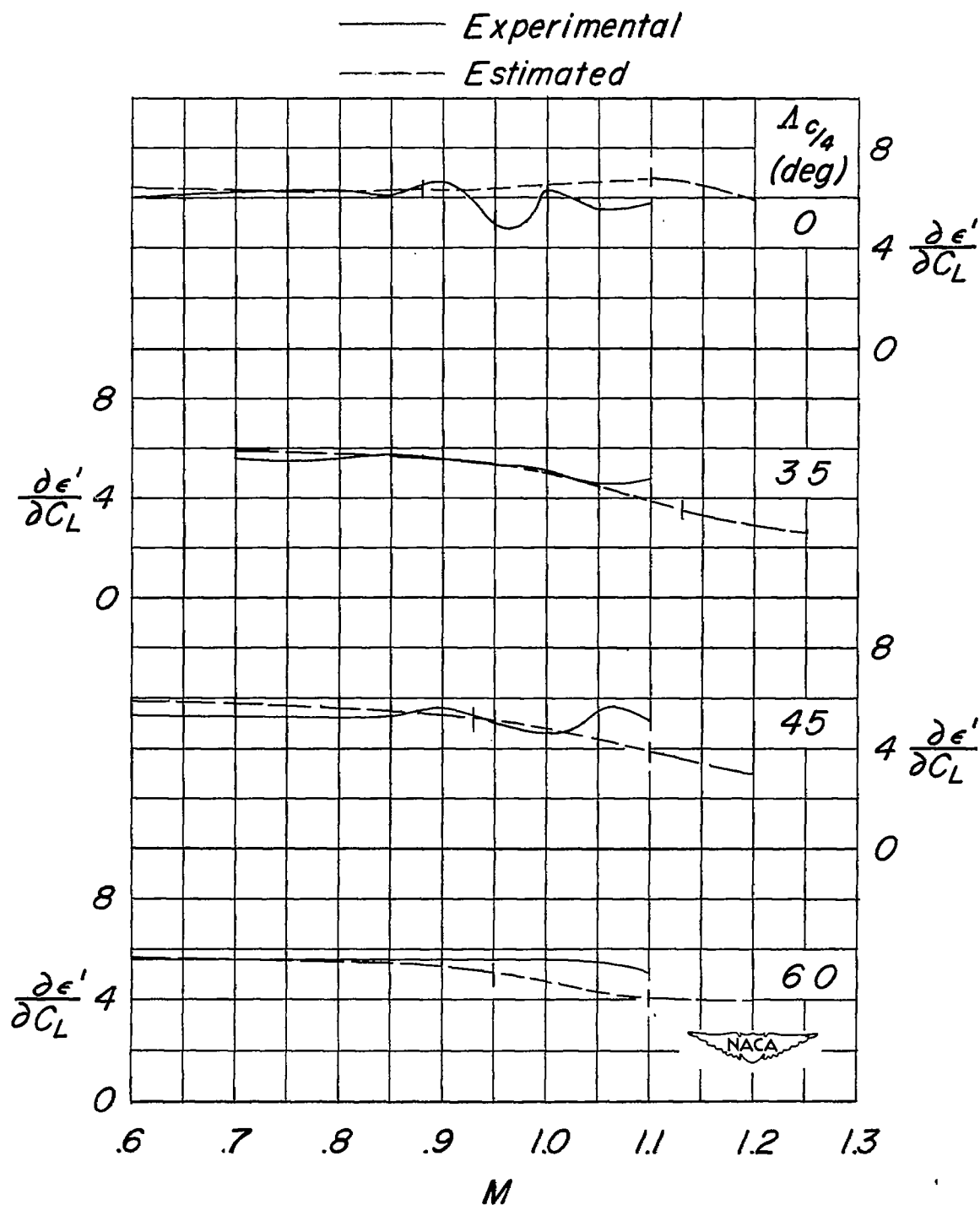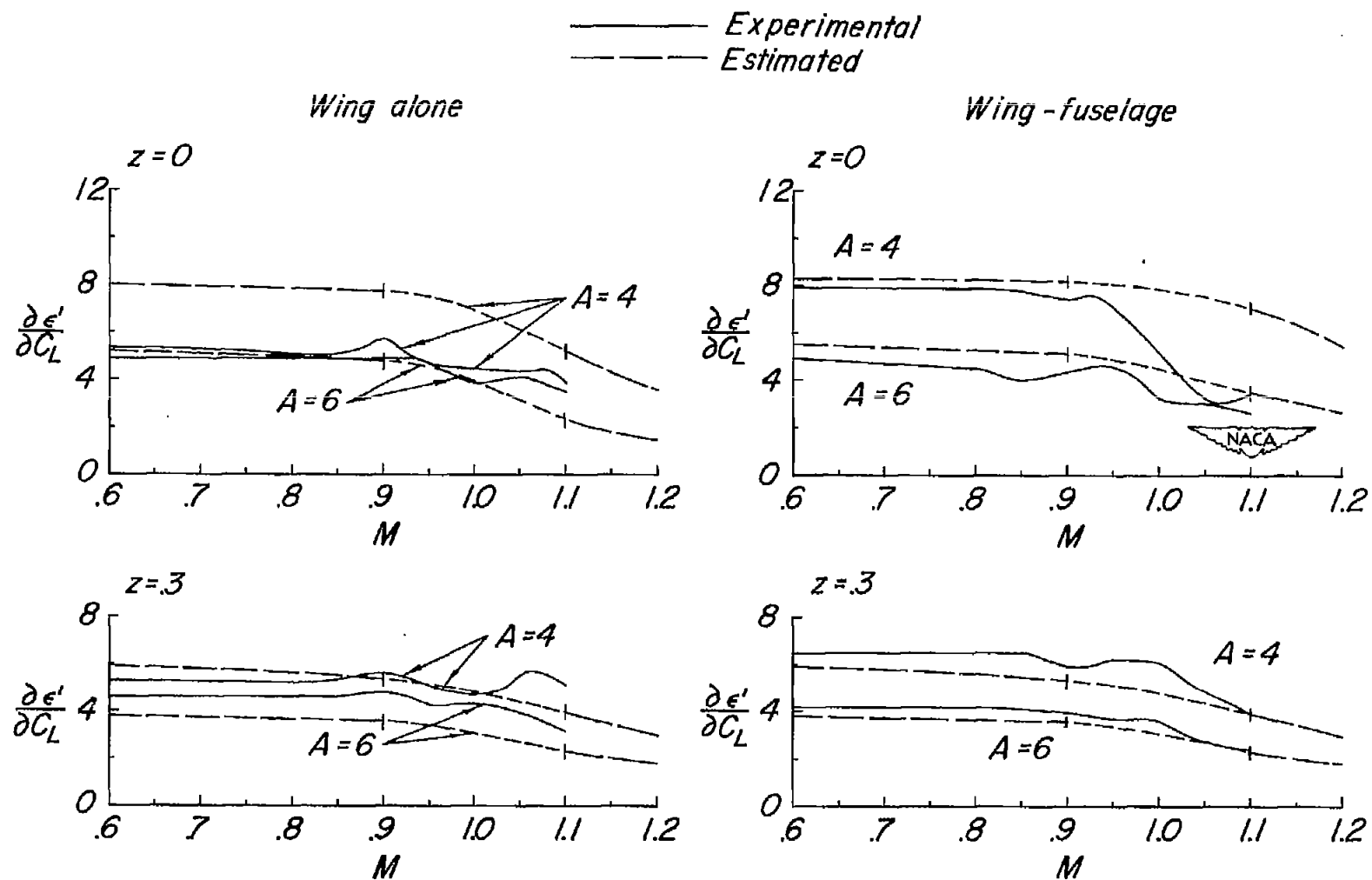
Figure 46.- Comparison of experimental and estimated variation of floating-angle parameter $\partial\epsilon'/\partial C_L$ with Mach number for various sweep angles. Wing alone; z = 0.3; A = 4; λ = 0.6; $\frac{t}{c}$ = 0.06.
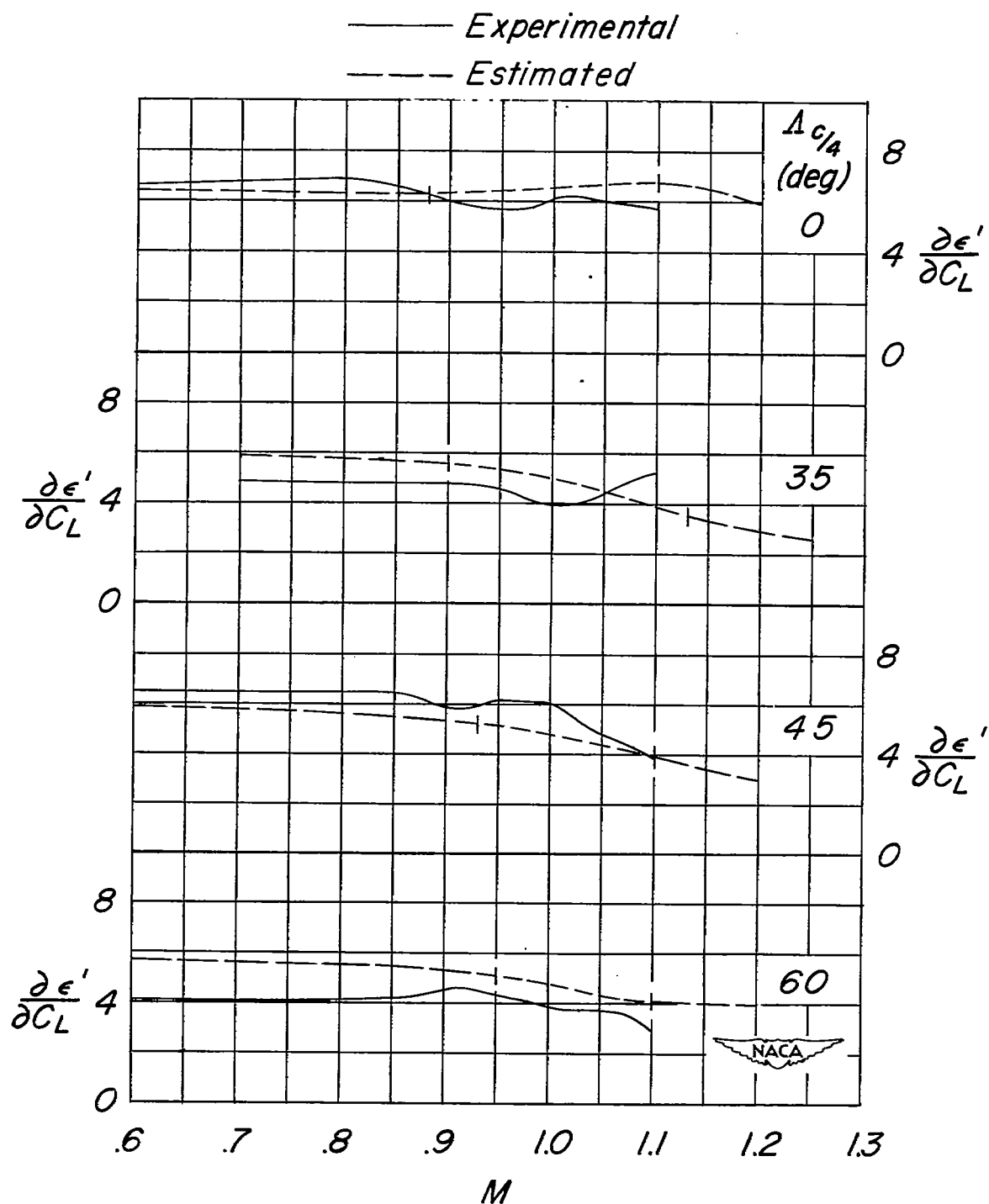
Figure 47.- Comparison of experimental and estimated variation of floating-angle parameter $\partial \epsilon'/\partial C_L$ with Mach number for various sweep angles. Wing and fuselage; $z = 0.3$; $A = 4$; $\lambda = 0.6$; $\frac{t}{c} = 0.06$.
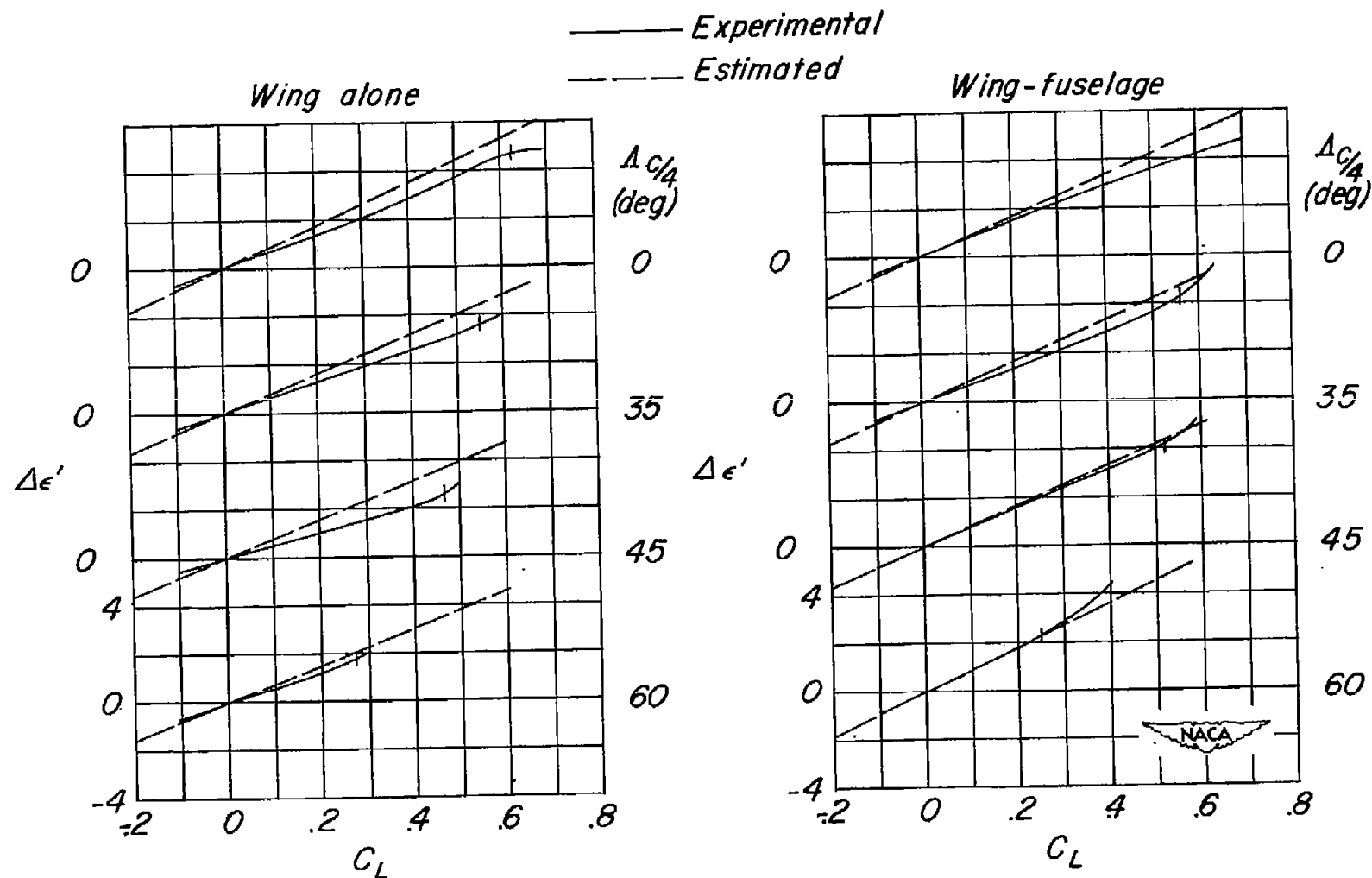
Figure 48.- Comparison of experimental and estimated variation of floating angle with lift coefficient for various sweep angles. M = 0.8; z = 0; A = 4; λ = 0.6; $\frac{t}{c}$ = 0.06.
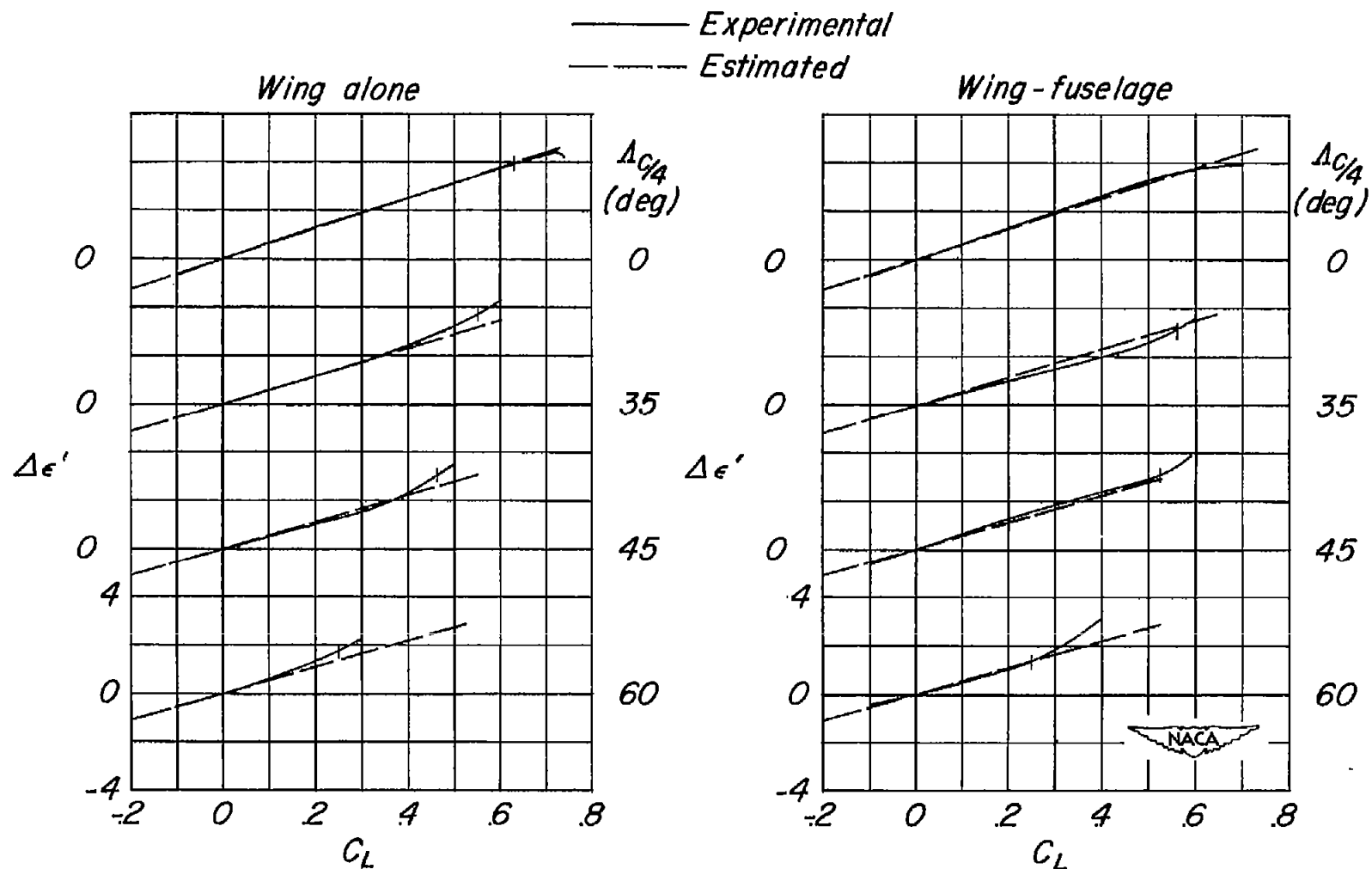
Figure 49.— Comparison of experimental and estimated variation of floating angle with lift coefficient for various sweep angles. M = 0.8; z = 0.3; A = 4; λ = 0.6; $\frac{t}{c}$ = 0.06.
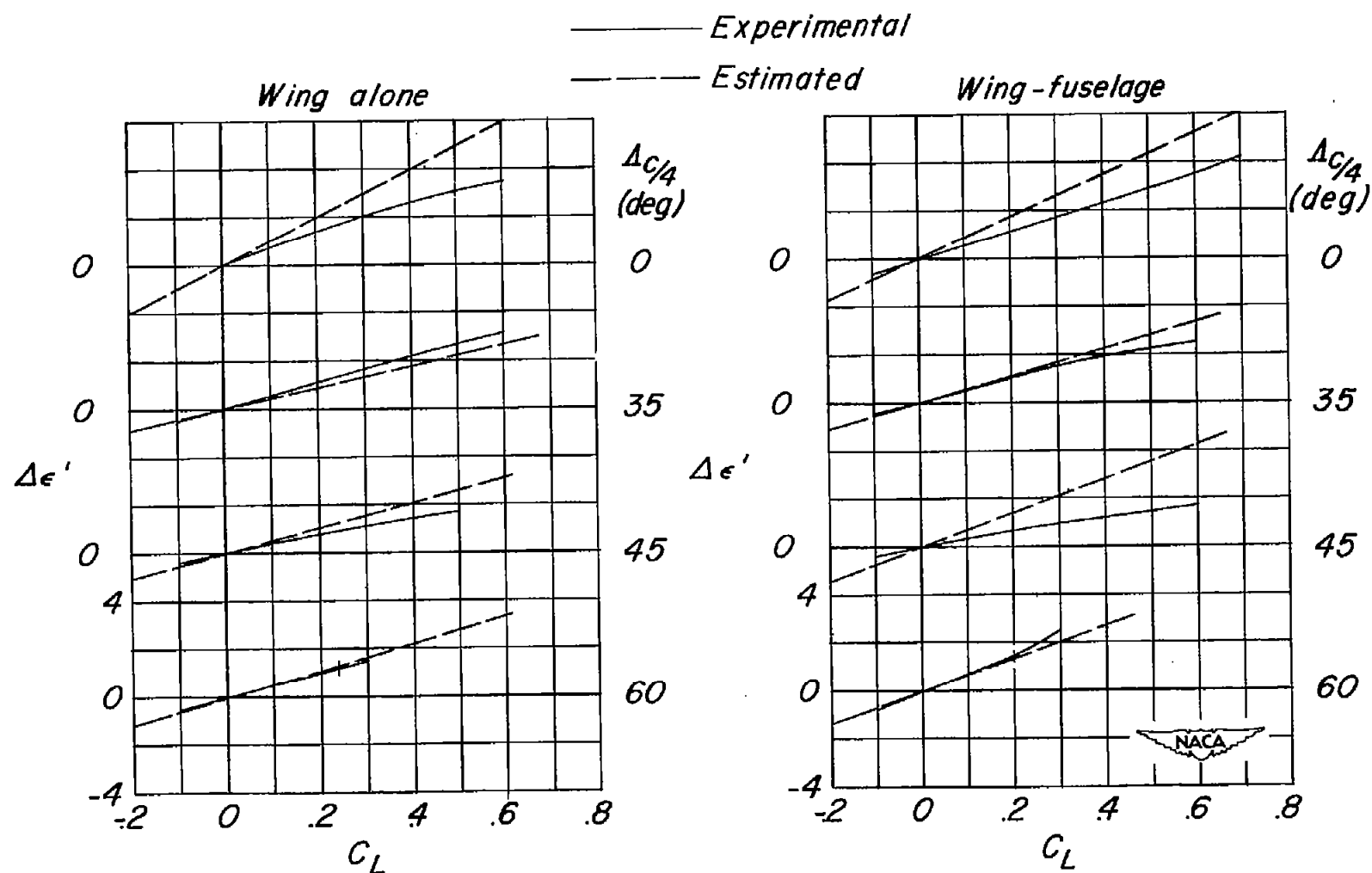
Figure 50.- Comparison of experimental and estimated variation of floating angle with lift coefficient for various sweep angles. $M = 1.1$; $z = 0$; $A = 4$; $\lambda = 0.6$; $\frac{t}{c} = 0.06$.
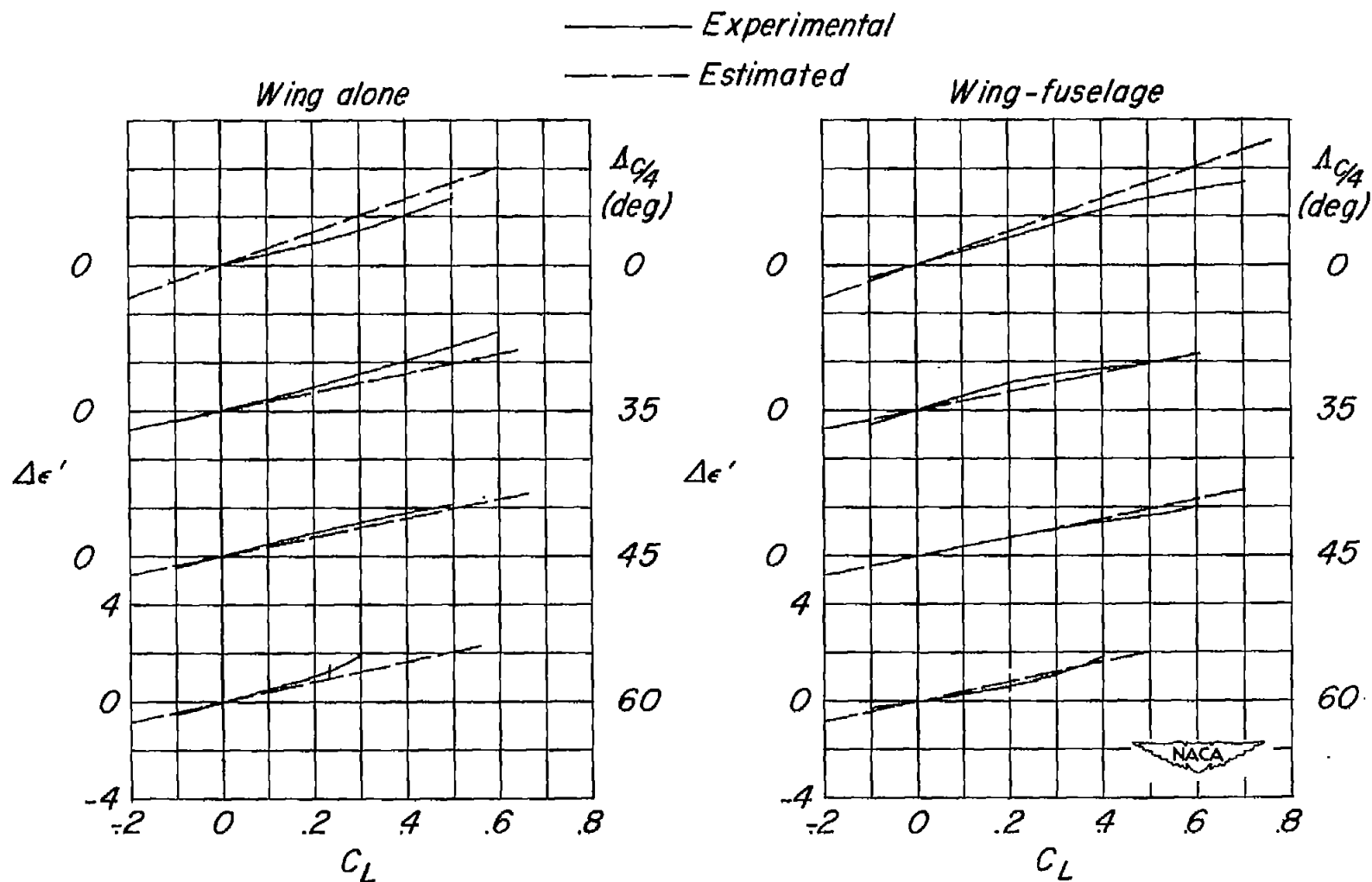
Figure 51.- Comparison of experimental and estimated variation of floating angle with lift coefficient for various sweep angles. $M = 1.1$; $z = 0.3$; $A = 4$; $\lambda = 0.6$; $\frac{t}{c} = 0.06$.
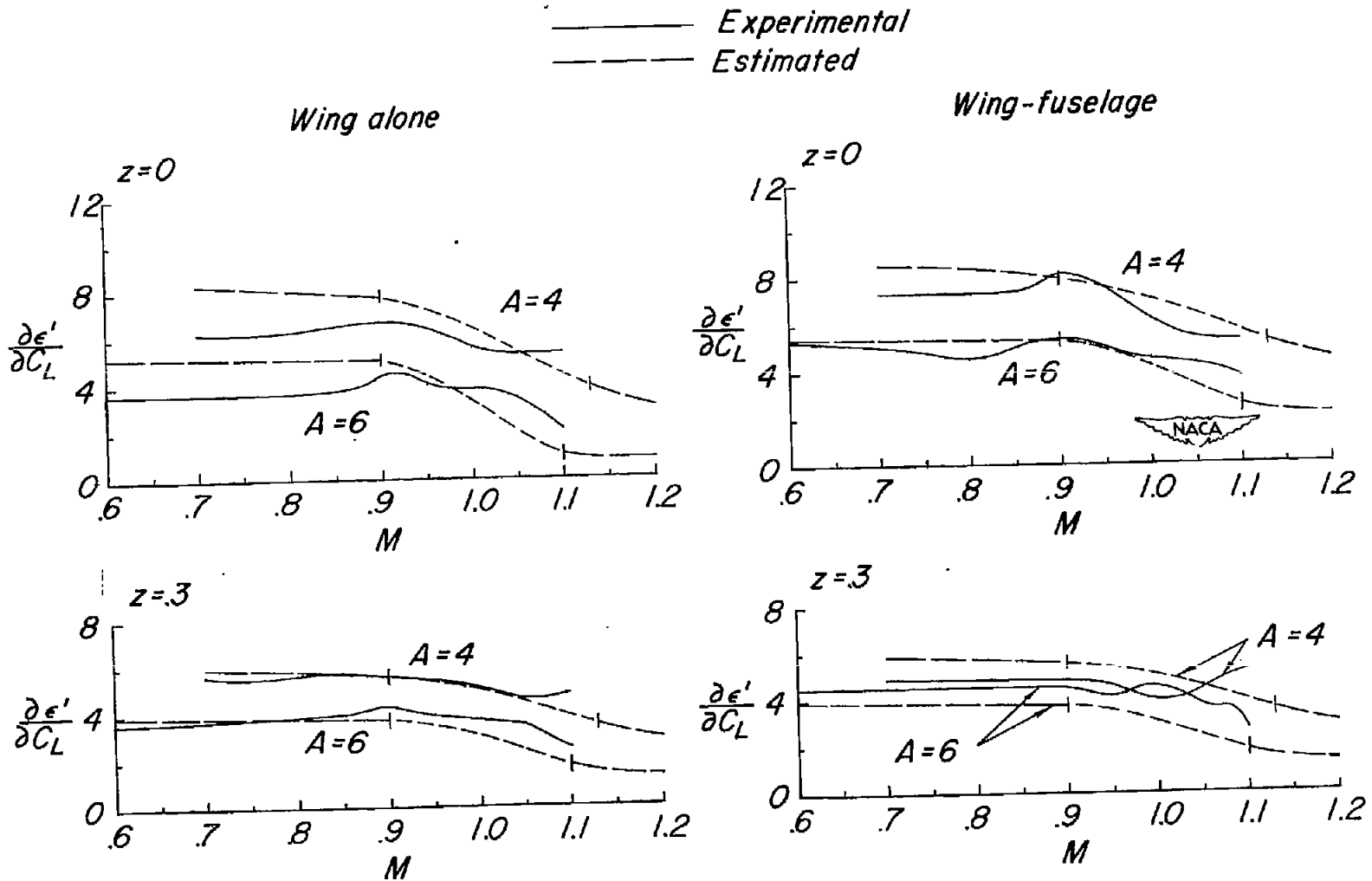
Figure 52.- Effect of aspect ratio on the experimental and estimated variation of floating-angle parameter $\partial \epsilon'/\partial C_L$ with Mach number. $\Lambda_{c/4} = 35°$; $\lambda = 0.6$; $\frac{t}{c} = 0.06$.
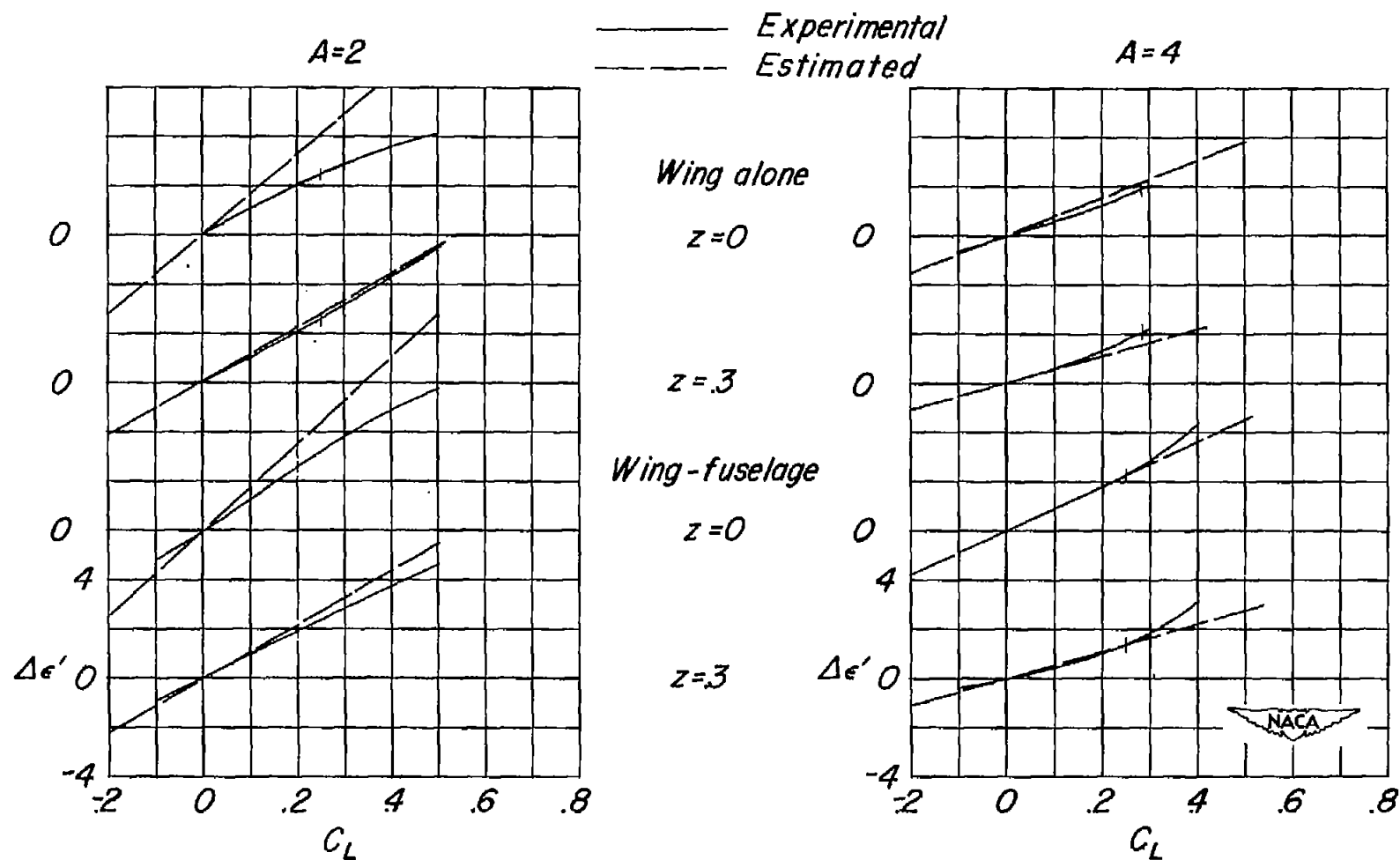
Figure 53.- Effect of aspect ratio on the experimental and estimated variation of floating angle with lift coefficient. $\Lambda_{c/4} = 35°$; $\lambda = 0.6$; $\frac{t}{c} = 0.06$; $M = 0.8$.

$\Lambda_{c/4} = 36.9°$
$A = 4$

——————— Experimental
— — — — Estimated

$\Lambda_{c/4} = 35°$
$A = 6$

Wing alone

$z = 0$

$z = .3$

Wing-fuselage

$z = 0$

$z = .3$
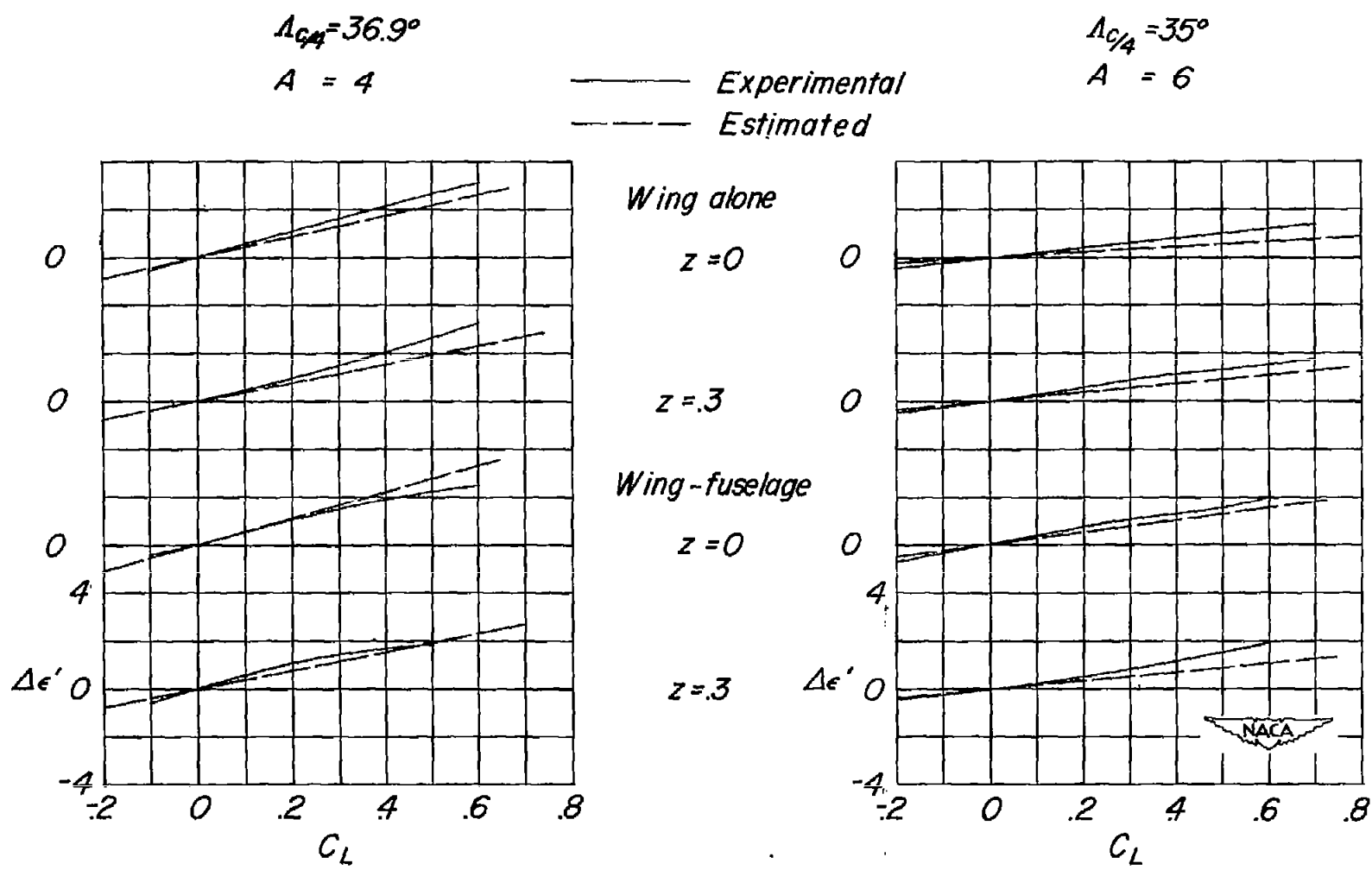
Figure 54.- Effect of aspect ratio on the experimental and estimated varia-
tion of floating angle with lift coefficient. $\Lambda_{c/4} = 35°$; $\lambda = 0.6$;
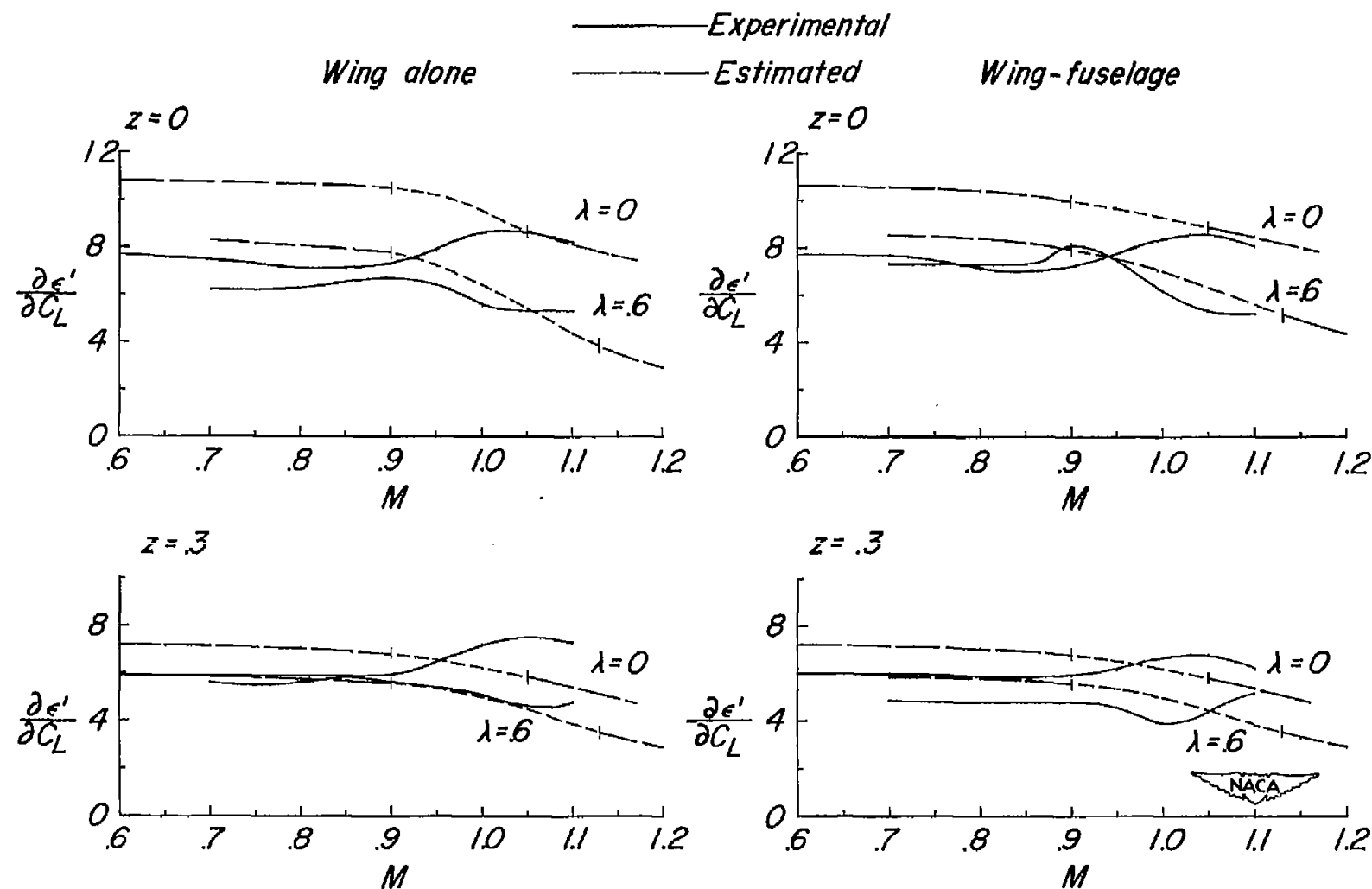$\frac{t}{c} = 0.06$; $M = 1.1$.

Figure 55.- Effect of aspect ratio on the experimental and estimated variation of floating-angle parameter $\partial \epsilon'/\partial C_L$ with Mach number. $\Lambda_{c/4} = 45°$; $\lambda = 0.6$; $\frac{t}{c} = 0.06$.
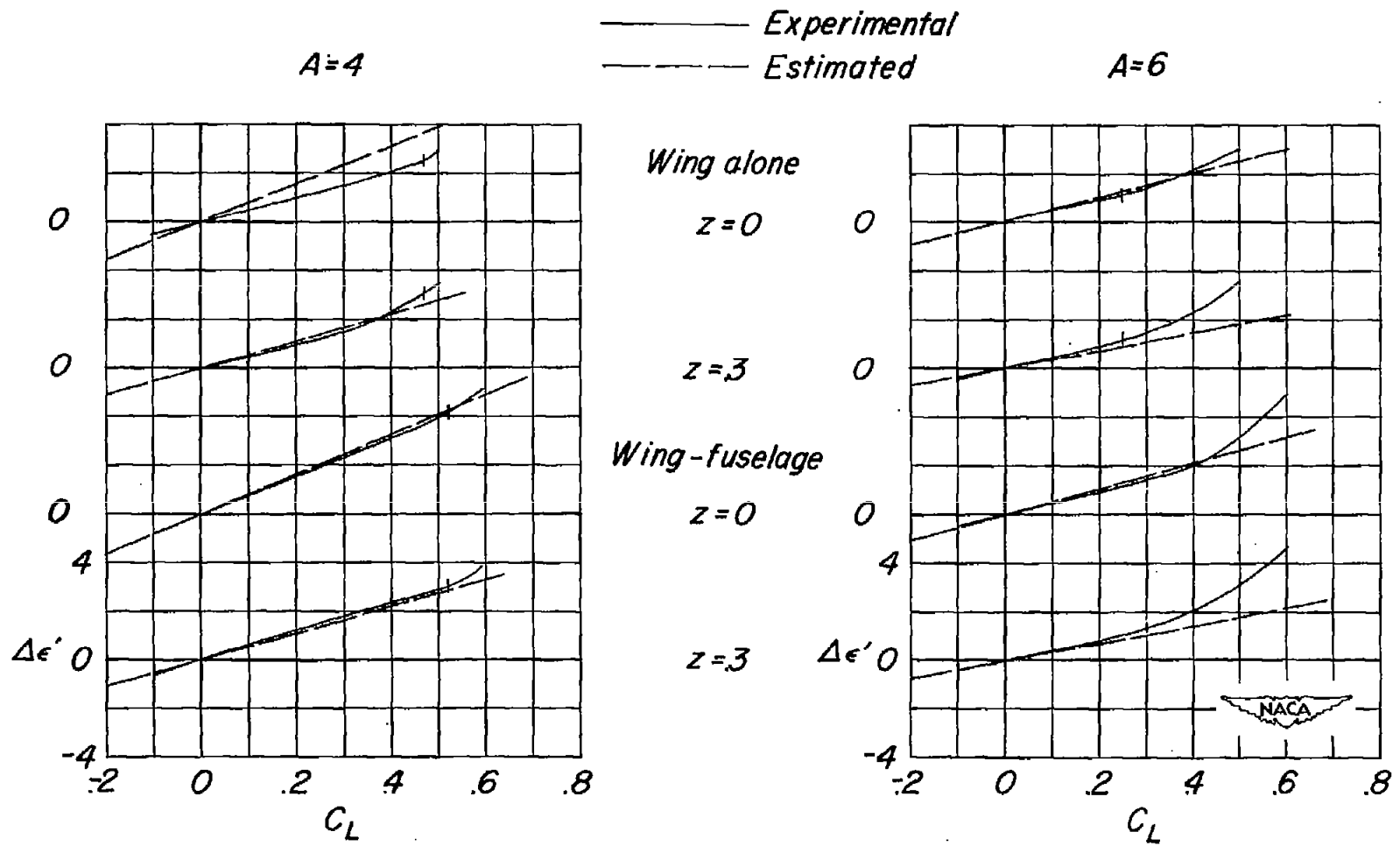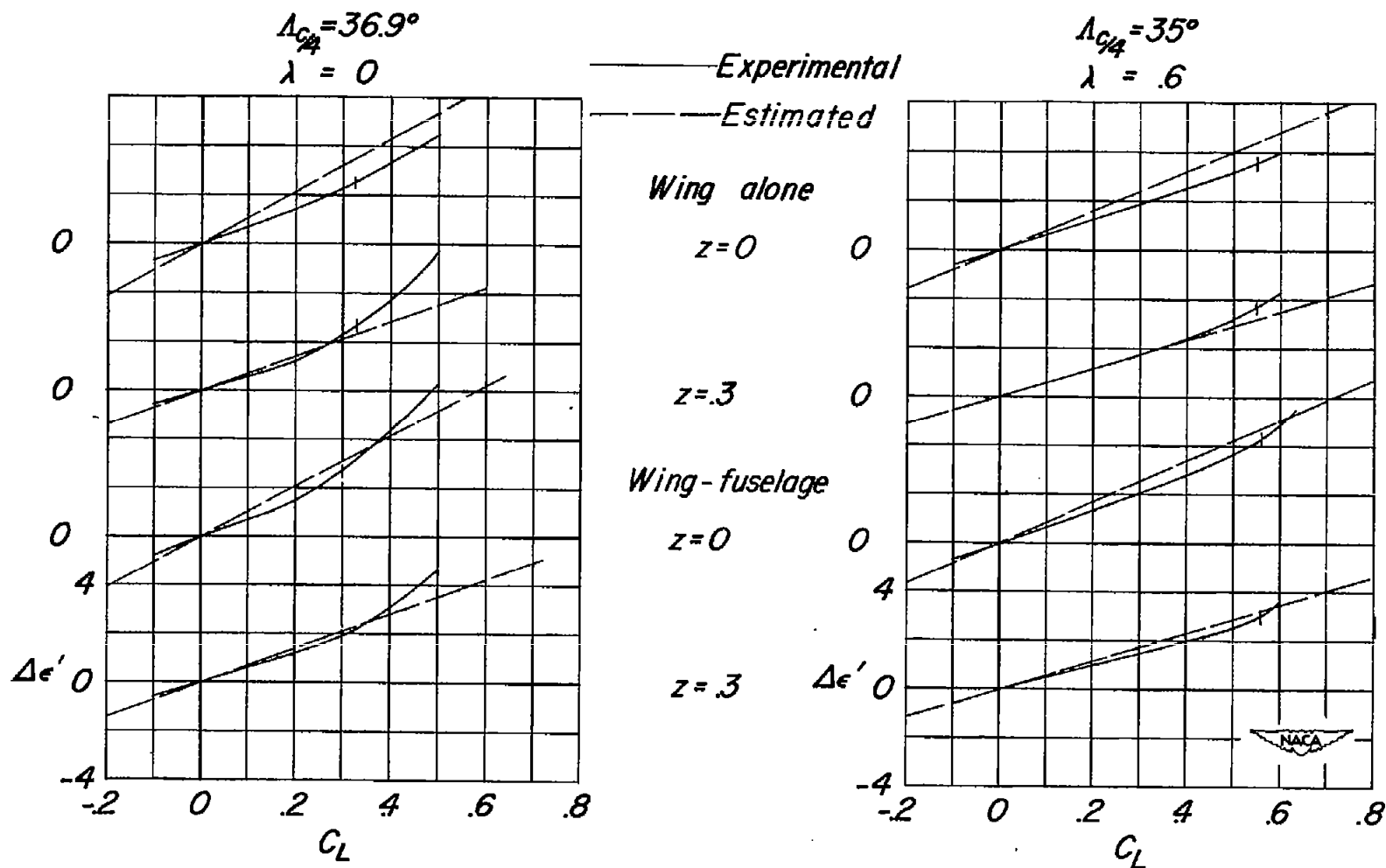
Figure 56.- Effect of aspect ratio on the experimental and estimated variation of floating angle with lift coefficient. $\Lambda_{c/4} = 45^\circ$; $\lambda = 0.6$; $\frac{t}{c} = 0.06$; $M = 0.8$.
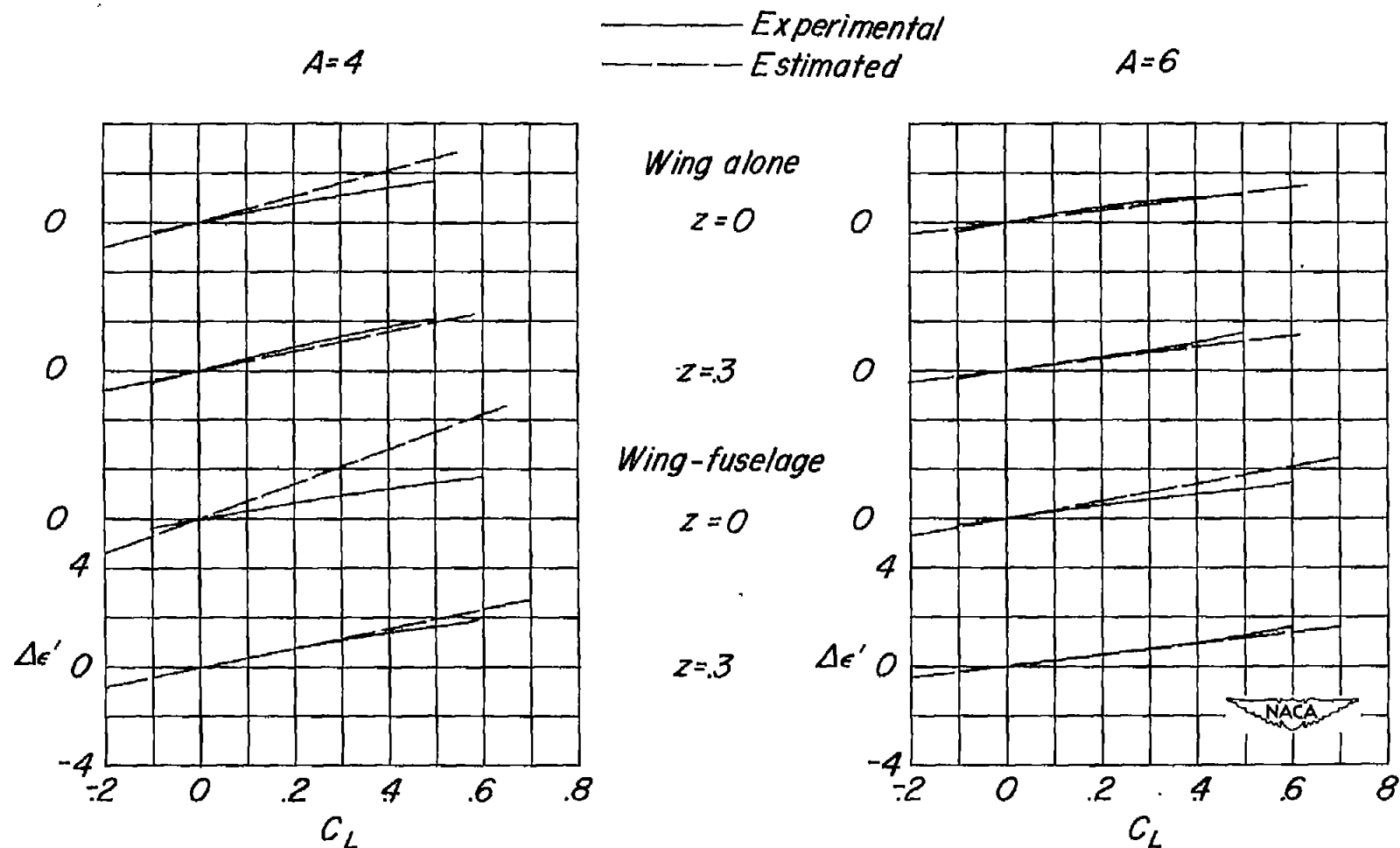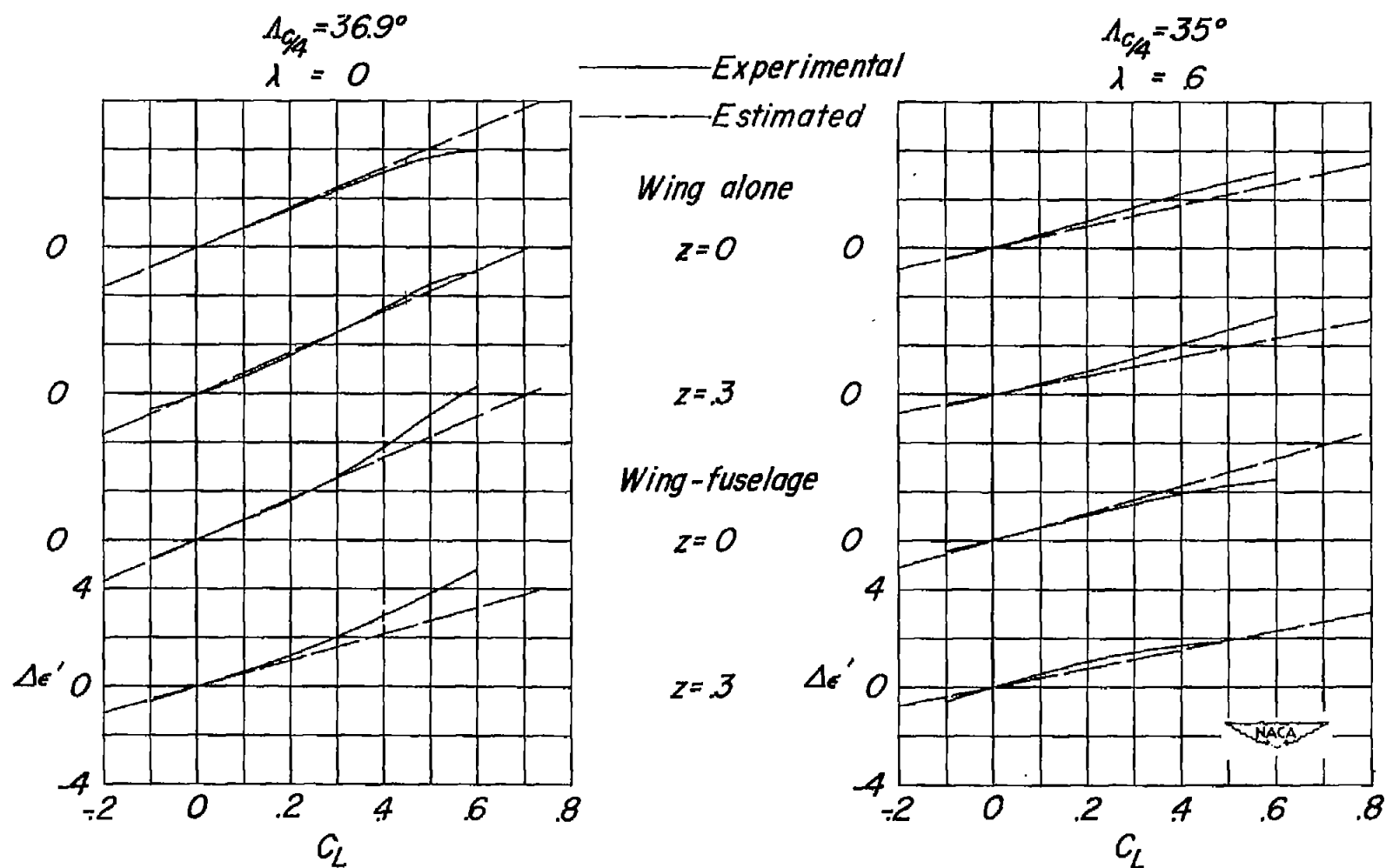
Figure 57.- Effect of aspect ratio on the experimental and estimated variation of floating angle with lift coefficient. $\Lambda_{c/4} = 45^\circ$; $\lambda = 0.6$; $\frac{t}{c} = 0.06$; $M = 1.1$.
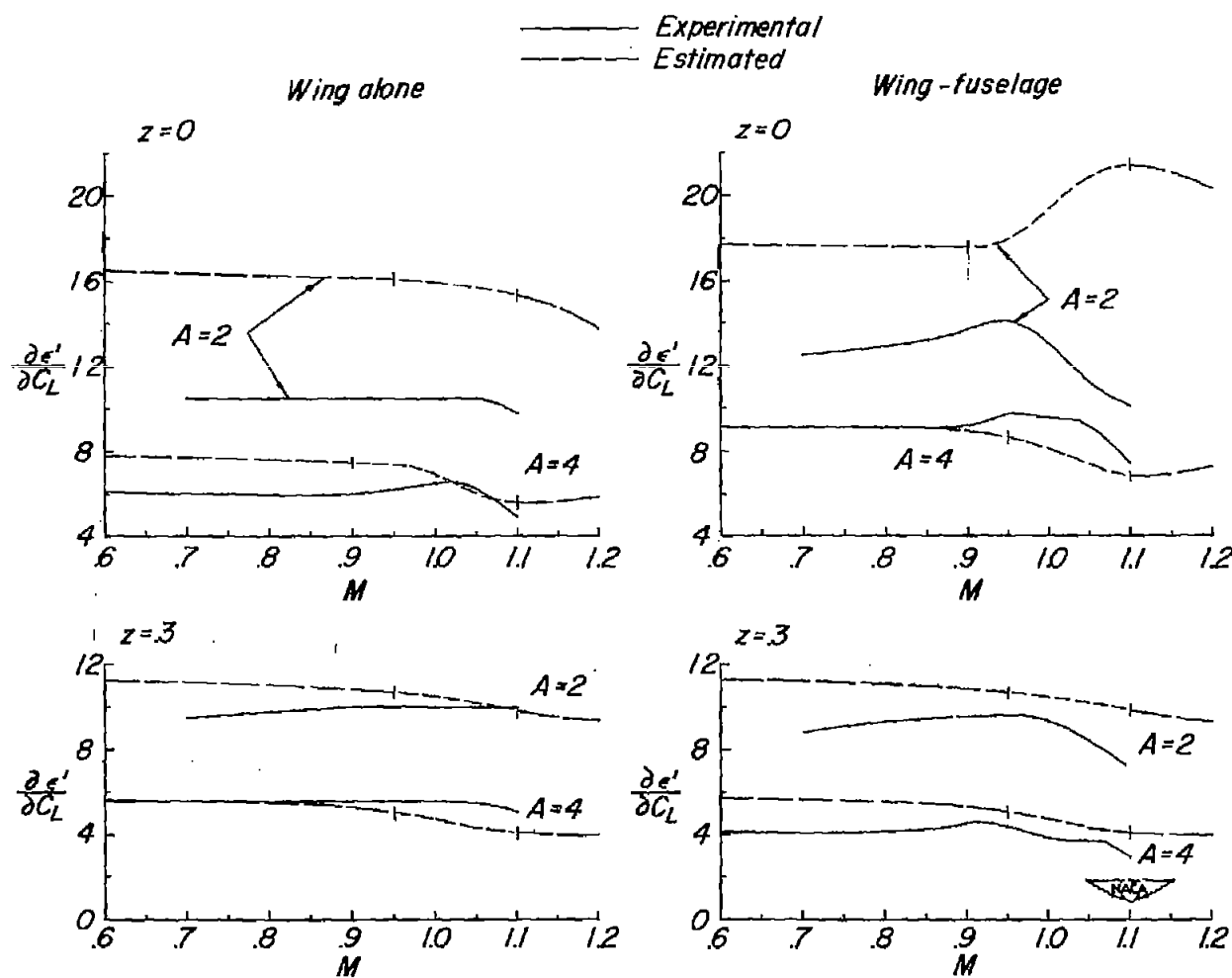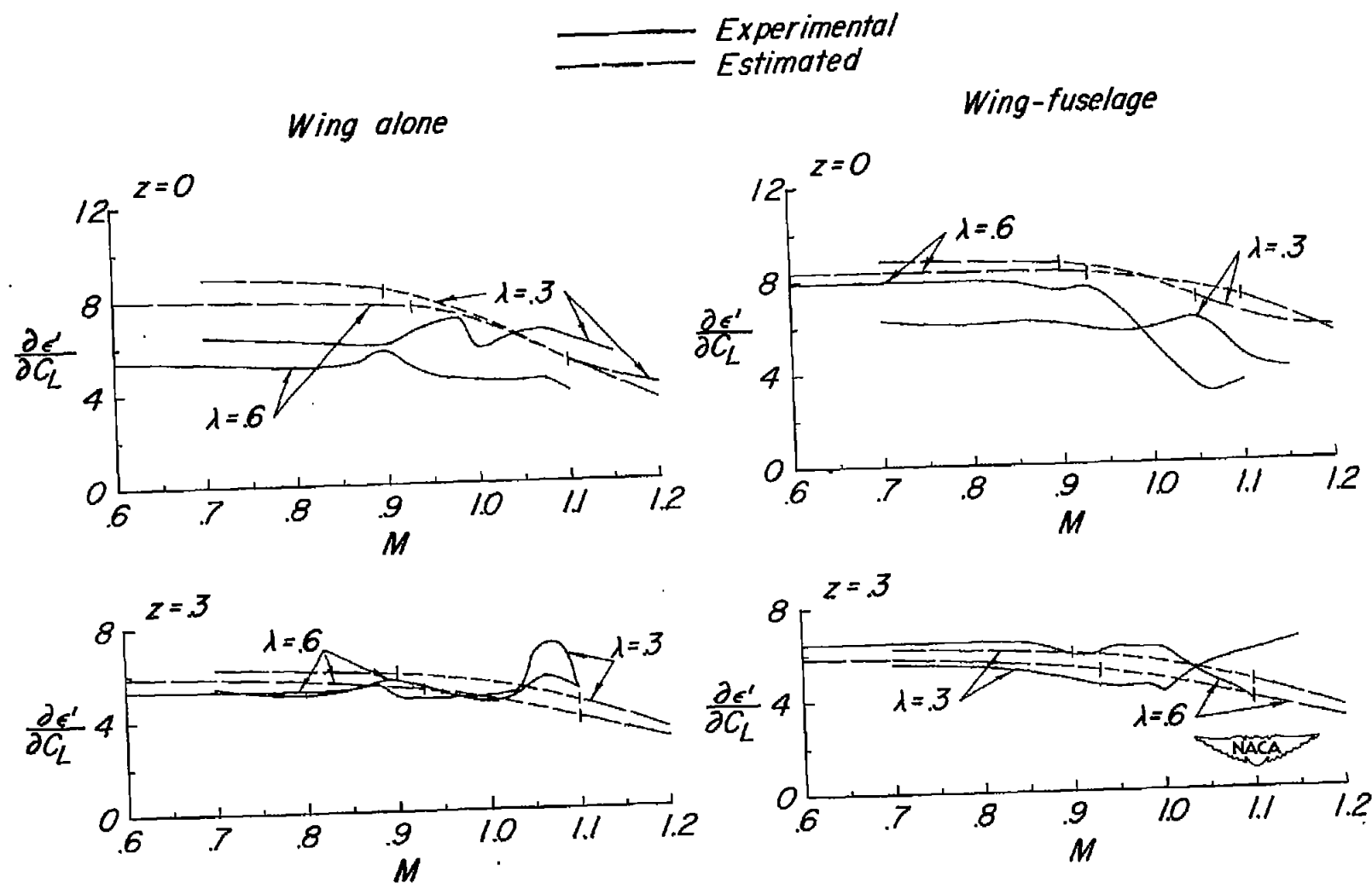
Figure 58.- Effect of aspect ratio on the experimental and estimated variation of floating-angle parameter $\partial \epsilon'/\partial C_L$ with Mach number. $\Lambda_{c/4} = 60^\circ$; $\lambda = 0.6$; $\frac{t}{c} = 0.06$.

Figure 59.- Effect of aspect ratio on the experimental and estimated variation of floating angle with lift coefficient. $\Lambda_{c/4} = 60°$; $\lambda = 0.6$; $\frac{t}{c} = 0.06$; $M = 0.8$.
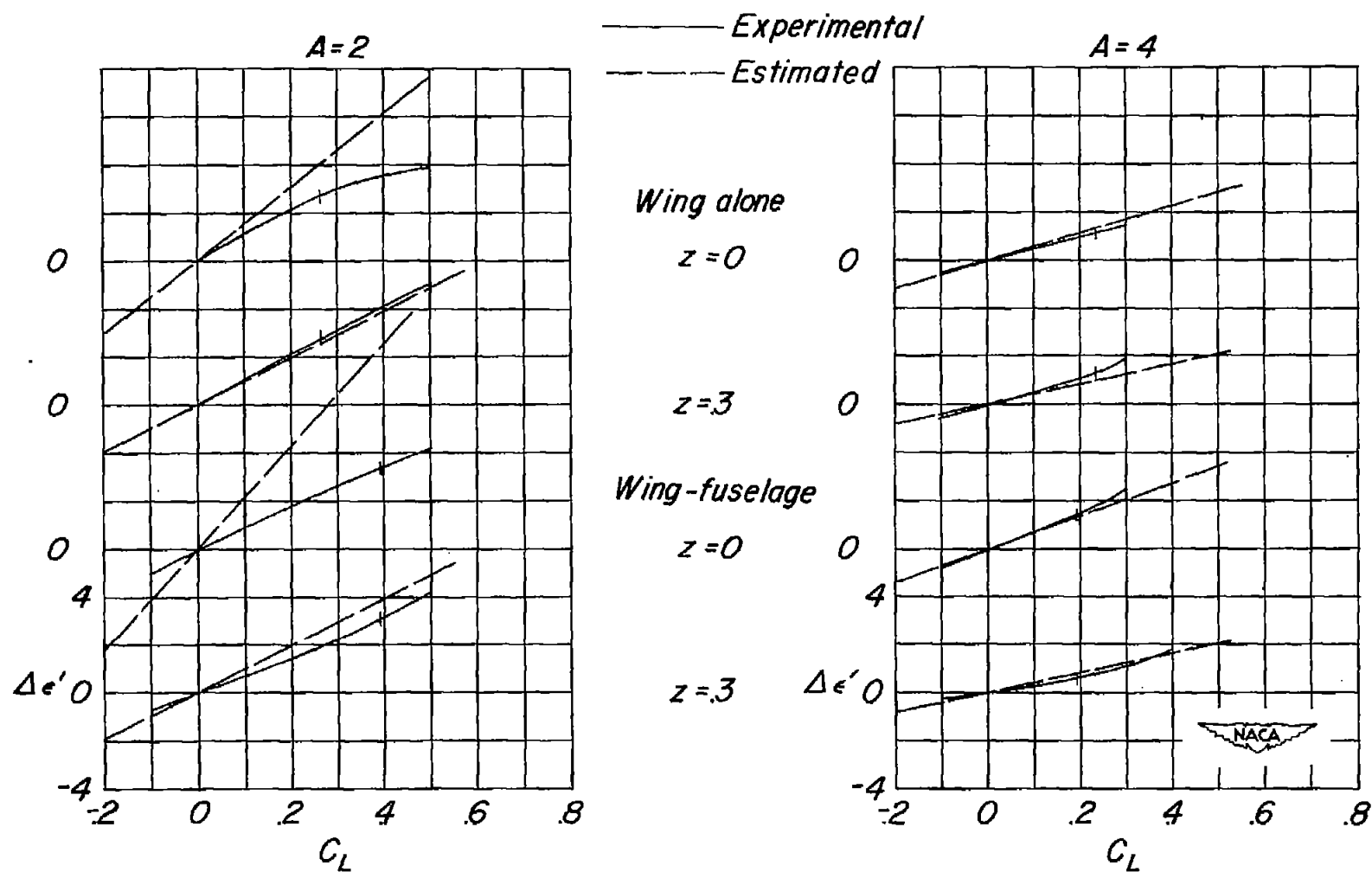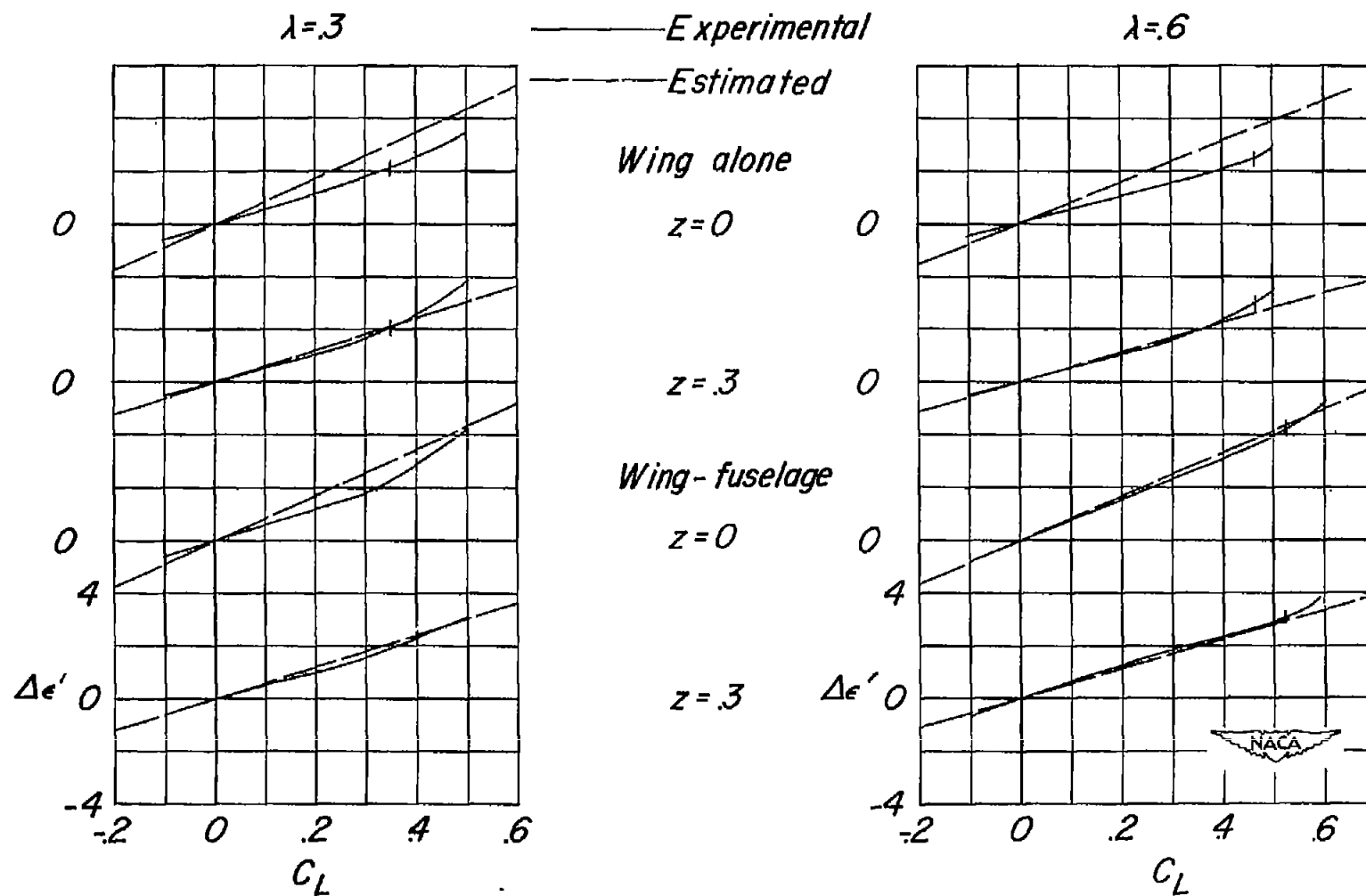
Figure 60.- Effect of aspect ratio on the experimental and estimated variation of floating angle with lift coefficient. $\Lambda_{c/4} = 60^\circ$; $\lambda = 0.6$; $\frac{t}{c} = 0.06$; $M = 1.1$.

Figure 61.- Effect of taper ratio on the experimental and estimated varia-
tion of floating-angle parameter $\partial \epsilon'/\partial C_L$ with Mach number. $\Lambda_{c/4} \approx 35°$;
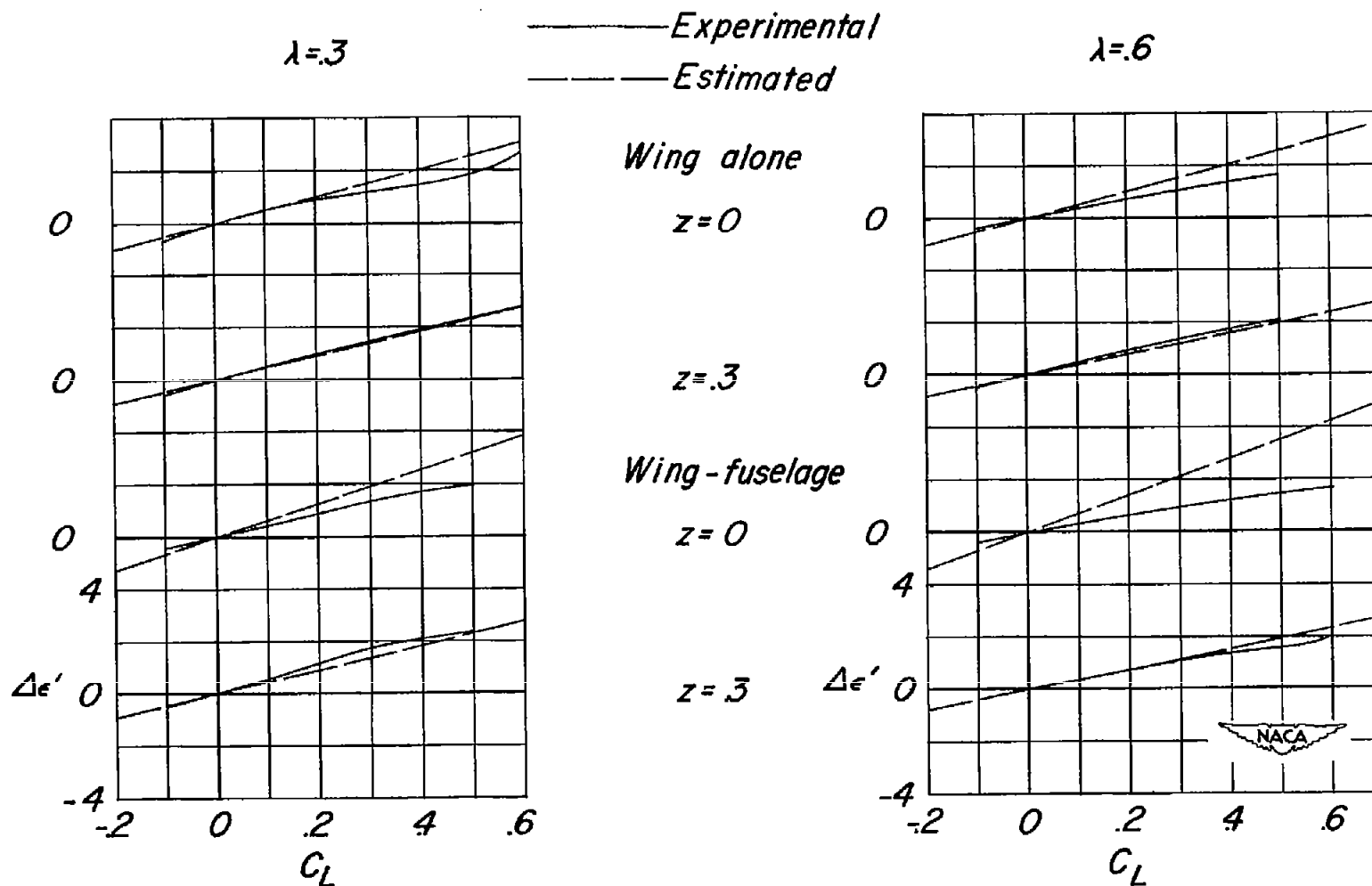$A = 4$; $\frac{t}{c} = 0.06$.

Figure 62.- Effect of taper ratio on the experimental and estimated variation of floating angle with lift coefficient. $\Lambda_{c/4} \approx 35°$; $A = 4$; $\frac{t}{c} = 0.06$; $M = 0.8$.

Figure 63.- Effect of taper ratio on the experimental and estimated variation of floating angle with lift coefficient. $\Lambda_{c/4} \approx 35°$; $A = 4$; $\frac{t}{c} = 0.06$; $M = 1.1$.

Figure 64.- Effect of taper ratio on the experimental and estimated variation of floating-angle parameter $\partial \epsilon'/\partial C_L$ with Mach number. $\Lambda_{c/4} = 45°$; $A = 4$; $\frac{t}{c} = 0.06$.

Figure 65.- Effect of taper ratio on the experimental and estimated variation of floating angle with lift coefficient. $\Lambda_{c/4} = 45^\circ$; $A = 4$; $\frac{t}{c} = 0.06$; $M = 0.8$.
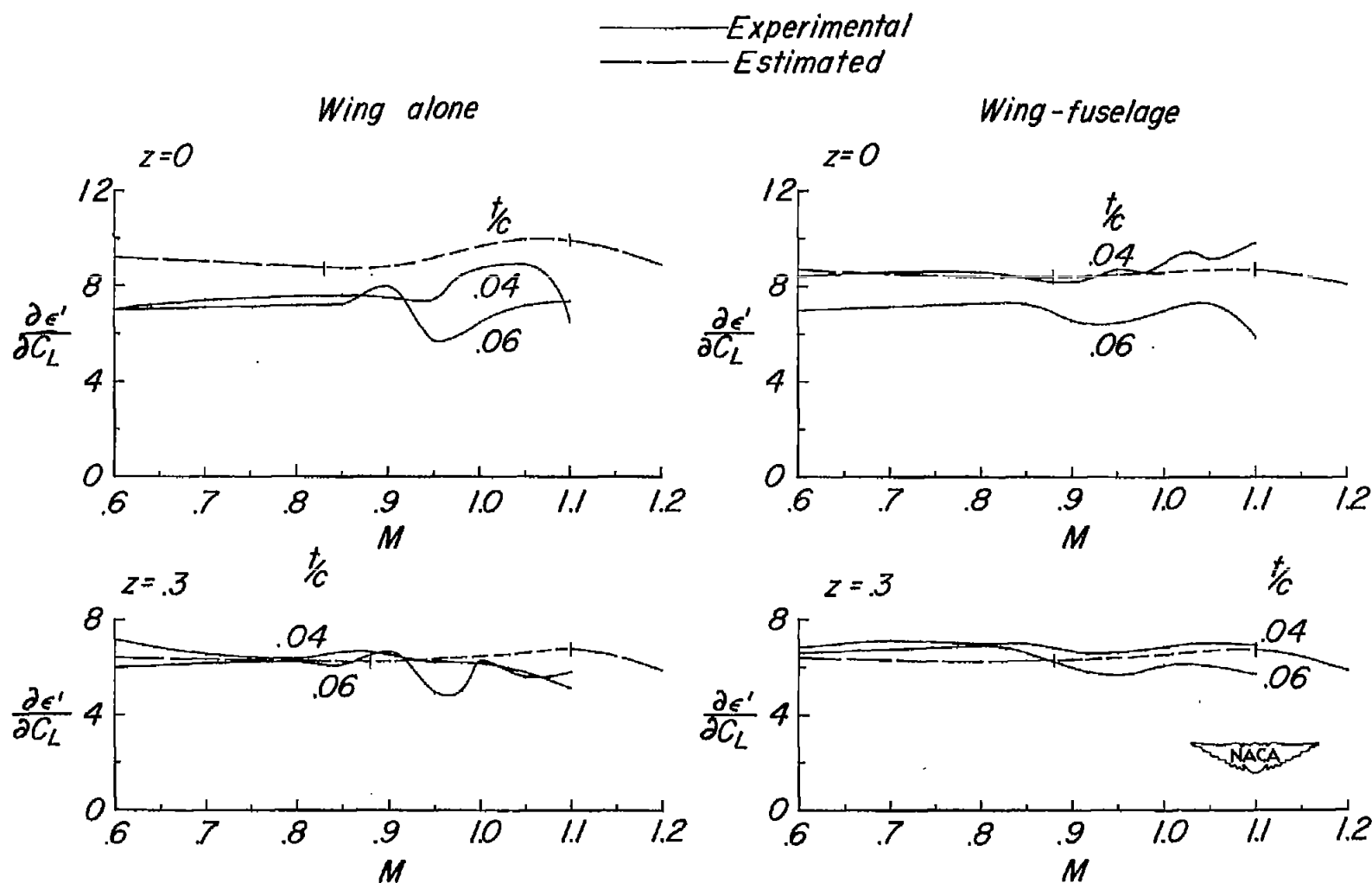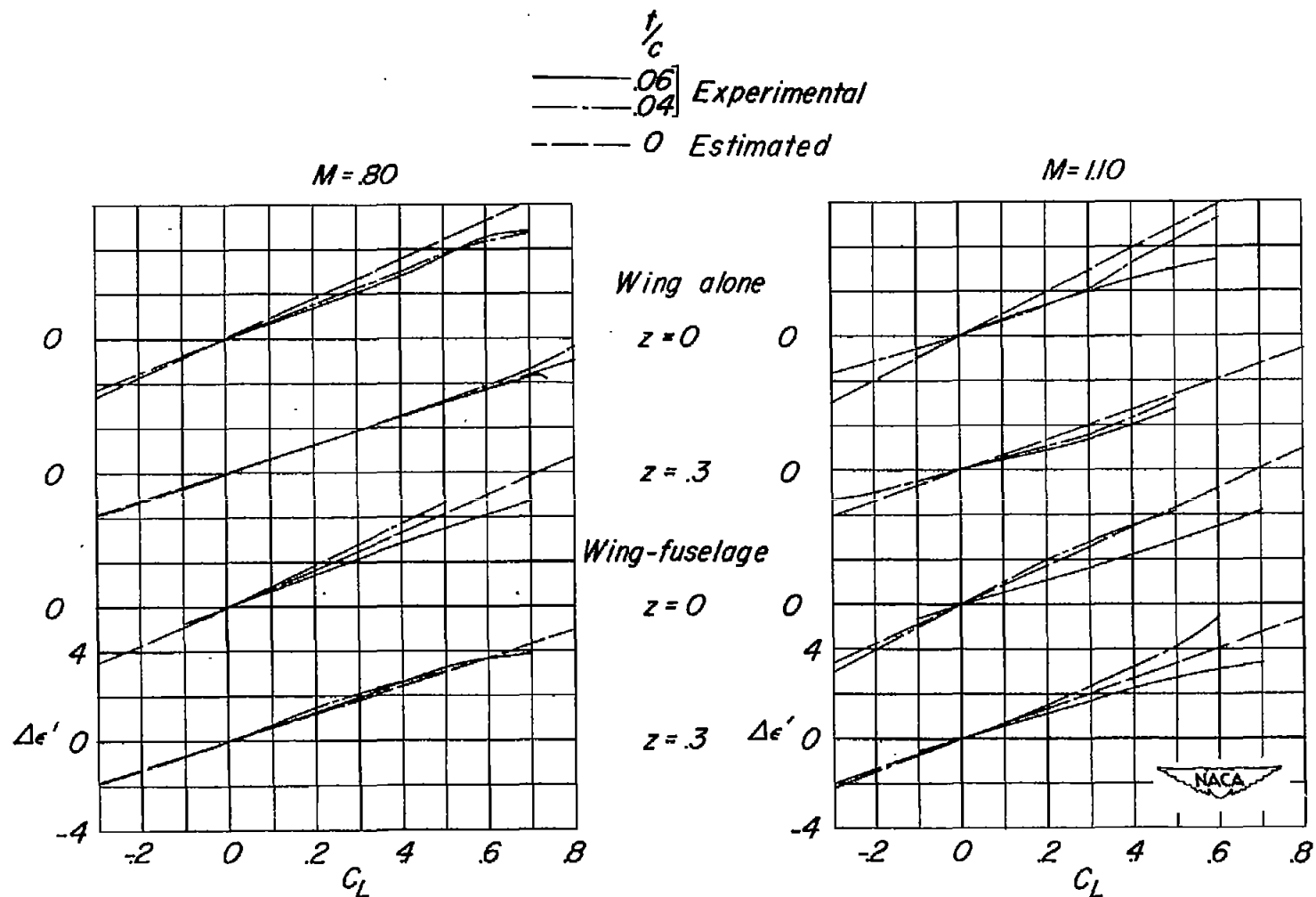
Figure 66.- Effect of taper ratio on the experimental and estimated variation of floating angle with lift coefficient. $\Lambda_{c/4} = 45°$; $A = 4$; $\frac{t}{c} = 0.06$; $M = 1.1$.
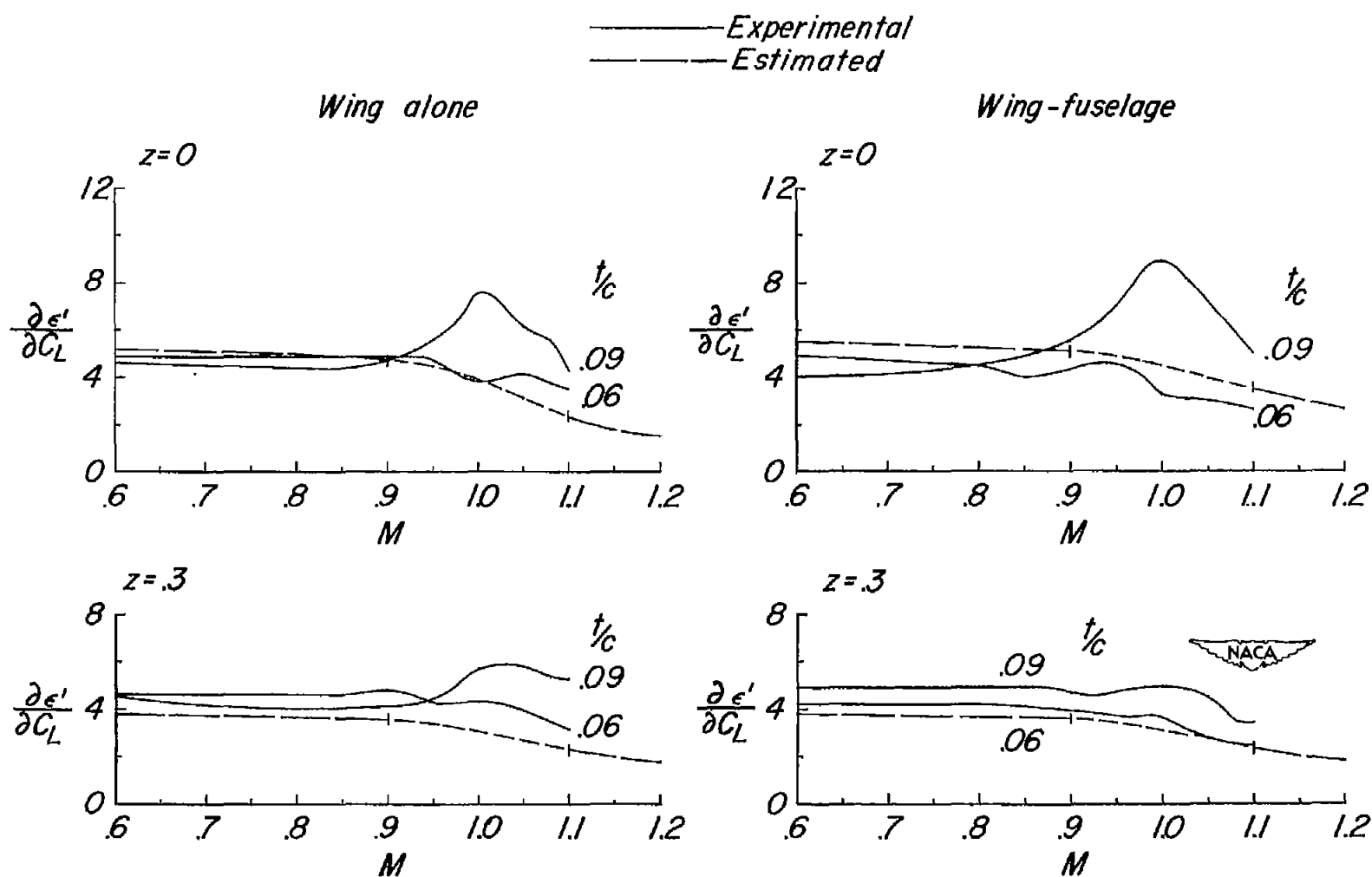
Figure 67.- Effect of wing thickness ratio on the experimental and estimated variation of floating-angle parameter $\partial \epsilon'/\partial C_L$ with Mach number. $\Lambda_{c/4} = 0$; $A = 4$; $\lambda = 0.6$.
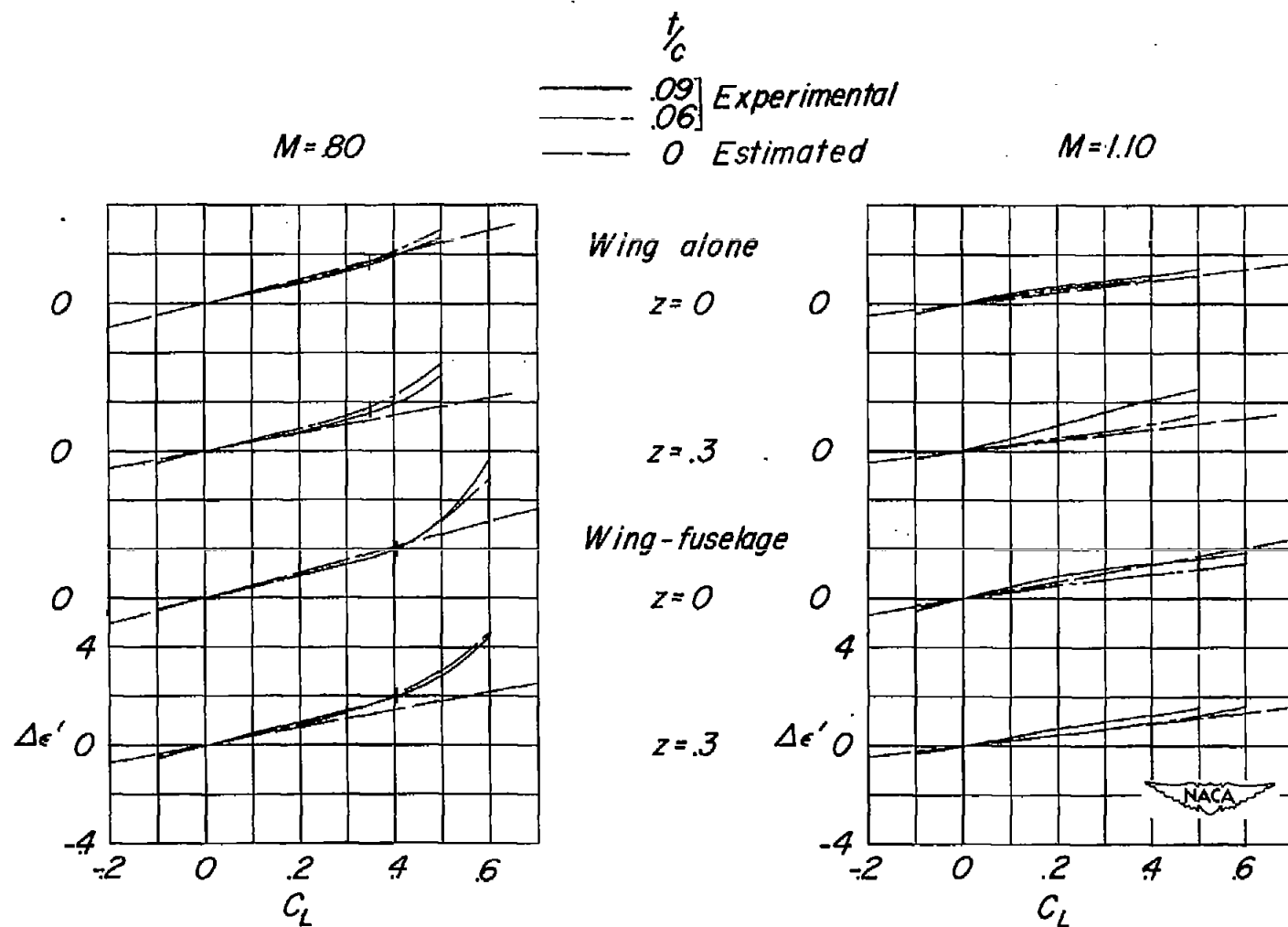
Figure 68.- Effect of wing thickness ratio on the experimental and estimated variation of floating angle with lift coefficient. $\Lambda_{c/4} = 0^\circ$; $A = 4$; $\lambda = 0.6$.

Figure 69.- Effect of wing thickness ratio on the experimental and estimated variation of floating-angle parameter $\partial\epsilon'/\partial C_L$ with Mach number. $\Lambda_{c/4} = 45°$; $A = 6$; $\lambda = 0.6$.

Figure 70.- Effect of wing thickness ratio on the experimental and estimated variation of floating angle with lift coefficient. $\Lambda_{c/4} = 45°$; $A = 6$; $\lambda = 0.6$.
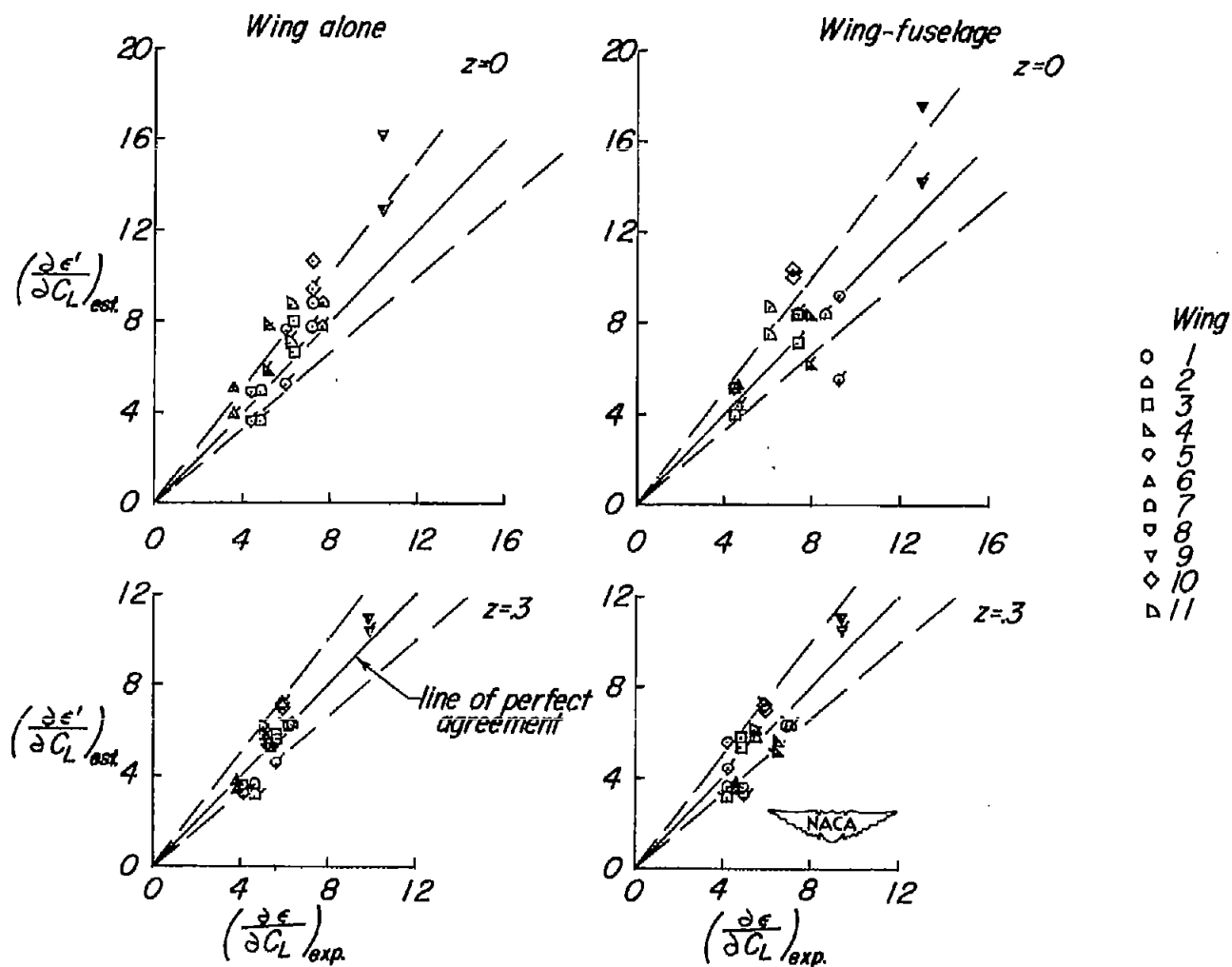
Figure 71.- Summary of correlation between experimental and estimated
parameter $\partial \epsilon'/\partial C_L$. M = 0.8; flat vortex theory, unflagged symbols;
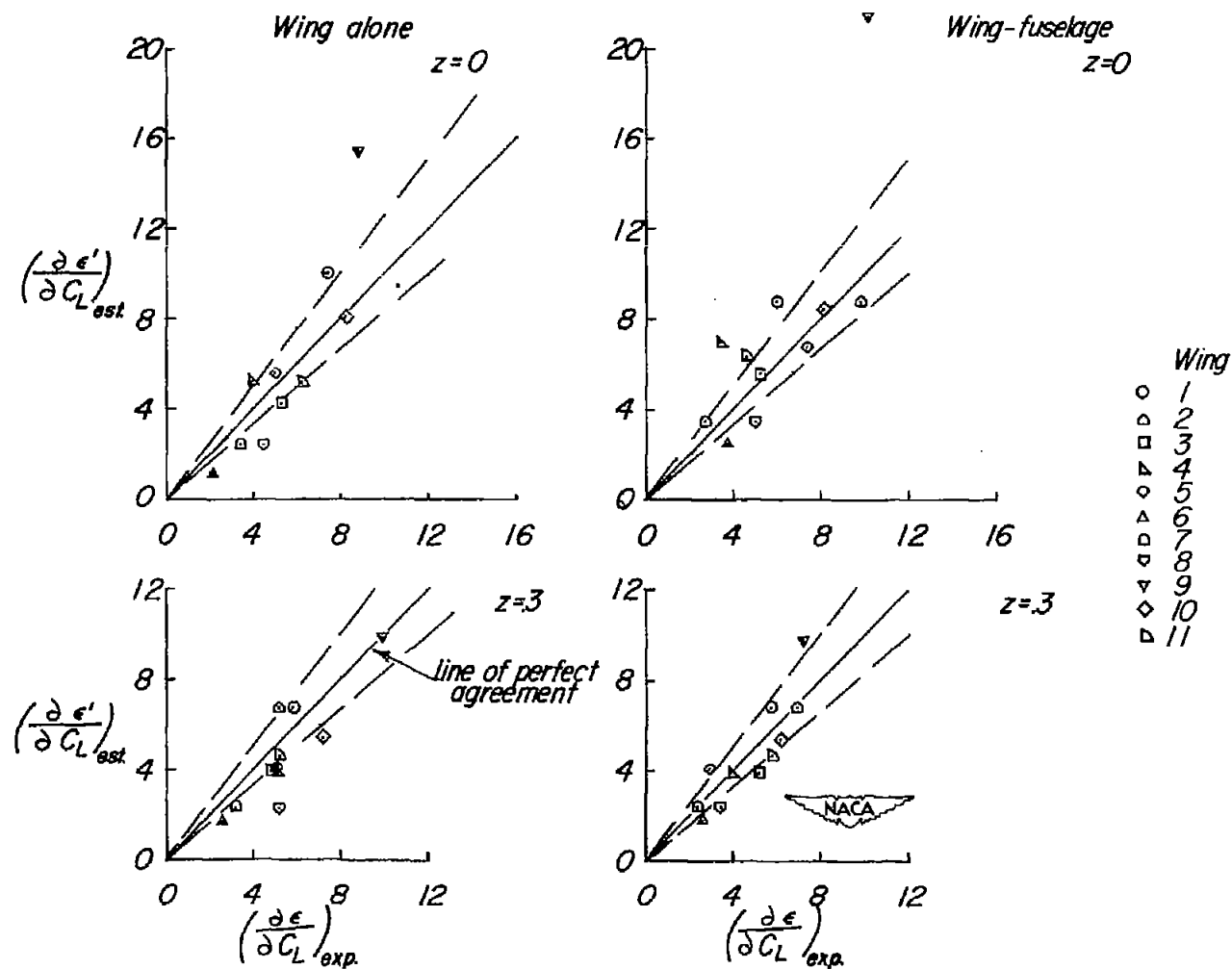single vortex theory, flagged symbols.

Figure 72.- Summary of correlation between experimental and estimated
parameter $\partial\epsilon'/\partial C_L$ using flat-vortex-sheet theory. M = 1.1.